To the Graduate Council:

I am submitting herewith a dissertation written by Sundaram C. Venkitarama entitled "An Acoustic Source Modeling Technique to Predict the Near Sound Field of Axisymmetric Turbulent Jets." I have examined the final copy of this dissertation for form and content and recommend that it be accepted in partial fulfillment of the requirements for the degree of Doctor of Philosophy, with a major in Mechanical Engineering.

James R. Maus

James R. Maus, Major Professor

We have read this dissertation and recommend its acceptance:

John E. Caruthers

[illegible]

[illegible]

[illegible]

Accepted for the Council:

L Evans Roth

Vice Chancellor
Graduate Studies and Research

AN ACOUSTIC SOURCE MODELING TECHNIQUE TO PREDICT THE NEAR SOUND FIELD OF AXISYMMETRIC TURBULENT JETS

A Dissertation

Presented for the

Doctor of Philosophy

Degree

The University of Tennessee, Knoxville

Sundaram C. Venkitarama

December 1981

3055596

ACKNOWLEDGMENTS

The author wishes to express his sincere gratitude and appreciation to Dr. J. R. Maus, Professor, Department of Aerospace and Mechanical Engineering, without whose help this study could not have been completed.

Special acknowledgments are due to Dr. B. H. Goethert, Dean Emeritus, whose acquaintance helped the author in realizing his dream of pursuing an educational career in this country.

The author expresses his gratefulness to Mr. J. Goodman, Engineer, Acoustics Laboratories, whose help in conducting the experiments reported in this study can never be overstated.

Special thanks are expressed to Mr. M. G. Scott and Mr. L. B. Bates, who helped in the various aspects of this research.

The author expresses his thanks to Wyle Laboratories of Huntsville, Alabama, for exhibiting an interest in this work and for providing free access to their facilities during the final stages of preparation of this study.

Words fail in expressing the gratitude the author feels towards Mr. N. S. Vidyasagaran and all other friends who provided utmost help during the last stages of preparation of this dissertation.

Special thanks are due to Jeannie Harper for her excellent typing of the manuscript.

The research reported herein was supported by fundings from Arnold Engineering Development Center/OIS, Air Force Systems Command, Arnold Air Force Station, Tullahoma, Tennessee, under Contract Number F40600-77-C-0009.

ABSTRACT

A procedure which allows the prediction of the near sound field of a circular jet by modeling the sound sources in the jet is developed. Far field, one-third octave sound pressure level data at various angles to the jet axis were obtained for an axisymmetric subsonic turbulent jet. The parameters varied were the jet exit velocities and stagnation temperature of the flow. The near field acoustic data at different radial locations and for the same test conditions were obtained. The strengths of the various source components at a particular frequency were determined by a constrained least-squares fit to the far field directivity pattern. The effects of sound source motion and distribution of the sources with frequency were taken into consideration and the near field sound pressure levels were predicted from the far field acoustic data. The experimental data for the near field and the predictions agreed fairly well.

The effect of Doppler shift in the observed frequency for a particular source frequency was studied. The Doppler shift correction was applied to the observed frequencies and the theoretical analysis was again carried out. This correction, however, did not indicate an improvement in the predicted results over that obtained before applying the correction.

TABLE OF CONTENTS

CHAPTER		PAGE
I.	INTRODUCTION	1
	Objective	1
	Physics of Sound Generation	2
II.	EXPERIMENTAL FACILITIES AND PROCEDURE	9
	Experimental Facilities	9
	Acoustic Data	11
III.	STATIONARY SOURCE MODEL	22
	Multipole Expansion	22
	Combination of Uncorrelated Sources	32
	Uniqueness Condition	36
	Source Synthesis for Jet Flow	39
	Results of Stationary Source Model	43
IV.	CONVECTED SOURCE MODEL	54
	Source Convection Effects	54
	General Aerodynamic Noise Theory	54
	Convection Effects on Source Model	65
	Extended Source Effects	73
	Results of Modified Source Modeling Procedure	76
V.	SUMMARY, CONCLUSIONS, AND RECOMMENDATIONS	98
	Summary	98
	Conclusions	99
	Recommendations	100

CHAPTER PAGE

BIBLIOGRAPHY 102

APPENDIX 105

VITA 113

LIST OF FIGURES

FIGURE		PAGE
1.	Elementary Sources of Sound [5]	3
2.	Elevation View of Free Field Facility	10
3.	Definition of Rectangular and Polar Coordinates for Stationary Source Model	14
4.	Far Field Spectrum for Test Condition 3 at ϕ = 30 degrees.	15
5.	Far Field Spectrum for Test Condition 3 at ϕ = 60 degrees.	16
6.	Far Field Spectrum for Test Condition 3 at ϕ = 90 degrees.	17
7.	One-Third Octave Far Field Directivity for a Center Frequency of 100 Hz (Test Condition 3)	18
8.	One-Third Octave Far Field Directivity for a Center Frequency of 1,000 Hz (Test Condition 3)	19
9.	One-Third Octave Far Field Directivity for a Center Frequency of 10,000 Hz (Test Condition 3).	20
10.	Definition of Position Vectors for Stationary Source Model	23
11.	Far Field Sound Pressure Directivity for Different Lengths of Source Region.	30
12.	Radial Variation of Sound Pressure Levels Showing Effect of Near Field Terms.	31

FIGURE PAGE

13. Comparison of Measured Sound Pressure Level Directivity with Least-Squares Fit for Test Condition 2 at 100 Hz. 44

14. Comparison of Measured Sound Pressure Level Directivity with Least-Squares Fit for Test Condition 2 at 1,000 Hz. 45

15. Comparison of Measured Sound Pressure Level Directivity with Least-Squares Fit for Test Condition 2 at 10,000 Hz 46

16. Comparison of Measured and Predicted Sound Pressure Levels for Test Condition 2 at 100 Hz 48

17. Comparison of Measured and Predicted Sound Pressure Levels for Test Condition 2 at 1,000 Hz 49

18. Comparison of Measured and Predicted Sound Pressure Levels for Test Condition 2 at 10,000 Hz. 50

19. Radial Variation of Sound Pressure Level for Test Condition 3 at 100 Hz. 52

20. Radial Variation of Sound Pressure Level for Test Condition 3 at 1,000 Hz. 53

21. Stationary Cold Jet: Measurements at Mach Number 0.3 and Reynolds Number 6×10^5 [11, 13]. 61

22. Increase of Emitting Volume and Emission Time Differences Because of Convection, by the Factor, $1/(1 - M_c \cos\phi)$ [11]. 63

FIGURE PAGE

23. Comparison of Measured Far Field Sound Directivity After Removal of Convection Effects with Least-Squares Fit for Test Condition 3 at 100 Hz. 69

24. Comparison of Measured Far Field Sound Directivity After Removal of Convection Effects with Least-Squares Fit for Test Condition 3 at 200 Hz. 70

25. Comparison of Measured Far Field Sound Directivity After Removal of Convection Effects with Least-Squares Fit for Test Condition 3 at 500 Hz. 71

26. Comparison of Measured Far Field Sound Directivity After Removal of Convection Effects with Least-Squares Fit for Test Condition 3 at 1,000 Hz. 72

27. RMS Error Between Microphone Data at 1 Ft and Predicted Sound Level as a Function of Assumed Source Location for 100 Hz. 74

28. Optimum Source Location as a Function of Strouhal Number 75

29. Comparison of Measured and Predicted Sound Pressure Levels Using Modified Source Modeling Technique for Test Condition 1 at 100 Hz. 77

30. Comparison of Measured and Predicted Sound Pressure Levels Using Modified Source Modeling Technique for Test Condition 1 at 200 Hz. 78

FIGURE PAGE

31. Comparison of Measured and Predicted Sound Pressure Levels Using Modified Source Modeling Technique for Test Condition 1 at 500 Hz. 79

32. Comparison of Measured and Predicted Sound Pressure Levels Using Modified Source Modeling Technique for Test Condition 1 at 1,000 Hz. 80

33. Comparison of Measured and Predicted Sound Pressure Levels Using Modified Source Modeling Technique for Test Condition 1 at 2,000 Hz. 81

34. Comparison of Measured and Predicted Sound Pressure Levels Using Modified Source Modeling Technique for Test Condition 2 at 100 Hz. 82

35. Comparison of Measured and Predicted Sound Pressure Levels Using Modified Source Modeling Technique for Test Condition 2 at 200 Hz. 83

36. Comparison of Measured and Predicted Sound Pressure Levels Using Modified Source Modeling Technique for Test Condition 2 at 500 Hz. 84

37. Comparison of Measured and Predicted Sound Pressure Levels Using Modified Source Modeling Technique for Test Condition 2 at 1,000 Hz. 85

38. Comparison of Measured and Predicted Sound Pressure Levels Using Modified Source Modeling Technique for Test Condition 2 at 2,000 Hz. 86

FIGURE PAGE

39. Comparison of Measured and Predicted Sound Pressure Levels Using Modified Source Modeling Technique for Test Condition 3 at 100 Hz. 87

40. Comparison of Measured and Predicted Sound Pressure Levels Using Modified Source Modeling Technique for Test Condition 3 at 200 Hz. 88

41. Comparison of Measured and Predicted Sound Pressure Levels Using Modified Source Modeling Technique for Test Condition 3 at 500 Hz. 89

42. Comparison of Measured and Predicted Sound Pressure Levels Using Modified Source Modeling Technique for Test Condition 3 at 1,000 Hz. 90

43. Comparison of Measured and Predicted Sound Pressure Levels Using Modified Source Modeling Technique for Test Condition 3 at 2,000 Hz. 91

44. Comparison of Measured and Predicted Sound Pressure Levels Using Modified Source Modeling Technique for Test Condition 4 at 100 Hz. 92

45. Comparison of Measured and Predicted Sound Pressure Levels Using Modified Source Modeling Technique for Test Condition 4 at 200 Hz. 93

46. Comparison of Measured and Predicted Sound Pressure Levels Using Modified Source Modeling Technique for Test Condition 4 at 500 Hz. 94

FIGURE PAGE

47. Comparison of Measured and Predicted Sound Pressure Levels Using Modified Source Modeling Technique for Test Condition 4 at 1,000 Hz. 95

48. Comparison of Measured and Predicted Sound Pressure Levels Using Modified Source Modeling Technique for Test Condition 4 at 2,000 Hz. 96

49. Comparison of Measured and Predicted Sound Pressure Levels After Doppler Shift Correction for Test Condition 1. 109

50. Comparison of Measured and Predicted Sound Pressure Levels After Doppler Shift Correction for Test Condition 2. 110

51. Comparison of Measured and Predicted Sound Pressure Levels After Doppler Shift Correction for Test Condition 3. 111

LIST OF SYMBOLS

A_1, A_2, A_3, A_4	Octupole coefficients, $K^6 M_{030}^2/(4\pi x)^2$, etc.
a	Radius of source region
a_o	Ambient speed of sound
C	Strength of source region
c	Local speed of sound
D	Nozzle diameter
D_1, D_2	Dipole coefficients, $K^2 M_{200}^2/(4\pi x)^2$, etc.
$F(\bar{y})$	Source function amplitude
f	Frequency
$f(\phi)$	Source directivity function
f_s	Source frequency
$f(x_1, x_2, x_3, t)$	Source function
I	Acoustic intensity
i	Imaginary unit, $\sqrt{-1}$
k	Wave number, ω/a_o
L	Length of source region
ℓ	Correlation radius
M	Mach number, U/a_o
M_c	Convection Mach number, V_c/a_o
$M_{jk\ell}$	Multipole moment amplitude
$m_{jk\ell}(t)$	Multipole moment
P_o	Stagnation pressure
P_a	Atmospheric pressure

p	Acoustic pressure
$\overline{p^2}$	Acoustic mean square pressure
p_d	Acoustic pressure associated with dipole terms
p_m	Acoustic pressure associated with monopole terms
p_q	Acoustic pressure associated with quadrupole terms
p_o	Acoustic pressure associated with octupole terms
P_1	Monopole coefficient, $M_{000}^2/(4\pi x)^2$
p_{ref}	Reference acoustic pressure
p_{ij}	Stress between adjacent elements of fluid
Q_1, Q_2, Q_3	Quadrupole coefficients, $K^4 M_{200}^2/(4\pi x)^2$, etc.
$q(t)$	Mass flow rate
$\dot{q}(t)$	Rate of variation of mass flow rate
R	Distance from source point to observation point, $\lvert\bar{x}-\bar{y}\rvert$
R_c	Ratio of convection velocity to jet velocity
r	Radius in cylindrical coordinates
SPL	Sound pressure level, $10 \log_{10} \overline{p^2}/p_{ref}^2$, dB
ST	Strouhal number, fD/U
T_{ij}	Equivalent applied stress
T_o	Stagnation temperature
t	Time
U	Velocity of jet
V	Turbulent flow region
V_e	Volume of region of flow in which the acoustic sources are well correlated
V_c	Convection velocity

v_i	Velocity vector
W	Acoustic power
x	Distance to field point
x_1, x_2, x_3	Coordinates of field point
x_s	Axial distance from nozzle exit plane to source location
$\bar{x}$	Position vector to field point
$\bar{y}$	Position vector to source point
y_1, y_2, y_3	Coordinates of source point
Z	Axis of symmetry of source region

Greek Symbols

δ_{ij}	Kronecker delta
θ	Azimuthal angle
λ	Wave length
ρ	Density
ρ_o	Stagnation or ambient density
ρ_m	Density in the mixing region
ϕ	Polar angle
Ω	Solid angle
ω	Radian frequency

CHAPTER I

INTRODUCTION

1.1. Objective

It is well known that sound pressure near an acoustic source can vary much more rapidly than the 1/R relation that applies in the far field. In this region the sound pressure is not in phase with the acoustic particle velocity and cannot be related directly to acoustic energy flux. The understanding of the near field data and their relation to the acoustic sources and the far field sound would be of great value in assessing the effect of jet noise on components located near the jet.

The primary objective of the present study is to determine the relationship between acoustic measurements in the near field and the far field sound produced by a free circular jet. The general approach taken in this study was to model the jet source region, for a given frequency, with a combination of uncorrelated elementary sources derived from the multipole expansion.

The basic theory of aerodynamic sound is derived from the classical acoustic theory of small disturbances of a gas at rest, the so-called elementary solutions of the equations of motion, namely, sources, dipoles, and so forth [1, 2].[1] The theory of aerodynamic

---

[1] Numbers in brackets refer to similarly numbered references in the Bibliography.

noise as it is known today was evolved from the fundamental work of Lighthill [3, 4] and has been contributed to by a number of workers in recent years.

In an earlier paragraph, it was mentioned that the theoretical prediction of the near sound field was achieved through a combination of the uncorrelated elementary sources in the source region as determined from the far field data. A physical explanation of these elementary sources of noise generating mechanisms would be in order here and is described in the next section.

1.2. Physics of Sound Generation

Perhaps the simplest of all noise generating mechanisms in a fluid flow would be the simple source, or a monopole. A balloon [5] caused to pulsate by an oscillatory air supply is often cited as a model for a simple source of sound. The sound waves arise from the radial acceleration (see Fig. 1a). An outward acceleration of fluid with the balloon removed will have the same effect. The + signs in Fig. 1a have a dual interpretation as radial acceleration (of the balloon) and as a time rate of injection of matter. The sound pressure radiated from the balloon is proportional to the product of surface area times radial acceleration and density. If new fluid is introduced at the source at a rate whose variation with time is expressed by the function $q(t)$, the strength of the source will be given by the rate of variation, $\dot{q}(t)$ at time t. The pressure at a distance R from the source takes the form,

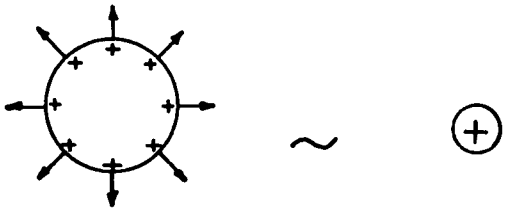

(a) Pulsating sphere as model of simple source of sound

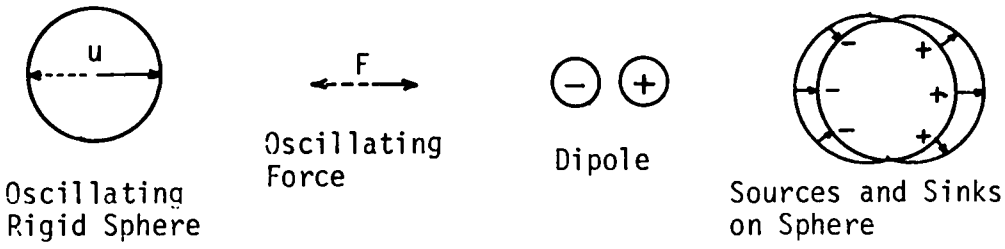

(b) Alternate models of dipole source of sound

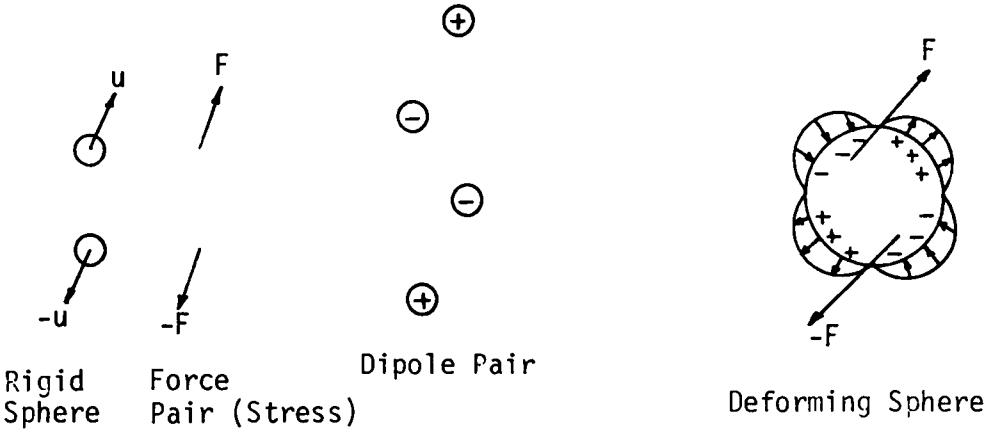

(c) Alternate models of oblique quadrupole source of sound

Figure 1. Elementary sources of sound [5].

$$p - p_o = \frac{\dot{q}\,(t - R/a_o)}{4\pi R} \quad . \tag{1.1}$$

It is proportional to the value of $\dot{q}$ at the "retarded time" $(t - R/a_o)$; that is, at the instant when a wave traveling at the speed of sound, a_o, had to leave the source in order to reach the point of observation at the current time, t.

The next simplest elementary solution is the dipole, where sound is generated by injection of momentum rather than mass. The model for a dipole source of sound is a rigid sphere that oscillates back and forth along a line. The outward or normal acceleration of the forward and rearward hemispheres is now opposite. The +'s and -'s shown in Fig. 1b are just an indication of the direction of acceleration at a given instant of time. There are equal "number" of +'s and -'s. If one takes an analogy from fluid mechanics and assumes the +'s as sources and the -'s as sinks, it would seem that the total efflux of matter from the sources would be ingested completely by the sinks, which in turn would lead one to believe that the net effect perceived externally to a dipole would be zero. However, occurrences at one face will be transmitted at the speed of sound to the other; that is, at a time proportional to D/c, where D is the diameter of the sphere; and c, the local acoustic speed. The transmitted pressure will fall short of canceling the local pressure disturbance by a fraction given by the phase shift proportional to fD/c. This contributes a factor proportional to $(fD/c)^2$ to the acoustic power as compared with that for the sources or sinks separately (a monopole). The idea that a source and a sink at close proximity generate a

dipole leads to the definition of dipole strength, from fluid mechanics, as the magnitude of the source strength times the separating distance. Thus, the acoustic dipole is equivalent to a force, concentrated at a point, and varies in magnitude and direction, or both. As far as generation of acoustic energy goes, the mechanism in a dipole is by the injection of momentum as compared with the injection of mass in a monopole.

If a pair of opposed forces are displaced, as in Fig. 1c, the result is a general type of quadrupole. Two spheres oscillating in opposite phase produce the same effect at large distances. Yet another model is a sphere deforming without change in volume. This approximates best the behavior of a fluid element.

Unlike a dipole, the quadrupole is characterized by two axes. One, a force vector, and the other a separation vector. If the forces are coaxial (i.e., length of separation vector is zero), the quadrupole is known as a longitudinal quadrupole. If the two vectors are perpendicular, there are lateral quadrupoles. Of course, a general quadrupole will have oblique axes, but they can always be resolved into the lateral and longitudinal types.

It is possible to replace a quadrupole distribution by an equivalent dipole distribution, which in turn can be replaced by an equivalent source distribution. For such an equivalent system, the total strength of either dipoles or sources is zero. The phase cancellation effects discussed in the case of dipoles earlier (equally present for a quadrupole, which is just a pair of dipoles) are present to some degree in an equivalent spatial source

distribution with total strength zero. Emission from such a distribution, according to Lighthill [3, 4, 6], has the nature of a quadrupole radiation. However, Ribner [5] considers this characterization somewhat of an oversimplification and discusses it in the following manner.

If one considers, for the sake of convenience, a two-dimensional space for a source distribution, then the sources and sinks can be pictured as hills and valleys, respectively. This pattern fluctuates in a random manner with time; however, with an average (in time) size or radius. The "source radius" is a measure of the extent of a source or sink patch radiating coherently. A very small source radius compared to the emitted wavelength/2 may consist of a number of source and sink patches and can still be considered to have simultaneous emission. The net emission from such a source/sink region will be zero if all the +'s and -'s cancel out in these regions. To retain the simultaneous emission approximation, it might be necessary to replace the equivalent source-sink distributions with an equivalent dipole distribution. If this again vanishes, consider a quadrupole distribution. Lighthill's [3, 4, 6] analysis of the flow noise in terms of quadrupoles follows in part from the vanishing of the volume integral of the equivalent sources. A necessary second assumption is that the "source radius" be very small compared to a sound wavelength/2 . In a jet flow this criterion is not fully met. The +,- source patches do not cancel out completely because the source radius is not very small. Hence, despite a net zero strength, there is little effective cancellation of the sound from the sources

and sinks. Hence, the distribution does not seem to have the essential quadrupole character, but rather, behaves more like a simple source/sink distribution of nonzero strength.

A brief explanation of the basics of aerodynamic noise generation has been presented in this section. However, the main point relevant to the present investigation that should be highlighted here, is that noise generation from a fluid flow can be approximated through a combination of monopole, dipoles, quadrupoles, octupoles, and so forth. These elementary sources are assumed to be uncorrelated. The strengths of these elementary sources can be derived from the sould characteristics in the radiation (far) field. These derived quantities can, in turn, be used for predicting the near sound field characteristics of a fluid flow.

The study started with a mathematical model in which the sources were considered stationary and located at the center of the nozzle exit plane. Less than satisfactory results from this oversimplified model resulted in the inclusion of the convection effects of the sources and studies on distribution of the sources with frequency. Incorporation of these factors resulted in a fairly good improvement in the predicted results. Finally, an attempt was made to incorporate the Doppler effects on frequency. However, the results did not seem to indicate a noticeable improvement from that without the Doppler effect. Discussion of the probable reasons for this will be taken up in Chapter V.

A longer range objective of this research effort is to establish techniques for predicting the far sound field from

measurements in the near-field. Such a prediction technique would be desirable in the study of the acoustic characteristics during flight simulation when it is not desirable or possible to build large flight simulation wind tunnels. Ahuja et al. [7] have conducted studies in predicting far field jet noise spectra from near field measurements. The importance of locating the acoustic sources as accurately as possible has been emphasized in this paper. The non-negligible distance of the sources, especially for the lower frequencies, is one of the reasons, according to this paper, that causes deviations from the inverse square law between mean square acoustic pressure and distance, as the distance is usually measured from the point of observation to the center of the nozzle exit plane; whereas, strictly, it should be from the observer to the source location point. The importance of obtaining a good estimate of the source location and also the convection velocity of the sources, was felt during the course of this study also. Of course, the nature and amount of deviation that would be introduced in the predicted results due to errors in these parameters would, to a large extent, also depend on the prediction scheme that is used.

CHAPTER II

EXPERIMENTAL FACILITIES AND PROCEDURE

2.1. Experimental Facilities

All acoustic data in this study were gathered in The University of Tennessee Space Institute (UTSI) free field facility shown in Fig. 2. The major elements of the free field test stand include the stilling chamber, which is 11 feet long and has an inside diameter of 25.75 inches, its supporting structure, and the microphone sweep arms. A kerosene-fueled heater makes it possible to conduct tests at temperatures up to $1{,}480^{o}R$. The stilling chamber may be raised and lowered from the horizontal to an angle of 35.5 degrees above the horizontal to facilitate changes in test configuration. For the present investigation it was positioned at 35.5 degrees to the horizontal during all tests.

Air is supplied to the test facility through a system of piping from three 250 ft^3, high-pressure storage tanks. Control of the airflow is achieved through the use of a 4-inch control valve and two dome regulators. A mass flowmeter is installed in the piping upstream of the test facility. The storage tanks are capable of delivering air mass flows in excess of 40 lbm/sec. At this flow rate, the heater is capable of raising the stagnation temperature up to $1{,}460^{o}R$. Being a blow-down facility, the run time is inversely proportional to the air mass flow rate, with a flow of 40 lbm/sec corresponding to about a three-minute run.

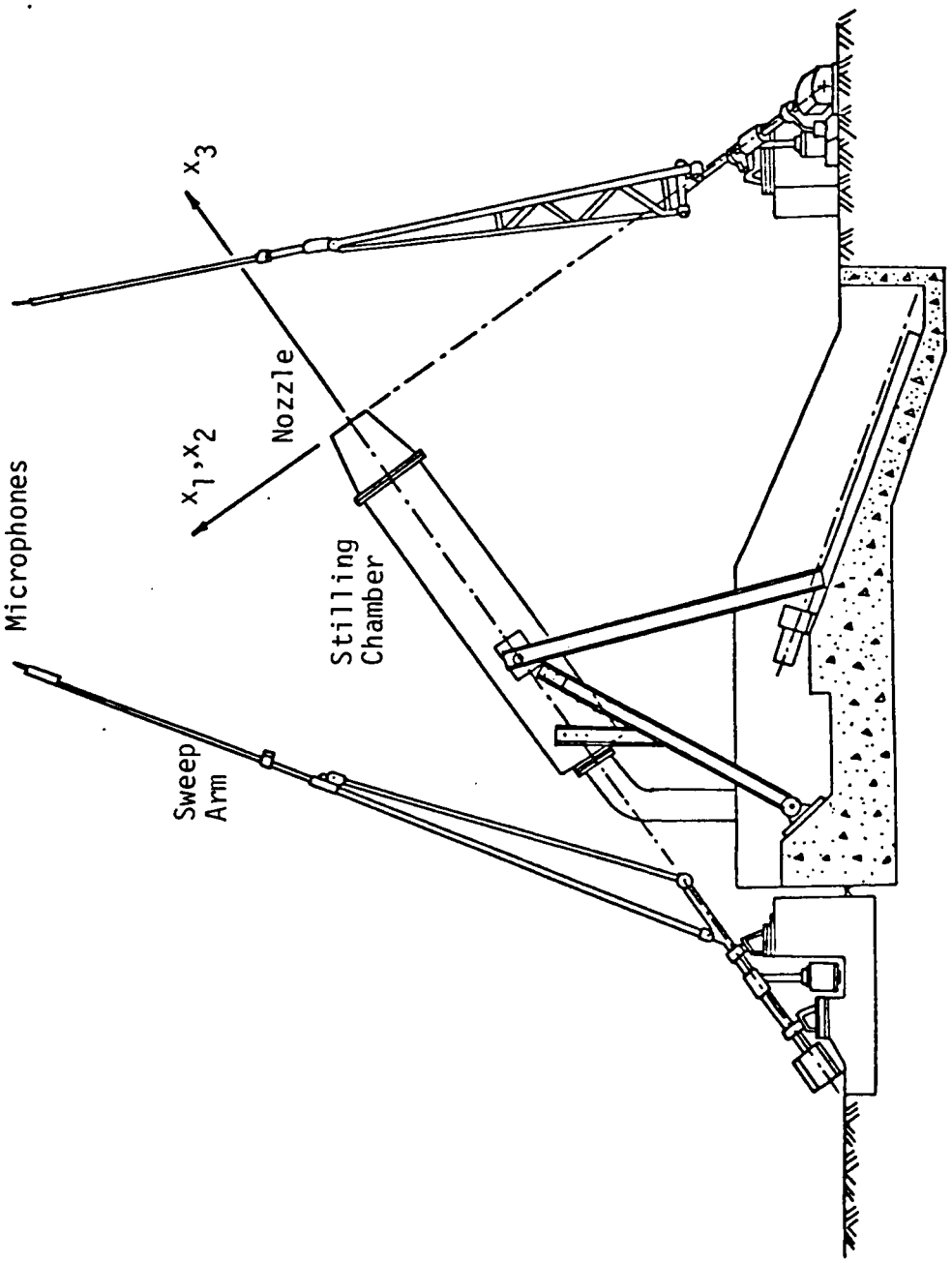

Figure 2. Elevation view of free field facility.

In the present study, the turbulent jet was obtained from a circular convergent nozzle with a nominal diameter of 2.82 inches.

The free field facility has the capability for positioning a microphone in any one or all of the three orthogonal planes centered about the nozzle. The motor-driven microphone sweep arms enable acoustic measurements at different angles to the jet axis, and being adjustable in length, the radial location of the microphone from the nozzle center can also be varied over a wide range.

The aeroacoustic instrumentation is composed of a flow measurement system and a sound measurement system. Sound measurements were made with 1/4-inch Bruël & Kjaër (B&K) 4136 condenser microphones. The signal from the microphone was fed into a B&K Frequency Analyzer Type 2112, and then recorded on the B&K Level Recorder Type 2305.

The bulk flow conditions at the nozzle exit were determined by measuring stilling chamber pressures and temperatures and then applying one-dimensional, isentropic flow relations for the expansion to atmospheric pressure.

2.2. Acoustic Data

All acoustic test data in the present study were taken on high velocity jets exhausting from a converging circular nozzle with a 2.82-inch exit diameter. In order to avoid noise sources associated with shocks in the flow, the exit Mach number of the jet exhaust was kept below one. Four different combinations of stagnation pressures and temperatures were used in order to vary the jet exit velocity,

and consequently, sound source power over a wide range. The flow conditions used in this study are given in Table 1.

A coordinate system with origin at the center of the nozzle exit plane and with x_1, x_2, and x_3 axes as defined in Fig. 3 was used for microphone sweep planes and for the development of the theoretical analysis. All of the acoustic data were obtained from a microphone in the x_1,x_3 plane. For normal operations, the microphone mounted on the arm is at a constant distance of 13 feet from the center of the nozzle exit plane during a sweep. At this distance, the microphone is in the far field for all frequencies greater than about 100 Hz. For each of the conditions in Table 1, a series of acoustic data was obtained. Far field data in the x_1,x_3 plane were taken first with the microphone located 13 feet from the origin of the coordinate system. One-third octave sound pressure spectra were obtained at 5-degree increments of polar angle, ϕ, starting at ϕ = 20 degrees to ϕ = 90 degrees. The polar angle, ϕ, is measured from the x_3 axis, the axis of the jet exhaust. Figures 4, 5, and 6 are examples of these far field spectra measured for Test Condition 3. From spectrograms such as these, the one-third octave, far field directivity patterns were plotted for center frequencies of 100, 200, 500, 1,000, 2,000, 5,000, and 10,000 Hz. Figures 7, 8, and 9 are examples of the far field directivities for Test Condition 3. It should be noted that the one-third octave frequency analysis is a constant percentage analysis with the filter bandwidths equal to 23 percent of the center frequency. Thus, the frequency bandwidth of the 100-Hz data in Fig. 7 is 23 Hz, and the bandwidth of the 1,000-Hz data in Fig. 8 is 230 Hz.

Table 1. Test Conditions

Condition	P_o/P_A	Jet Exit Mach No.	T_o, ^oR	Jet Exit Velocity (ft/sec)
1	1.387	0.7	540	755
2	1.691	0.9	530	943
3	1.691	0.9	1,160	1,396
4	1.787	0.95	1,260	1,524

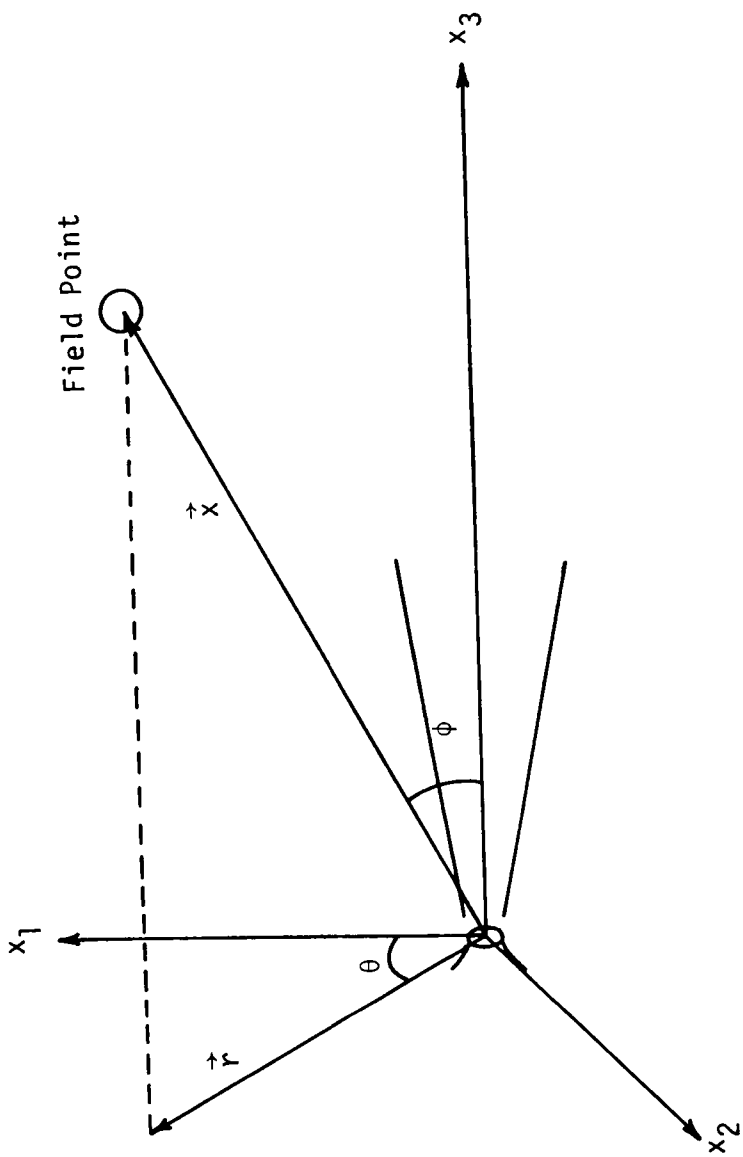

Figure 3. Definition of rectangular and polar coordinates for stationary source model.

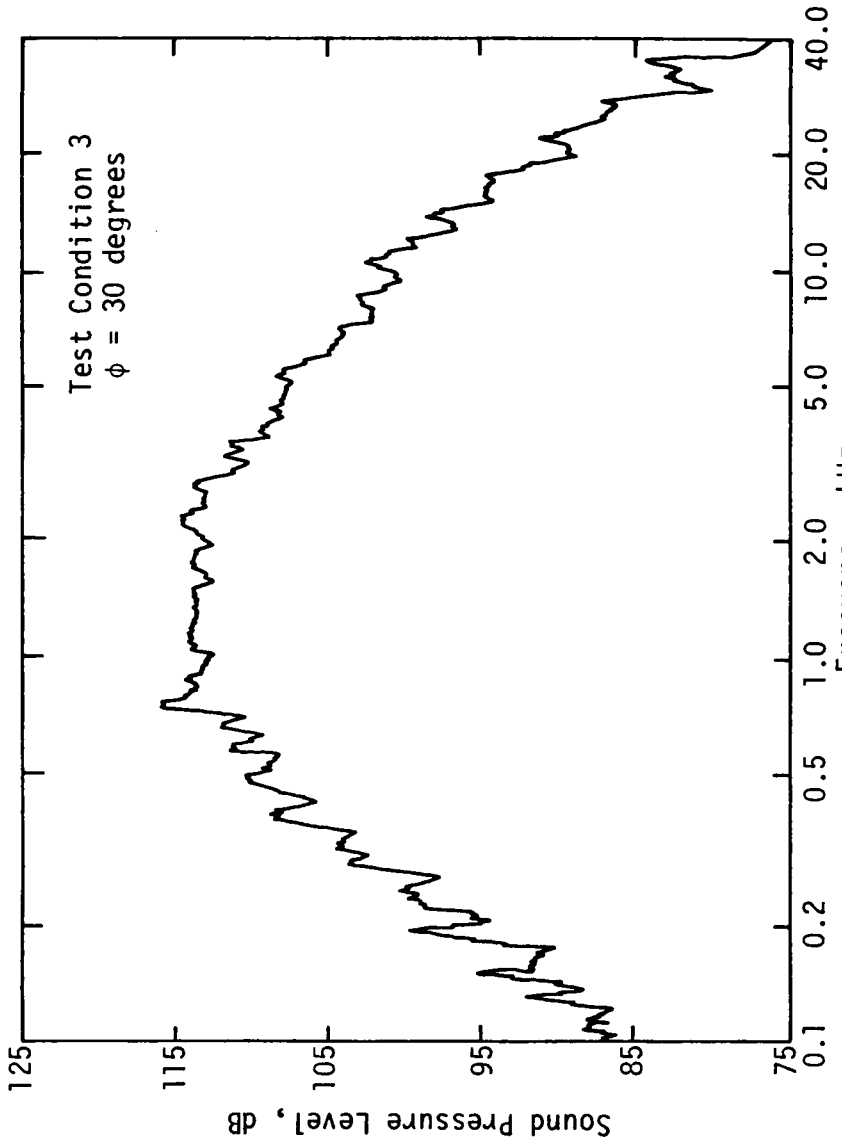

Figure 4. Far field spectrum for Test Condition 3 at ϕ = 30 degrees.

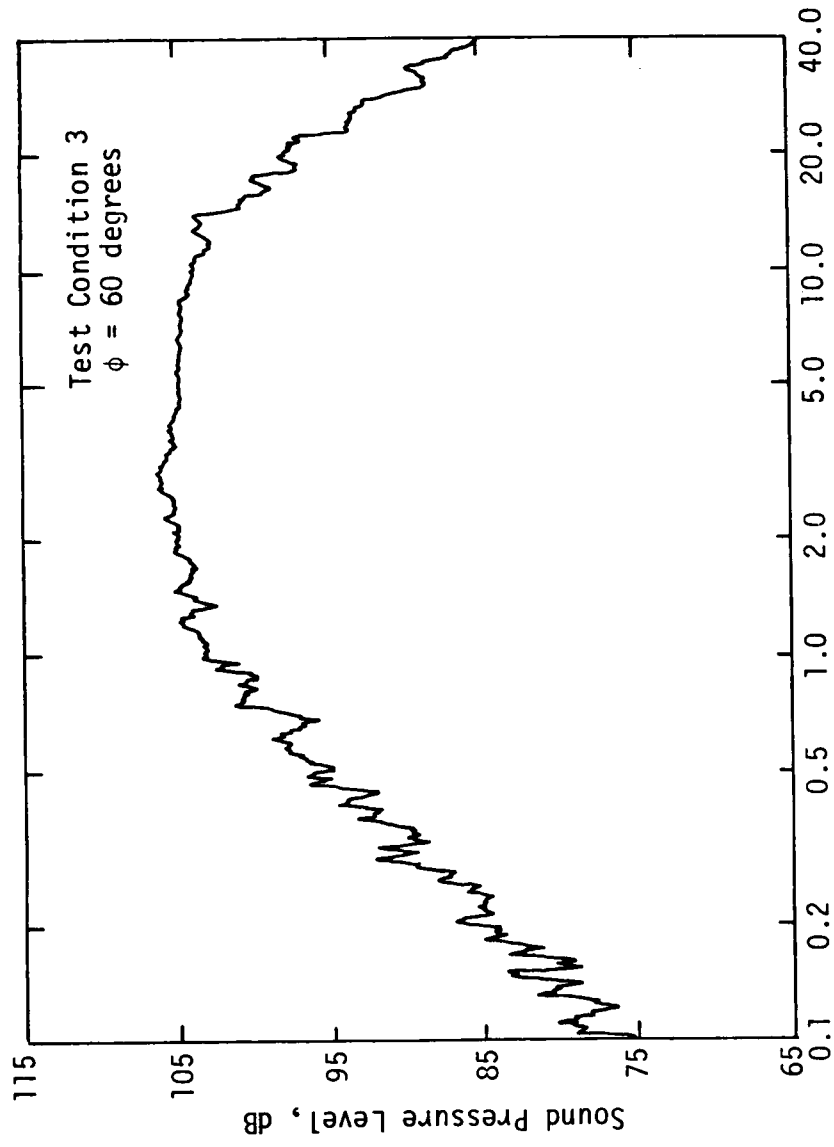

Figure 5. Far field spectrum for Test Condition 3 at ϕ = 60 degrees.

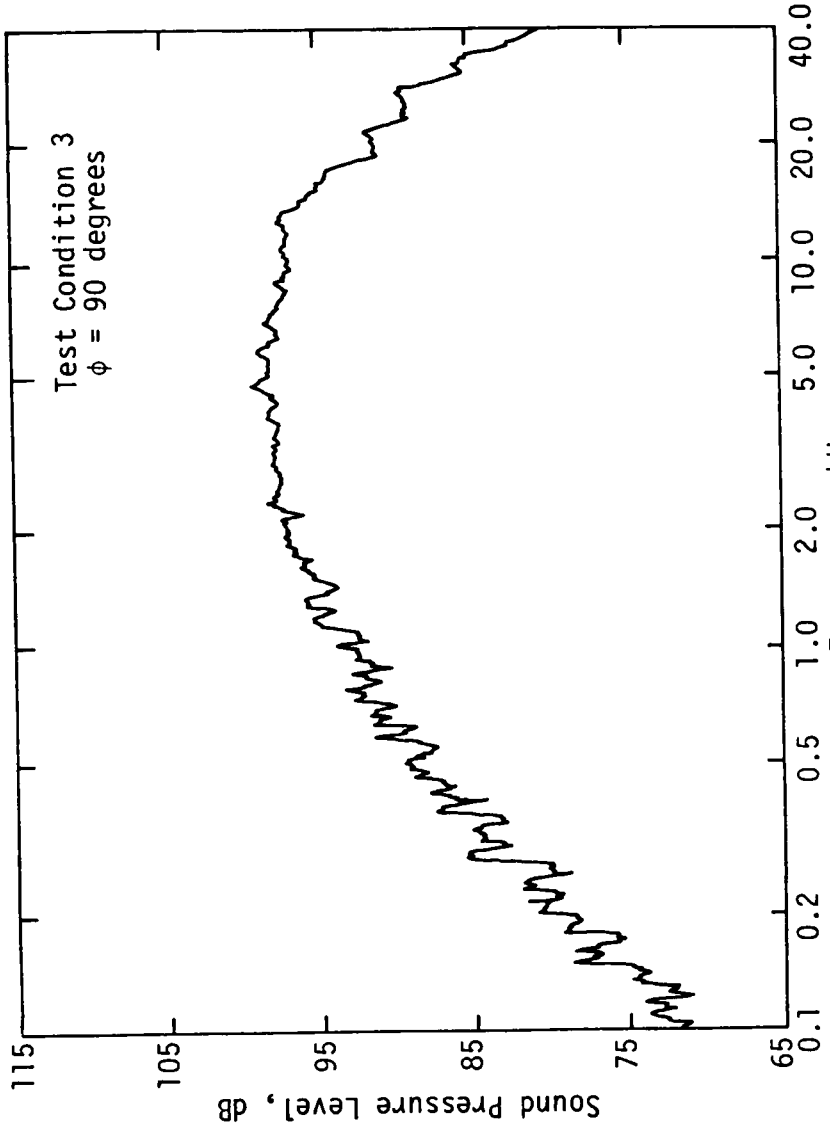

Figure 6. Far field spectrum for Test Condition 3 at ϕ = 90 degrees.

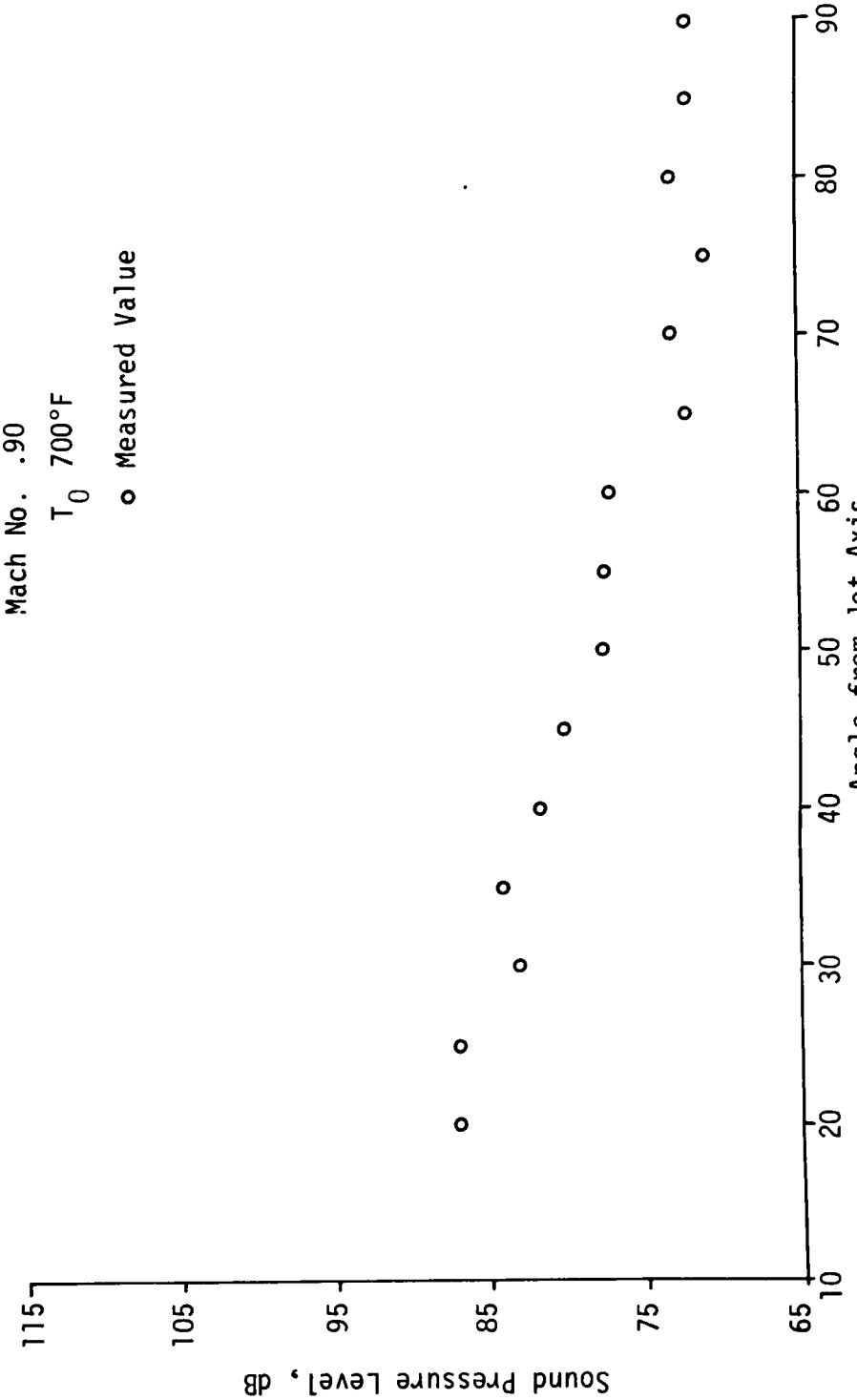

Figure 7. One-third octave far field directivity for a center frequency of 100 Hz (Test Condition 3).

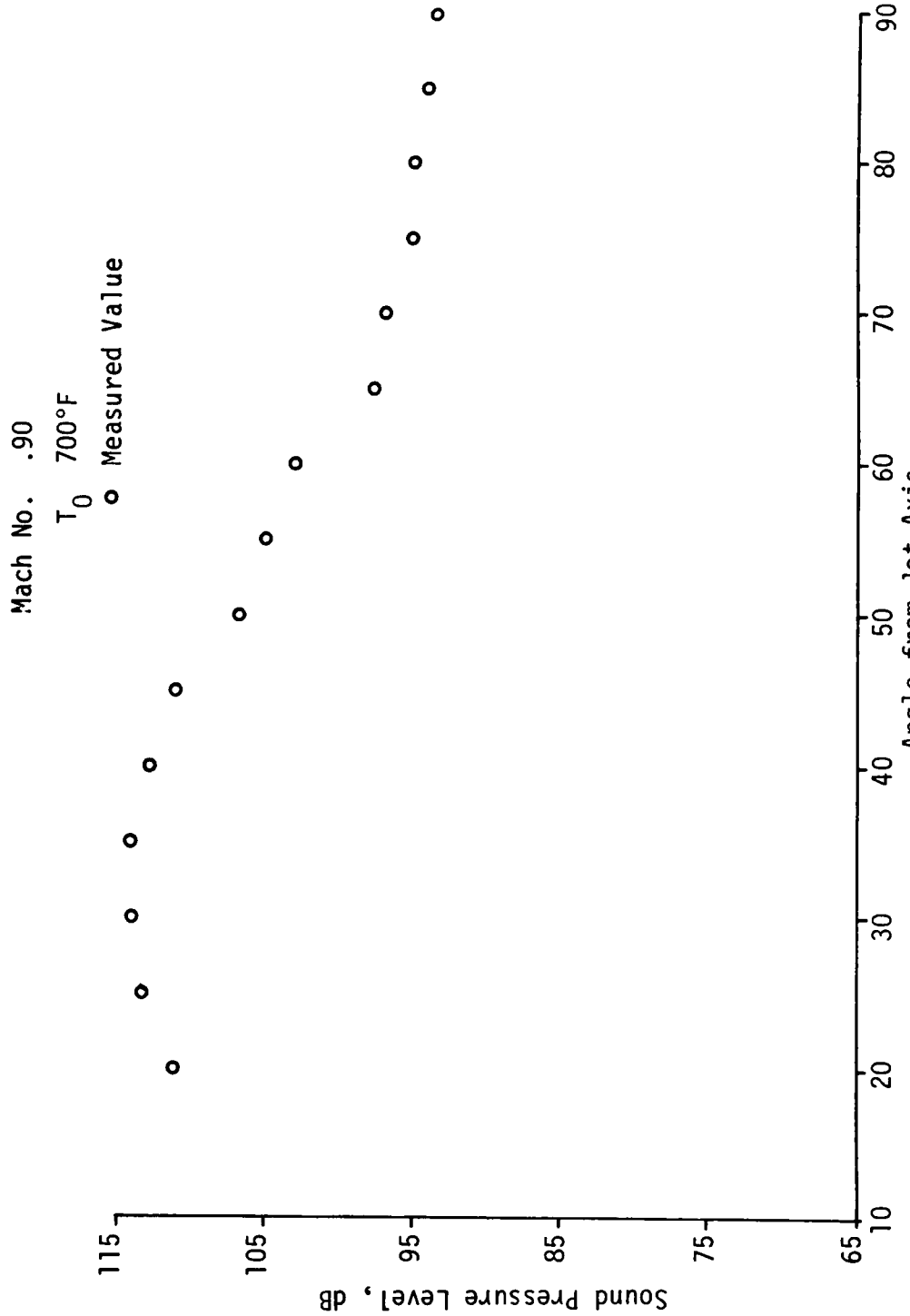

Figure 8. One-third octave far field directivity for a center frequency of 1,000 Hz (Test Condition 3).

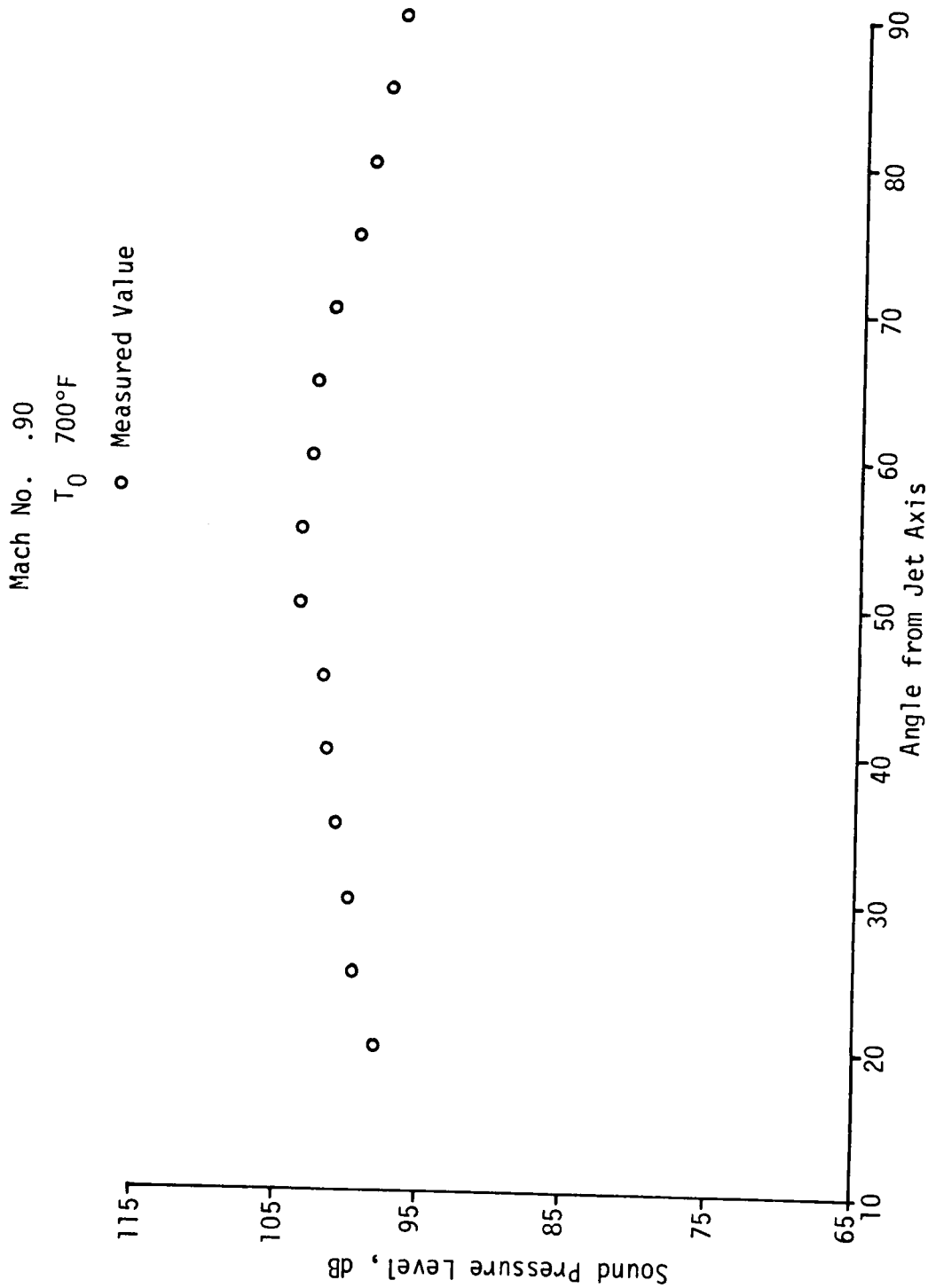

Figure 9. One-third octave far field directivity for a center frequency of 10,000 Hz (Test Condition 3).

Data such as shown in Figs. 7, 8, and 9 were used to obtain the strengths of the uncorrelated elementary sources, as described in Chapter III.

Near field data for the test conditions listed in Table 1, page 13, were obtained by readjusting the sweep arm to bring the microphone closer to the center of the nozzle exit plane. Data were obtained in the x_1,x_3 plane for radial distances between 1 and 4 feet at approximately 1-foot intervals. At each radial distance, one-third octave spectra were taken at several angular positions so the radial variation of sound pressure could be plotted for different frequencies and angular orientations. This variation was compared against the far field approximation of $\overline{p^2} \propto 1/R^2$ for acoustic pressure drop. A discussion of this comparison is presented in in Chapter III where, it is felt, it is more relevant.

CHAPTER III

STATIONARY SOURCE MODEL

In this chapter, equations are developed for synthesizing the source region for an axisymmetric turbulent jet, assuming that the true noise sources can be replaced by an equivalent stationary source distribution.

2.1. Multipole Expansion

The sound pressure field produced by a stationary distributed source, $f(x_1, x_2, x_3, t)$, is governed by the nonhomogeneous wave equation,

$$\frac{\partial^2 p}{\partial x_1^2} + \frac{\partial^2 p}{\partial x_2^2} + \frac{\partial^2 p}{\partial x_3^2} - \frac{1}{a_0^2}\frac{\partial^2 p}{\partial t^2} = - f(x_1, x_2, x_3, t) \ . \qquad (3.1)$$

In the absence of any reflecting walls, the free field solution to this equation is given by

$$p(\bar{x},t) = \int_S \frac{f(\bar{y}, t-R/a_o)}{4\pi R} \, d\bar{y} \ , \qquad (3.2)$$

where $\bar{x}$ is the position vector to the field point, $\bar{y}$ is the position vector to a source point, and $R = |\bar{x} - \bar{y}|$. The geometry under consideration is illustrated in Fig. 10. It is assumed that the distributed source is located in the neighborhood of the origin of the coordinate system.

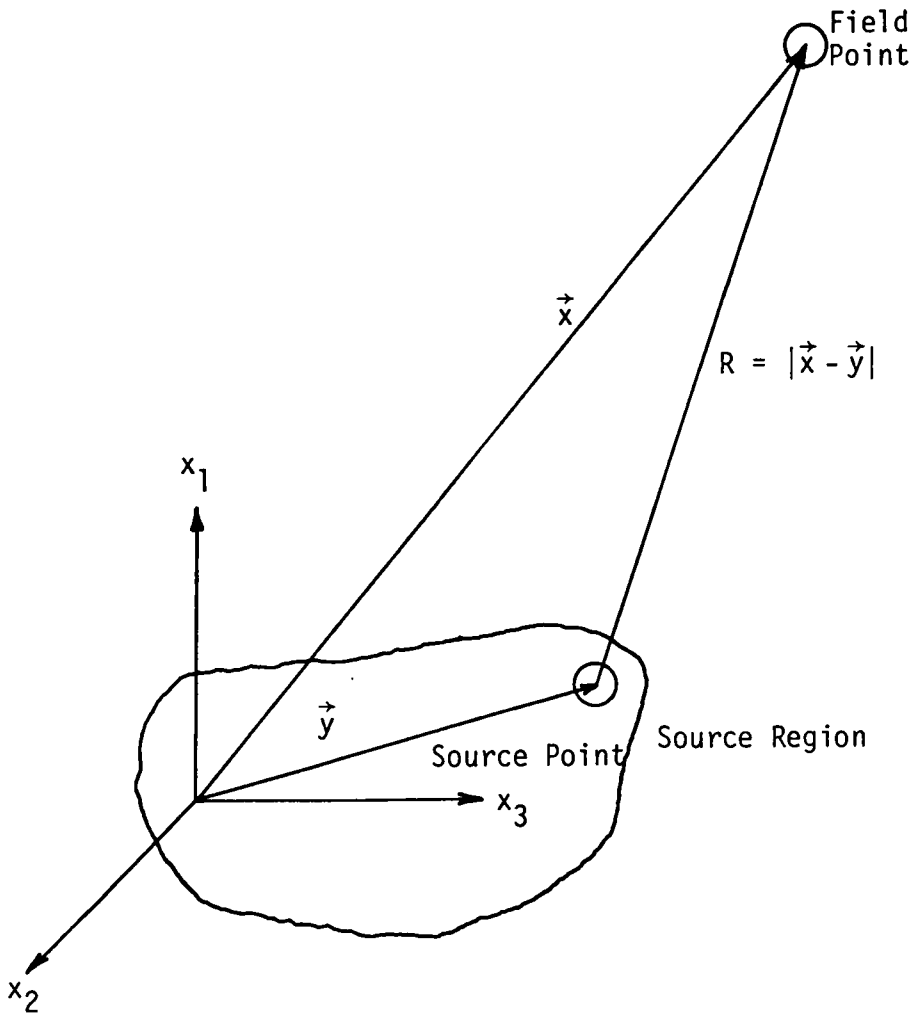

Figure 10. Definition of position vectors for stationary source model.

The integral solution for $p(\bar{x},t)$ is difficult to evaluate because the acoustic source function is an unknown function. It was decided that a multipole expansion technique offered the most promise for evaluating the integral. A sufficiently well-behaved source distribution function in the neighborhood of the origin can be expanded in a Taylor series about the origin. This expansion leads to a series solution for the sound pressure field of the form [8]:

$$p(\bar{x},t) = \sum_{j,k,\ell=0}^{\infty} \frac{\partial^{j+k+\ell}}{\partial x_1^j \, \partial x_2^k \, \partial x_3^\ell} \frac{(-1)^{j+k+\ell}}{4\pi x} m_{jk\ell}\left(t - \frac{x}{a_o}\right) , \qquad (3.3)$$

where,

$$m_{jk\ell}(t) = \int_S \frac{y_1^j \, y_2^k \, y_3^\ell}{j! \; k! \; \ell!} f(\bar{y},t) d\bar{y} \qquad (3.4)$$

are called the multipole moments of the expansion. The multipole moments can be computed for a specified source distribution, or they can be treated as adjustable constants to synthesize a sound source with certain far field characteristics. The multipole expansion, in effect, replaces the distributed source by an infinite combination of elementary point sources located at the origin of the coordinate system. The leading term of Eq. (3.3) where $j = k = \ell = 0$ represents a monopole source with sound pressure field

$$p_m = \frac{1}{4\pi x} m_{000}\left(t - x/a_o\right) . \qquad (3.5)$$

The next three terms of the series in the $j + k + \ell = 1$ correspond to dipole sources with sound pressure fields,

$$p_{d_1} = -\frac{\partial}{\partial x_1}\left[\frac{m_{100}(t - x/a_o)}{4\pi x}\right]$$

$$p_{d_2} = -\frac{\partial}{\partial x_2}\left[\frac{m_{010}(t - x/a_o)}{4\pi x}\right] . \qquad (3.6)$$

$$p_{d_3} = -\frac{\partial}{\partial x_3}\left[\frac{m_{001}(t - x/a_o)}{4\pi x}\right]$$

The six terms corresponding to $j + k + \ell = 2$ are known as quadrupole terms, and the ten terms with $j + k + \ell = 3$ are known as octupole terms. In general, terms with $j + k + \ell = n$ correspond to multipoles of order 2^n.

During the initial phase of the theoretical modeling it was assumed that the source region had a harmonic time dependence and that all parts of the source region are oscillating in phase, at a single frequency. Under this assumption, the source function can be written as,

$$f(\bar{y},t) = F(\bar{y})e^{i\omega t} . \qquad (3.7)$$

The multipole moments can then be written as,

$$m_{jk\ell} = M_{jk\ell}\, e^{i\omega t} ,$$

where,

$$M_{jk\ell} = \int_S y_1^j\, y_2^k\, y_3^\ell\, F(\bar{y})\, d\bar{y} .$$

The variations with time can be made more complex by a superpositioning of harmonic sources.

Introducing spherical polar coordinates, as defined in Fig. 3, page 14,

$$\frac{x_1}{x} = \cos\theta\cdot\sin\phi \ ,$$

$$\frac{x_2}{x} = \sin\theta\cdot\sin\phi \ ,$$

$$\frac{x_3}{x} = \cos\phi \ .$$

The multipole expansion for the acoustic pressure field can then be written as,

$$\begin{aligned} p(\bar{x},t) = \Bigg[& M_{000} + ik\cos\phi\, M_{001}\,(1 - i/kx) \\ & + k^2 M_{200}\left\{\sin^2\phi\left(-1 + \frac{3i}{kx} + \frac{3}{(kx)^2}\right) - \frac{2i}{kx} - \frac{2}{(kx)^2}\right\} \\ & + k^2 M_{002}\left\{\cos^2\phi\left(-1 + \frac{3i}{kx} + \frac{3}{(kx)^2}\right) - \frac{i}{kx} - \frac{1}{(kx)^2}\right\} \\ & + k^3 M_{201}\left\{\sin^2\phi\cos\phi\left(-i - \frac{6}{kx} + \frac{15i}{(kx)^2} + \frac{15}{(kx)^3}\right)\right. \\ & \quad \left. + \cos\phi\left(+\frac{2}{kx} - \frac{6i}{(kx)^2} - \frac{6}{(kx)^3}\right)\right\} \\ & + K^3 M_{003}\left\{\cos^3\phi\left(-i - \frac{6}{kx} + \frac{15i}{(kx)^2} + \frac{15}{(kx)^3}\right)\right. \\ & \quad \left. + \cos\phi\left(\frac{3}{kx} - \frac{9i}{(kx)^2} - \frac{9}{(kx)^3}\right)\right\}\Bigg] \ \frac{e^{i\omega(t - x/a_o)}}{4\pi x} \ , \end{aligned} \tag{3.8}$$

where,

$$k = \omega/a_o = 2\pi/\lambda$$

is called the wave number.

The $1/(kx)$ and higher powers of this term in the above equation determines the contribution of near field effect in the expression for $p(\bar{x},t)$. As $k\bar{x} = 2\pi x/\lambda$ becomes much larger than unity, the near field effects tend to be of less importance. The simplified expression for far field sound pressure field can result through an increase in x (observer at a great distance from the source region) or through a decrease in the wavelength, λ (as the source frequency under consideration increases). That the definition of near field and far field of a source region is dependent on the source frequency under consideration is evident from this, because, it is the number of wavelengths by which an observer is removed from the source, that determines whether he is in the far field or near field and not the actual distance, x. For $kx >> 1$, the far field approximation of Eq. (3.8) becomes

$$p(\bar{x},t) = \left(M_{000} + M_{001}\ ik\cos\phi - M_{200}\ k^2 \sin^2\phi - M_{002}\ k^2 \cos^2\phi \right.$$
$$\left. - M_{201}\ ik^3 \sin^2\phi\cos\phi - M_{003}\ ik^3 \cos^3\phi \right) \frac{e^{i\omega(t-x/a_o)}}{4\pi x} \quad . \quad (3.9)$$

The mean square pressure in the far field is obtained by taking the sum of squares of the real and imaginary parts of Eq. (3.9),

$$\overline{p^2} = \left(\frac{M_{000}}{4\pi x} - \frac{M_{200}}{4\pi x} k^2 \sin^2\phi - M_{002} k^2 \cos^2\phi \right)^2 + \left(\frac{M_{001}}{4\pi x} k \cos\phi - \frac{M_{201}}{4\pi x} k^3 \sin^2\phi \cos\phi - \frac{M_{003}}{4\pi x} k^3 \cos^3\phi \right)^2 . \quad (3.10)$$

In order to better understand the relative importance of various terms of the multipole expansion series, a cylindrical source region whose strength decreases in the axial direction was assumed and calculations for mean square pressures were carried out.

The source distribution assumed was,

$$f(\bar{y},t) = f(r,Z,t) = C\left(1 - \frac{Z}{L}\right)e^{i\omega t} \begin{cases} r \le a \\ 0 < Z \le L \end{cases}$$

$$= 0 \qquad \begin{cases} r > a \\ Z < 0,\ Z > L \end{cases} , \quad (3.11)$$

where r,Z are cylindrical coordinates and Z being the axis of symmetry, a is the radius of the source region, and L its length. The calculations were carried out for a = 0.5. The strength of the source region, C, was assumed to be inversely proportional to L, so that monopole moment was constant at unity for all calculations.

Given,

$$F(y) = F(r,Z) = C(1 - Z/L) ,$$

the coefficients of the multipole moments, $M_{jk\ell}$ when evaluated, yield,

$$
\begin{aligned}
M_{000} &= \frac{CL}{2}\pi a^2 = M \\
M_{001} &= \frac{CL^2}{6}\pi a^2 = \frac{ML}{3} \\
M_{200} &= \frac{CL}{16}\pi a^4 = \frac{Ma^2}{8} \\
M_{002} &= \frac{CL^3}{24}\pi a^2 = \frac{ML^2}{12} \\
M_{201} &= \frac{CL^2}{48}\pi a^4 = \frac{MLa^2}{24} \\
M_{003} &= \frac{CL^4}{120}\pi a^2 = \frac{ML^3}{60}
\end{aligned}
\qquad (3.12)
$$

It is clear from the form of the multipole expansion given in Eq. (3.9) and the multipole moments given in Eq. (3.12) that, the higher order terms of the expansion become increasingly important as L increases and as the frequency, ω, increases. This tendency is displayed in Fig. 11 for far field sound pressure levels. In Fig. 11, for L/D = 0.5, where D is the diameter of the source region, the sound pressure level is nearly independent of radiation angle, indicating that the monopole term is dominant in that expansion. As the length of the source region increases, the directivity is increasingly distorted by the contribution of the higher order terms.

Figure 12 shows the comparison between the "exact solution" and the far field approximation. The dashed lines in this figure represent the far field approximation where the sound pressure level is reduced by 6 dB each time the distance from the source is doubled. The individual points of the figure represent the calculated values,

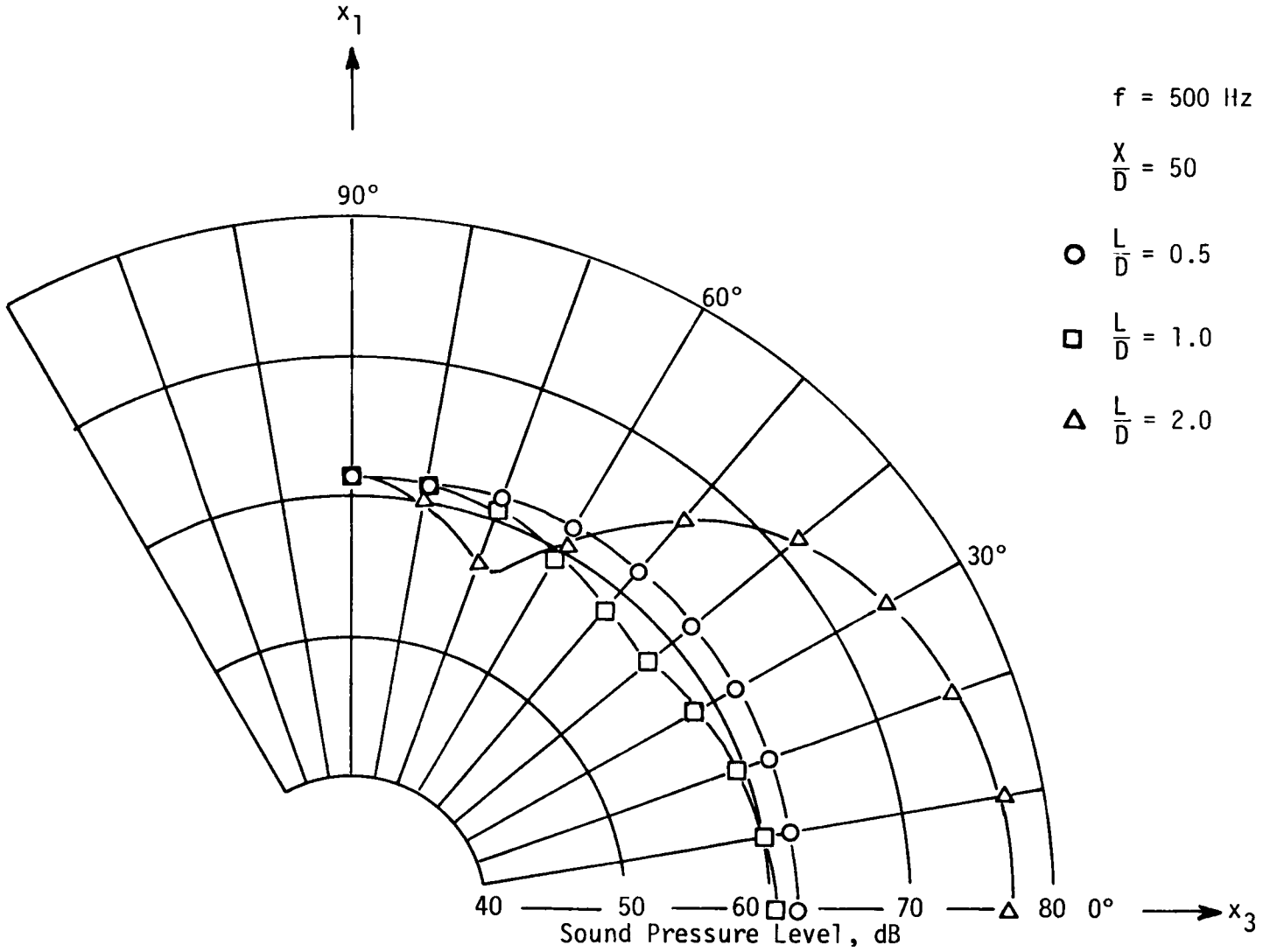

Figure 11. Far field sound pressure directivity for different lengths of source region.

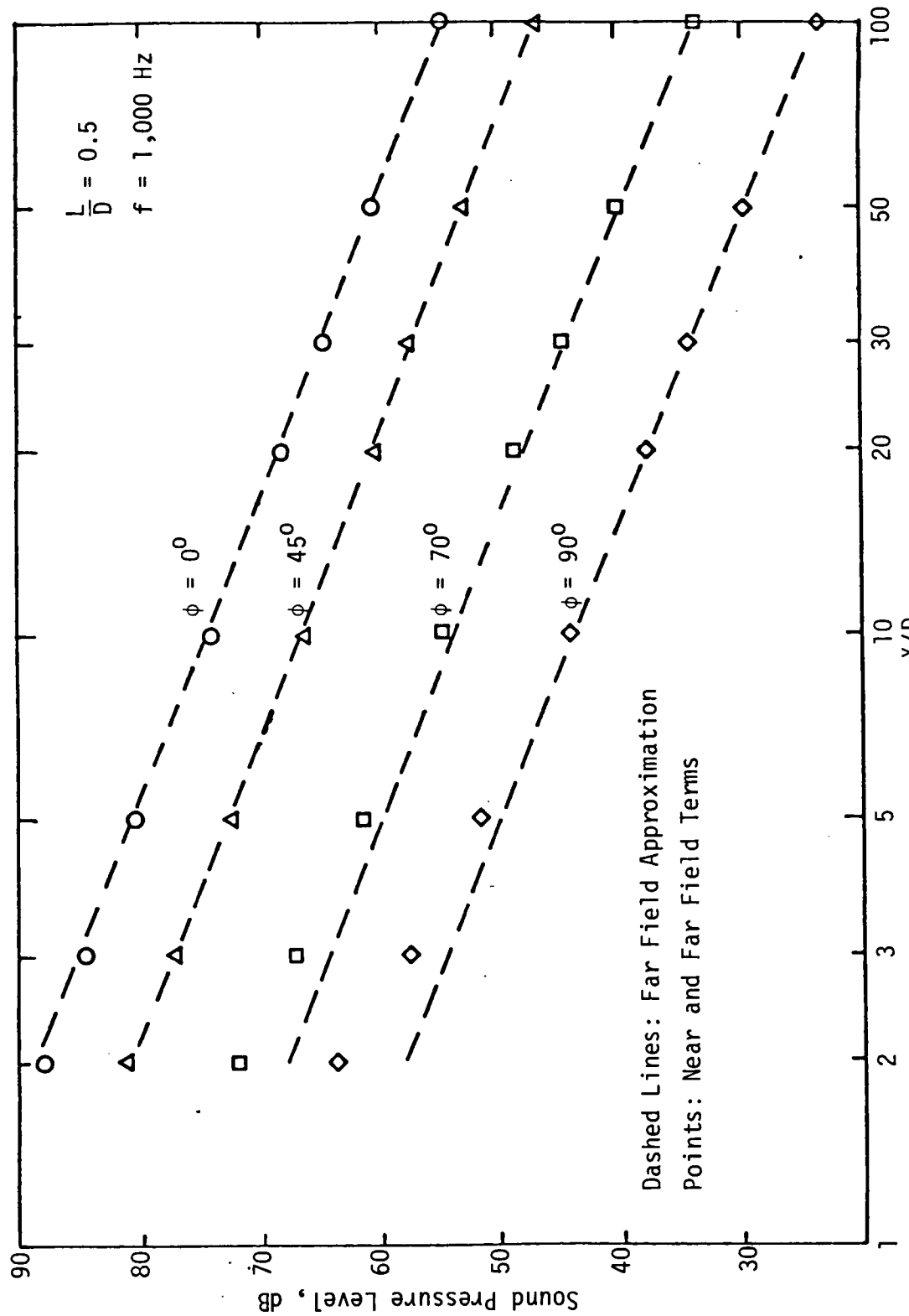

Figure 12. Radial variation of sound pressure levels showing effect of near field terms.

including the near field terms. For radiation angles less than 45 degrees, there is very little difference between the "exact solution" and the far field approximation down to x/D = 2.0. At ϕ = 90 degrees the difference is 6 dB for x/D = 2.0, indicating that the near field terms contribute approximately the same amount to the sound field as the far field terms.

The calculations and results discussed above for the assumed source distributions serve the purpose of only demonstrating the behavior of the multipole expansion technique. The far field sound radiated does not display the features characteristic of aerodynamic noise, as the criteria used in selecting the source distribution function was to obtain simple analytical expressions for multipole moments and does not represent the source distribution that would exist in an actual flow.

3.2. Combination of Uncorrelated Sources

Considering the source region as the axisymmetric turbulent jet flow from a circular nozzle, the sound field produced by this source distribution should possess axial geometry. Thus, in the nonhomogeneous wave equation (Eq. (3.1)), the source distribution for a particular frequency was assumed to have the form,

$$f(\bar{y},t) = F(r,y_3)e^{i\omega t} , \tag{3.13}$$

where,

$$r^2 = y_1^2 + y_2^2 .$$

With this assumption, many of the multipole moments associated with the source distribution were found to be zero. In particular, the dipole moments, M_{100} and M_{010}, were zero, and the dipole contribution to the sound pressure field becomes (see Eq. (3.8)):

$$p_d = \frac{ik \cos\phi \, M_{001}}{4\pi x} \left(1 - \frac{i}{kx}\right) e^{i\omega(t - x/a_o)} .$$

This pressure field was added to that for the monopole and surviving higher order poles to produce a sound field that is axially symmetric.

Further reflection, however, revealed that the assumptions made in writing Eq. (3.8) are much too restrictive. The acoustic sources in a jet flow are directly related to the flow turbulence and are random in nature. Thus, while the acoustic source distribution may be axially symmetric with respect to the average amplitude, it is probably not axisymmetric on an instantaneous basis with respect to amplitude and phase, as was assumed. Said another way, it appears that the acoustic source distribution for an axisymmetric jet cannot be modeled adequately by an axisymmetric source region oscillating in phase.

A second method that appeared more realistic was to model the source with an assemblage of uncorrelated elementary sources (monopole, dipole, etc.). These sources can be combined in such a way as to produce a sound field that is axisymmetric with respect to mean square pressure. This technique has been used by Mani et al. [9] to model the source distribution for a small circular jet in an open-jet wind tunnel.

To illustrate this approach, consider the contribution due only to dipole radiation. In the general multipole expansion for a nonsymmetric source distribution there arise three dipole terms, each corresponding to a dipole with its axis aligned along one of the coordinate directions. The acoustic pressures associated with these dipoles are:

$$p_{d_1}(\bar{x},t) = \frac{ik \sin\phi \cos\theta \, M_{100}}{4\pi x}\left(1 - \frac{i}{kx}\right) e^{i\omega(t - x/a_o)}$$

$$p_{d_2}(\bar{x},t) = \frac{ik \sin\phi \sin\theta \, M_{010}}{4\pi x}\left(1 - \frac{i}{kx}\right) e^{i\omega(t - x/a_o)} . \qquad (3.14)$$

$$p_{d_3}(\bar{x},t) = \frac{ik \cos\phi \, M_{001}}{4\pi x}\left(1 - \frac{i}{kx}\right) e^{i\omega(t - x/a_o)}$$

If it is assumed that these three dipoles are uncorrelated, these acoustic pressures add in a mean square sense so that the mean square of the acoustic pressure contributed by the dipoles alone is,

$$\overline{p_d^2} = \overline{p_{d_1}^2} + \overline{p_{d_2}^2} + \overline{p_{d_3}^2}$$

$$= \frac{k^2}{(4\pi x)^2}\left[1 + \frac{1}{(kx)^2}\right]\left(M_{100}^2 \sin^2\phi \cos^2\theta + M_{010}^2 \sin^2\phi \sin^2\theta + M_{001}^2 \cos^2\phi\right) . \qquad (3.15)$$

The sound field given by this equation is not symmetric about the jet axis for arbitrary values of dipole moments. However, if the strengths of the x_1 and x_2 dipoles are the same so that $M_{100} = M_{010}$, the dependence on azimuthal angle, θ, disappears, yielding

$$\overline{p_d^2} = \frac{k^2}{(4\pi x)^2}\left[1+\frac{1}{(kx)^2}\right]\left(M_{100}^2 \sin^2\phi + M_{001}^2 \cos^2\phi\right) . \qquad (3.16)$$

The corresponding far field expression will be,

$$\overline{p_d^2} = \frac{k^2}{(4\pi x)^2}\left(M_{100}^2 \sin^2\phi + M_{001}^2 \cos^2\phi\right) . \qquad (3.17a)$$

Similarly, the far field approximation for mean square pressures for monopole, quadrupole, and octupole singularities can be written as,

Monopole:

$$\overline{p_m^2} = \frac{M_{000}^2}{(4\pi x)^2}$$

Quadrupole:

$$\overline{p_q^2} = \frac{k^4}{(4\pi x)^2}\left[M_{200}^2 \sin^4\phi + M_{110}^2 \sin^2\phi \cos^2\phi + M_{002}^2 \cos^4\phi\right] \qquad (3.17b)$$

Octupole:

$$\overline{p_o^2} = \frac{k^6}{(4\pi x)^2}\left[M_{030}^2 \sin^6\phi + M_{021}^2 \sin^4\phi \cos^2\phi + M_{012}^2 \sin^2\phi \cos^4\phi + M_{003}^2 \cos^6\phi\right]$$

The total mean square pressure is obtained by combining the contributions of the above singularities, assuming that they are uncorrelated,

$$\overline{p^2} = \overline{p_m^2} + \overline{p_d^2} + \overline{p_q^2} + \overline{p_o^2} .$$

3.3. Uniqueness Condition

In the source synthesis procedure, constants, M^2_{000}, M^2_{100}, M^2_{001}, and so forth, are determined by a least-squares technique to best fit the far field sound pressure data at a particular frequency. The constants, however, are not uniquely determined by the least-squares fit. To illustrate this, suppose the far field sound pressure at some frequency is given accurately by the combination of monopole and two dipoles. Then,

$$\overline{p^2} = \frac{M^2_{000}}{(4\pi x)^2} + \frac{k^2}{(4\pi x)^2}\left[M^2_{100}\sin^2\phi + M^2_{001}\cos^2\phi\right] ; \qquad (3.18)$$

by using the identity, $\sin^2\phi + \cos^2\phi = 1$, this can be rewritten as,

$$\overline{p^2} = \frac{k^2}{(4\pi x)^2}\left[M^{*2}_{100}\sin^2\phi + M^{*2}_{001}\cos^2\phi\right] , \qquad (3.19)$$

where,

$$M^{*2}_{100} = M^2_{100} + \frac{M^2_{000}}{k^2} ,$$

$$M^{*2}_{001} = M^2_{001} + \frac{M^2_{000}}{k^2} .$$

Similarly, if $M^2_{001} > M^2_{100}$, the mean square pressure can be written as,

$$\overline{p^2} = \frac{M'^2_{000}}{(4\pi x)^2} + \frac{k^2}{(4\pi x)^2} M'^2_{001}\cos^2\phi , \qquad (3.20)$$

where,

$$M'^2_{001} = M^2_{001} - M^2_{100} ,$$

$$M'^2_{000} = M^2_{000} + k^2 M^2_{100} .$$

While these three expressions give the same sound pressure in the far-field, the near field pressures are not the same because the near field terms are different for a monopole and a dipole.

In order to uniquely determine the multipole moments, an additional condition is imposed based on the intuitive concept that the lower order singularities should have their maximum possible strength. Using this condition in the example above specifies Eq. (3.20), since M'_{000} in that equation is the largest possible monopole moment.

Carrying this a step further, suppose the far field sound pressure is expressed accurately in terms of a combination of quadrupoles,

$$\overline{p^2} = Q_1 \sin^4\phi + Q_2 \sin^2\phi \cos^2\phi + Q_3 \cos^4\phi , \qquad (3.21)$$

where,

$$Q_1 = \frac{k^4 M_{200}}{(4\pi x)^2} , \quad Q_2 = \frac{k^4 M_{110}}{(4\pi x)^2} , \quad Q_3 = \frac{k^4 M_{002}}{(4\pi x)^2} .$$

The identity, $\sin^4\phi + 2 \sin^2\phi \cos^2\phi + \cos^4\phi = 1$, can be used to extract the largest embedded monopole. Let,

$$P_1 = \min (Q_1, Q_2/2, Q_3) = \frac{M_{000}^2}{(4\pi x)^2}$$

and redefining,

$$Q_1' = Q_1 - P_1 ,$$

$$Q_2' = Q_2 - 2P_1 ,$$

$$Q_3' = Q_3 - P_1 .$$

Now the mean square pressure can be written as,

$$\overline{p^2} = P_1 + Q_1' \sin^4\phi + Q_2' \sin^2\phi \cos^2\phi + Q_3' \cos^4\phi . \qquad (3.22)$$

Now using the identity $\sin^2 + \cos^2 = 1$, to remove the embedded dipoles, let

$$D_1 = \min (Q_1', Q_2') = \frac{k^2 M_{100}^2}{(4\pi x)^2} ,$$

and redefining,

$$Q_1'' = Q_1' - D_1 ,$$

$$Q_2'' = Q_2' - D_1 ,$$

$$Q_3'' = Q_3' ;$$

again, defining,

$$D_2 = \min (Q_2'', Q_3'') = \frac{k^2 M_{001}^2}{(4\pi x)^2} ;$$

leading to,

$$Q_1''' = Q_1'' ,$$

$$Q_2''' = Q_2'' - D_2 ,$$

$$Q_3''' = Q_3'' - D_2 .$$

This gives the least singular representation for the source region,

$$\overline{p^2} = P_1 + D_1 \sin^2\phi + D_2 \cos^2\phi + Q_1''' \sin^4\phi + Q_2''' \sin^2\phi \cos^2\phi + Q_3''' \sin^4\phi . \qquad (3.23)$$

The above procedure has been extended to octupole level to determine the least singular multipole moments corresponding to a far field sound pressure distribution.

3.4. Source Synthesis for Jet Flow

From the one-third octave spectra measurements for the circular jet, narrow band sound pressure level directivity patterns were constructed and used to determine multipole moments for the uncorrelated singularities. In carrying out this procedure, the sound pressure level values were converted to mean square pressure values by the relation,

$$\overline{p^2} = p_{ref}^2 \, 10^{SPL/10} ,$$

where,

$$\overline{p^2_{ref}} = 2\times10^{-5}\ N/m^2 \ .$$

The coefficients, A_1, A_2, A_3, and A_4, of uncorrelated octupoles were then determined to best fit the mean square pressure values, which are given by,

$$\overline{p^2} = A_1 \sin^6\phi + A_2 \sin^4\phi \cos^2\phi + A_3 \sin^2\phi \cos^4\phi + A_4 \cos^6\phi \ , \quad (3.24)$$

where,

$$A_1 = \frac{k^6 M^2_{030}}{(4\pi x)^2} \ ,$$

$$A_2 = \frac{k^6 M^2_{021}}{(4\pi x)^2} \ ,$$

$$A_3 = \frac{k^6 M^2_{012}}{(4\pi x)^2} \ ,$$

$$A_4 = \frac{k^6 M^2_{003}}{(4\pi x)^2} \ .$$

It should be noted that the above constants must all be non-negative according to the derivation. Consequently, a simple least-squares procedure cannot be used to determine these quantities. In Reference [10], a constrained least-squares algorithm based on the Kuhn-Tucker theorem is presented. A Fortran subroutine based on this algorithm was adapted to the present problem to determine the values of A_1, A_2, A_3, and A_4 that best fit the measured sound pressure data, subject to the constraint, $A_i \geq 0$.

From the above values of A_i, the embedded monopole, dipoles, quadrupoles, and octupoles were evaluated. These values were used in the evaluation of the mean square pressure calculation. The mean square pressures associated with the monopole, dipole, quadrupole, and octupole type singularities taking into account the near field and far field terms are given below:

Monopole (no near field terms):

$$\overline{p_m^2} = \frac{M_{000}^2}{(4\pi x)^2} , \tag{3.25a}$$

Dipole:

$$\overline{p_d^2} = \frac{k^2}{(4\pi x)^2}\left[1+\frac{1}{(kx)^2}\right]\left(M_{100}^2 \sin^2\phi + M_{001}^2 \cos^2\phi\right) , \tag{3.25b}$$

Quadrupole:

$$\begin{aligned}\overline{p_q^2} = {} & \frac{k^4 M_{200}^2}{(4\pi x)^2}\left[\sin^4\phi+\frac{1}{(kx)^2}\left(3\sin^4\phi-4\sin^2\phi+2\right)\right. \\ & \left. +\frac{1}{(kx)^4}\left(9\sin^4\phi-6\sin^2\phi+2\right)\right] \\ & + \frac{k^4 M_{002}^2}{(4\pi x)^2}\left[\cos^4\phi+\frac{1}{(kx)^2}\left(3\cos^4\phi-4\cos^2\phi+1\right)\right. \\ & \left. +\frac{1}{(kx)^4}\left(9\cos^4\phi-6\cos^2\phi+1\right)\right] \\ & + \frac{k^4 M_{101}^2}{(4\pi x)^2}\sin^2\phi\cos^2\phi\left[1+\frac{3}{(kx)^2}+\frac{9}{(kx)^4}\right] ,\end{aligned} \tag{3.25c}$$

Octupole:

$$\overline{p_0^2} = \frac{k^6 M_{300}^2}{(4\pi x)^2}\left[\sin^6\phi + \frac{6}{(kx)^2}\left(\sin^6\phi - 3\sin^4\phi + 2\sin^2\phi\right)\right.$$

$$+ \frac{1}{(kx)^4}\left(45\sin^6\phi - 72\sin^4\phi + 36\sin^2\phi\right)$$

$$\left. + \frac{1}{(kx)^6}\left(225\sin^6\phi - 270\sin^4\phi + 108\sin^2\phi\right)\right]$$

$$+ \frac{k^6 M_{003}^2}{(4\pi x)^2}\left[\cos^6\phi + \frac{3}{(kx)^2}\left(2\cos^6\phi - 6\cos^4\phi + 3\cos^2\phi\right)\right.$$

$$+ \frac{9}{(kx)^4}\left(5\cos^6\phi - 8\cos^4\phi + 3\cos^2\phi\right)$$

$$\left. + \frac{1}{(kx)^6}\left(225\cos^6\phi - 270\cos^4\phi + 81\cos^2\phi\right)\right]$$

$$+ \frac{k^6 M_{021}^2}{(4\pi x)^2}\left[\sin^4\phi\cos^2\phi + \frac{6\cos^2\phi}{(kx)^2}\left(\sin^4\phi - \sin^2\phi + 2\right)\right.$$

$$+ \frac{3\cos^2\phi}{(kx)^4}\left(15\sin^4\phi - 8\sin^2\phi + 2\right)$$

$$\left. + \frac{9\cos^2\phi}{(kx)^6}\left(25\sin^4\phi - 10\sin^2\phi + 2\right)\right]$$

$$+ \frac{k^6 M_{102}^2}{(4\pi x)^2}\left[\cos^4\phi\sin^2\phi + \frac{\sin^2\phi}{(kx)^2}\left(6\cos^4\phi - 6\cos^2\phi + 1\right)\right.$$

$$+ \frac{3\sin^2\phi}{(kx)^4}\left(15\cos^4\phi - 8\cos^2\phi + 1\right)$$

$$\left. + \frac{9\sin^2\phi}{(kx)^6}\left(25\cos^4\phi - 10\cos^2\phi + 1\right)\right] \quad . \qquad (3.25d)$$

These equations were used in a computer code to evaluate the complete sound field when the wave number, k, and multipole moments, M_{000}, M_{100}, etc., are prescribed.

3.5. Results of Stationary Source Model

In this section, a comparison of the results of the stationary source model with the acoustic data obtained are presented. Figures 13 through 15 illustrate the degree to which the far field directivity patterns can be represented by a combination of uncorrelated singularities through the octupole level.

The curves in these figures were obtained by calculating the mean square pressure using the equation,

$$\overline{p^2} = A_1' \sin^6\phi + A_2' \sin^4\phi \cos^2\phi + A_3' \sin^2\phi \cos^4\phi + A_4' \cos^6\phi \ ,$$

where, A_1', A_2', A_3', and A_4' are the four positive constants selected to give the best fit in least-squares sense to the experimental directivity pattern. The acoustic pressures in these and all other figures are given as sound pressure levels in a decibel scale.

$$SPL = 10 \log_{10} \frac{\overline{p^2}}{p_{ref}^2} \text{ dB} \ ,$$

where,

$$p_{ref} = 2 \times 10^{-5} \text{ N/m}^2 \ .$$

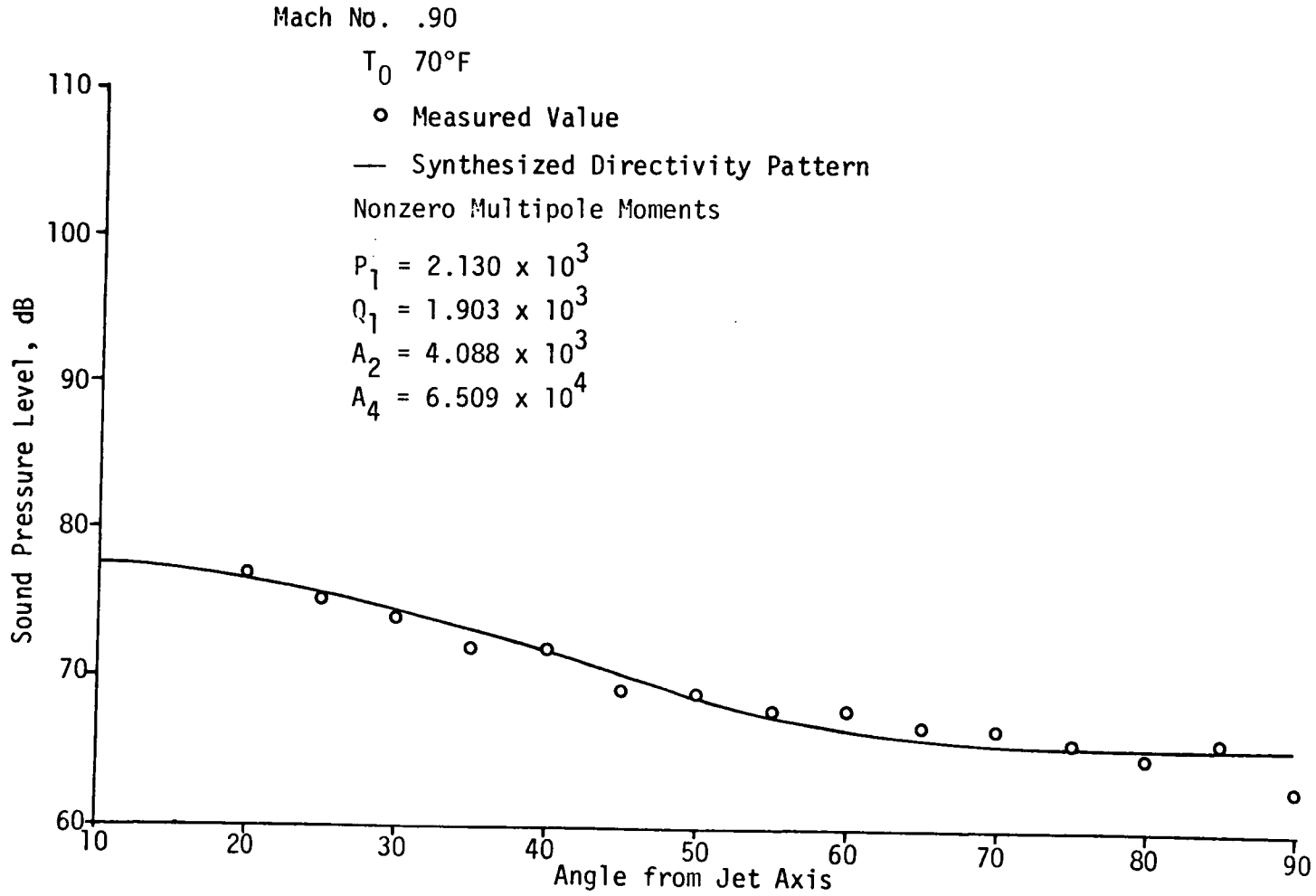

Figure 13. Comparison of measured sound pressure level directivity with least-squares fit for Test Condition 2 at 100 Hz.

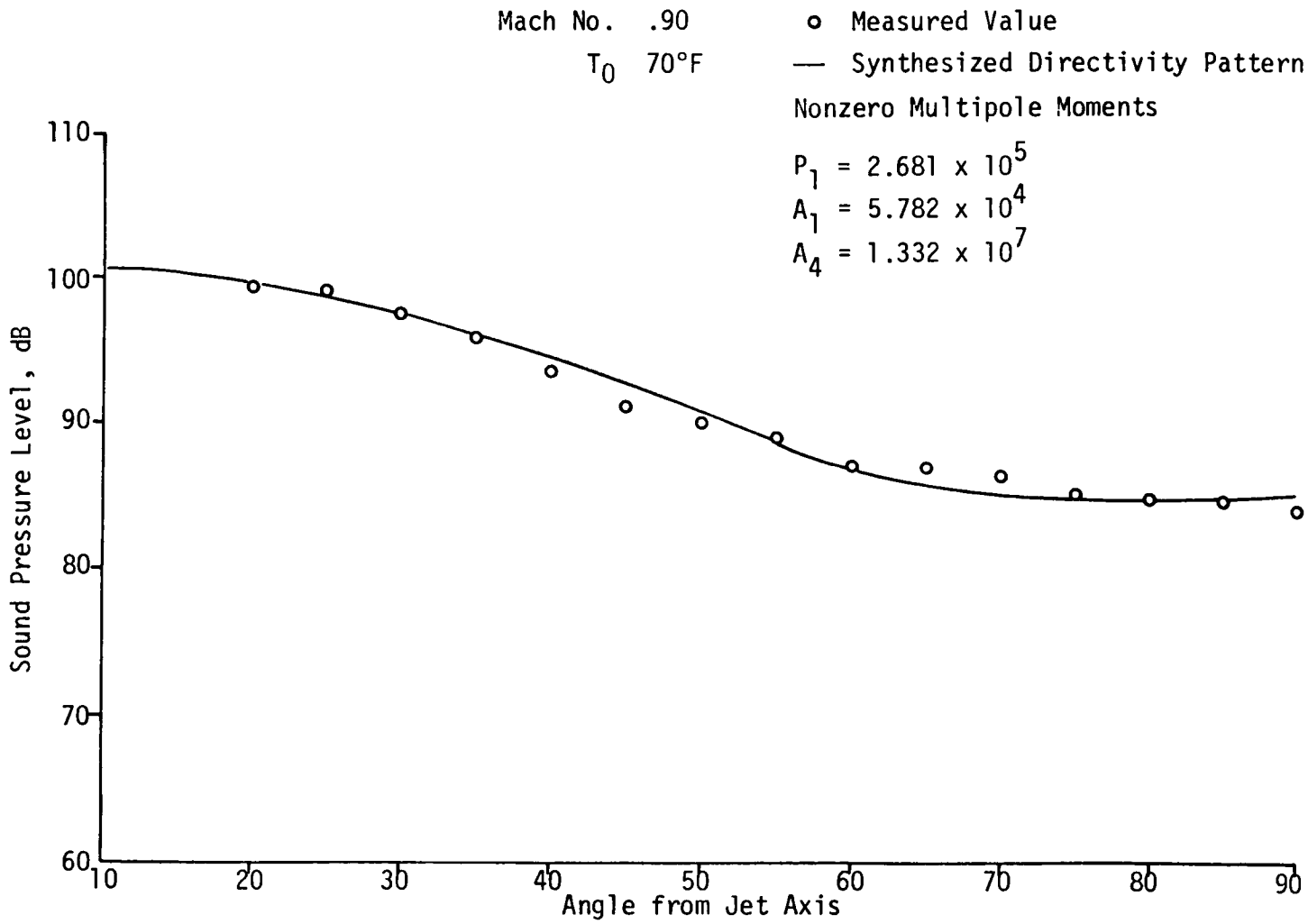

Figure 14. Comparison of measured sound pressure level directivity with least-squares fit for Test Condition 2 at 1,000 Hz.

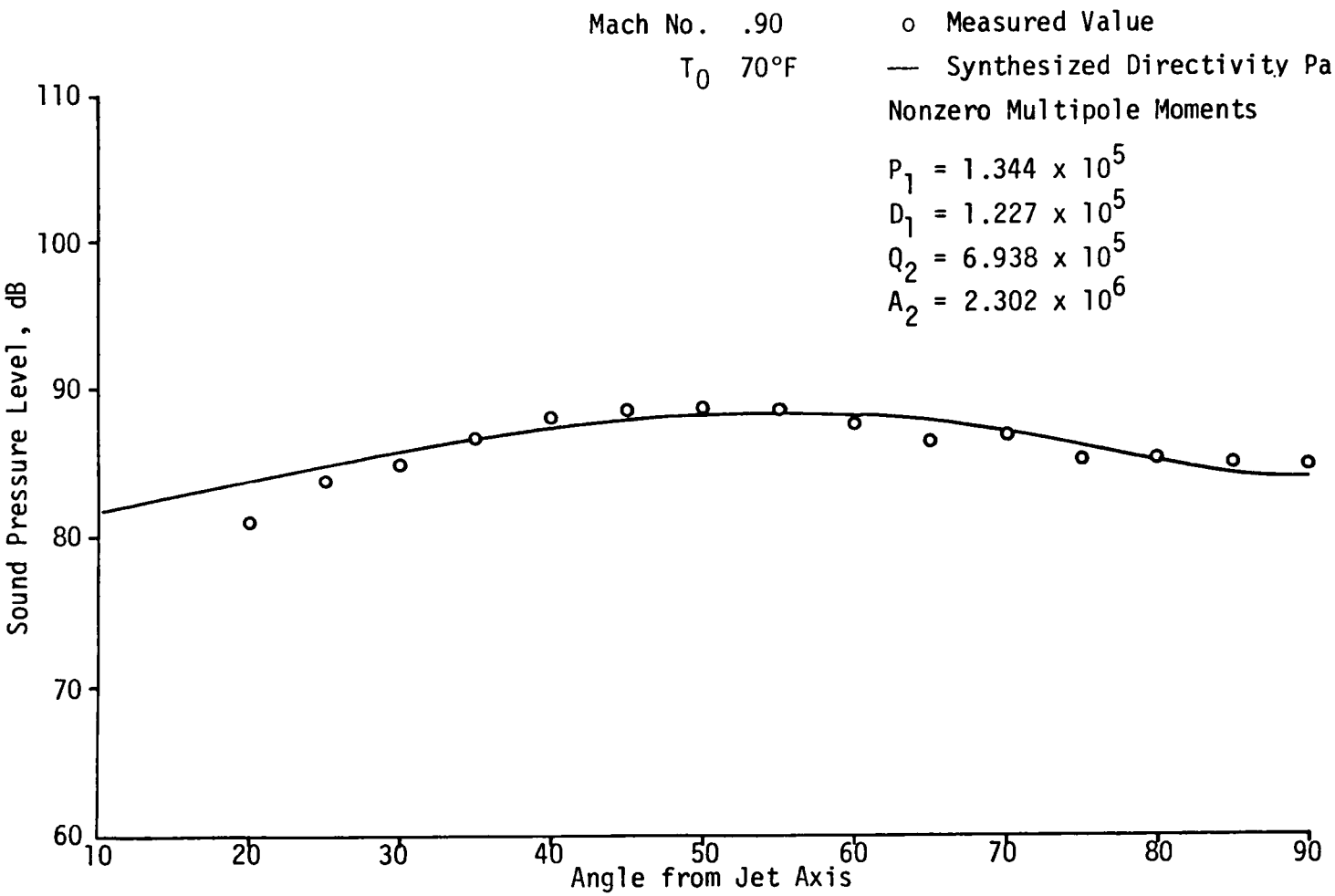

Figure 15. Comparison of measured sound pressure level directivity with least-squares fit for Test Condition 2 at 10,000 Hz.

As explained in Section 3.3, the moments of the largest embedded monopole, P_1, were determined as,

$$P_1 = \min \left[A_1', A_2'/3, A_2'/3, A_4' \right] .$$

The dipole moments, D_1 and D_2; the quadrupole moments, Q_1, Q_2, and Q_3; and the reduced octupole moments, A_1, A_2, A_3, and A_4, were obtained as described earlier. These values are given in the legends of Figs. 13 through 15. Curves similar to those shown in Figs. 13 through 15 were obtained for the four test conditions given in Table 1, page 13, and for the seven frequencies: 100, 200, 500, 1,000, 2,000, 5,000, and 10,000 Hz. For all test conditions and all frequencies considered, the discrepancy between the experimental data and the best fit for the multipole expansion was less than 4 dB.

A comparison of the radial distribution of sound pressure, as computed for the multipole expansion and measured in the experimental program, is presented in Figs. 16 through 18.

Using the coefficients listed in Figs. 13 through 15 in the full multipole expansion, including the near field terms, the sound pressure level was computed along rays emanating from the center of the nozzle exit plane. Examination of the results shown in Figs. 16 through 18 shows that the multipole expansion predicts reasonably well the sound field at high frequencies where the near field terms are of minor importance. As the frequency under consideration decreases and the near field terms in the multipole expansion become increasingly important, the measured and predicted sound pressure

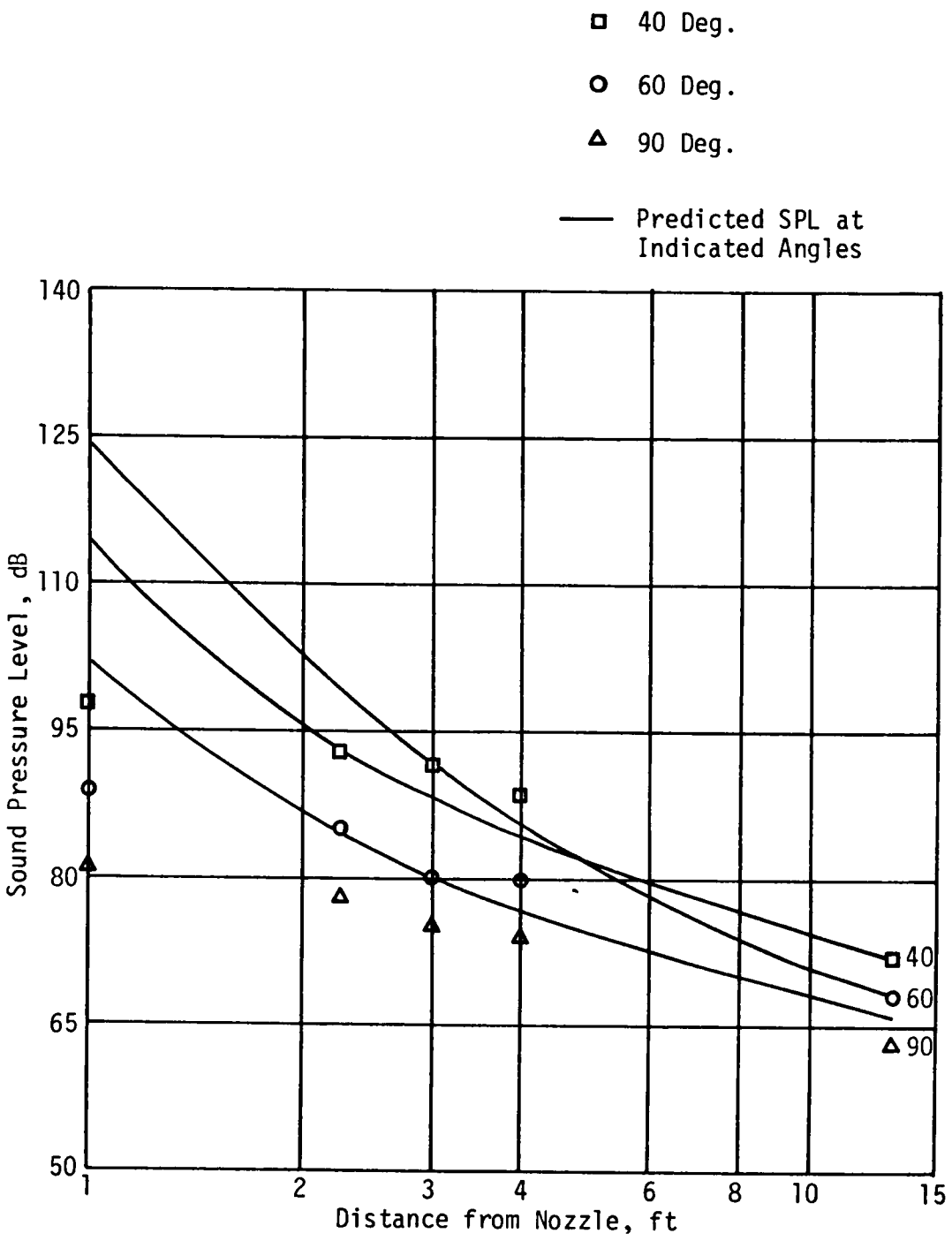

Figure 16. Comparison of measured and predicted sound pressure levels for Test Condition 2 at 100 Hz.

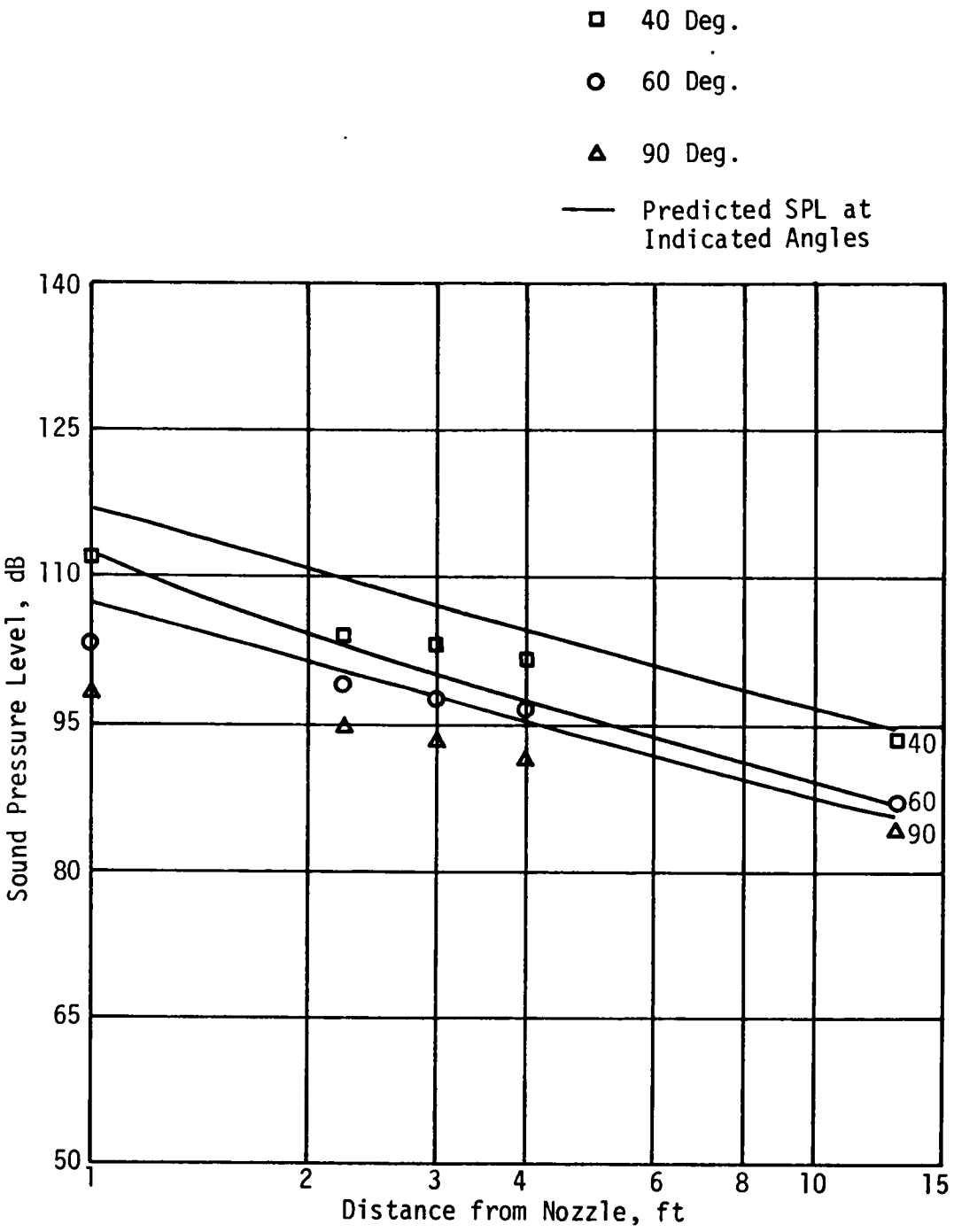

Figure 17. Comparison of measured and predicted sound pressure levels for Test Condition 2 at 1,000 Hz.

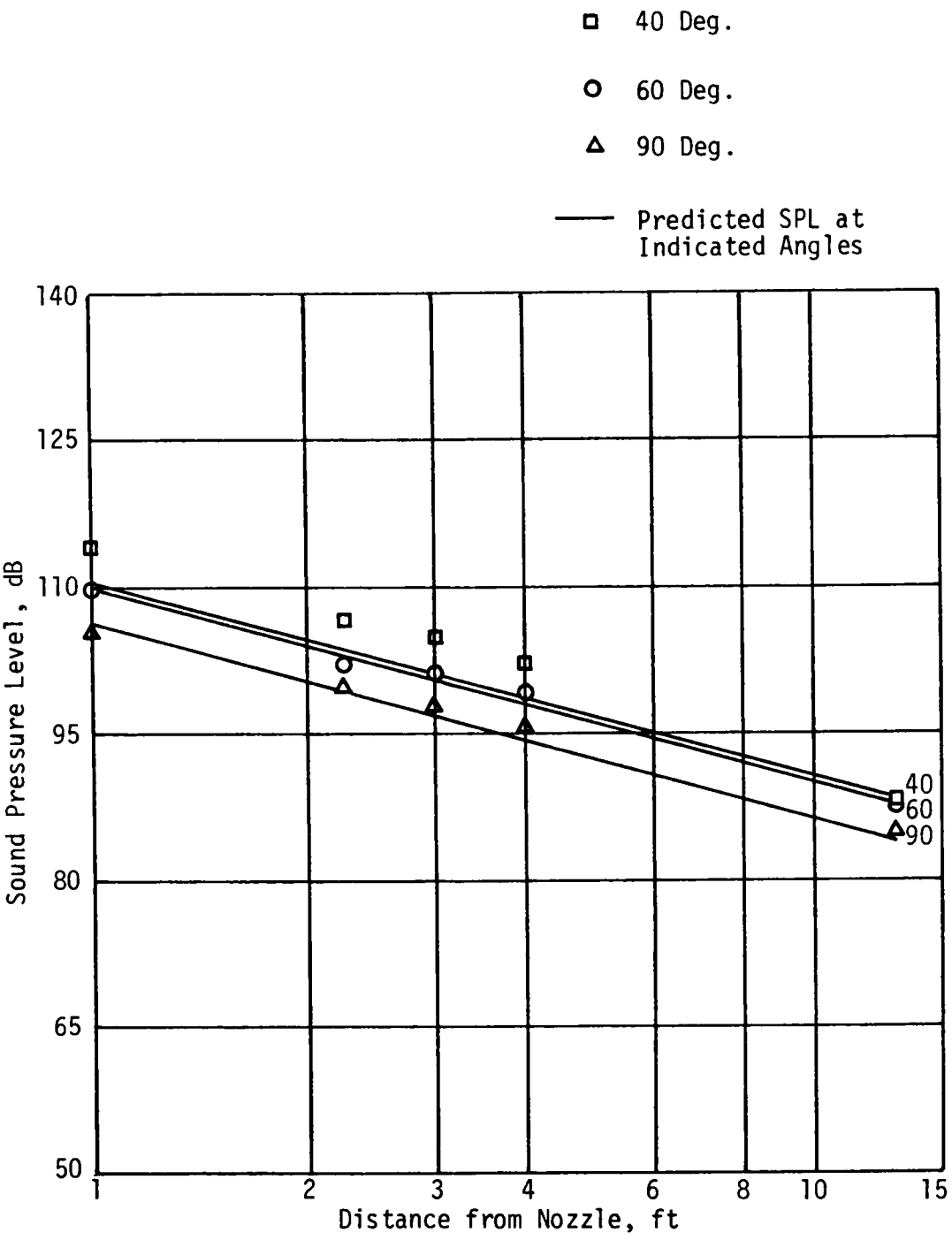

Figure 18. Comparison of measured and predicted sound pressure levels for Test Condition 2 at 10,000 Hz.

values near the jet exhaust diverge. The computed values in almost all the cases are greater than those measured. This trend suggests that the stationary source model is giving too large a near field contribution to the calculated sound field. Referring to Eq. (3.25) shows that importance of the near field terms increases with order of the pole: monopole having no near field terms; dipole's near field terms proportional to $1/(kx)^2 = (\lambda/2\pi x)^2$; the quadrupole near field terms being proportional to $1/(kx)^4$; and for octupole, these terms are of the order $1/(kx)^6$. Thus, the stationary source model is resulting in too great a contribution from the higher order poles. This, in turn, is due to the directionality of the far field sound distribution which can be modeled adequately only with the inclusion of these higher order terms.

Closer examination of the measured radial sound pressure distribution for low frequencies reveals that the mean square sound pressure drops off even more slowly than $\overline{p^2} \propto 1/R^2$ predicted for the far field. This is perhaps best seen in Figs. 19 and 20, where the straight lines represent the far field relation of 6-dB drop for a doubling of distance. This discrepancy obviously cannot be overcome by the inclusion of near field terms, but must be accounted for in some other way.

In Chapter IV, modifications of the stationary source model are introduced, which result in substantial improvement in the agreement with the experimental data.

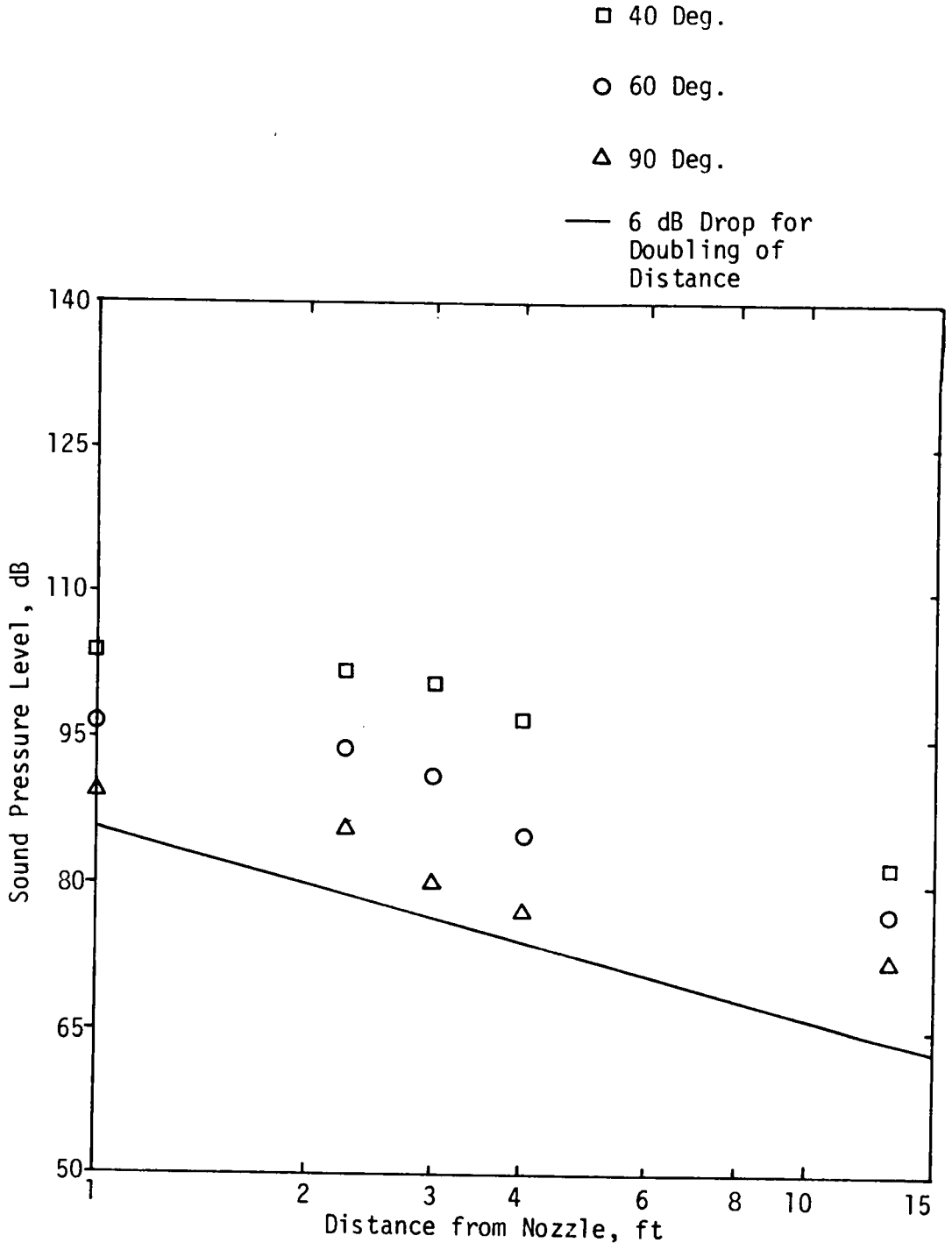

Figure 19. Radial variation of sound pressure level for Test Condition 3 at 100 Hz.

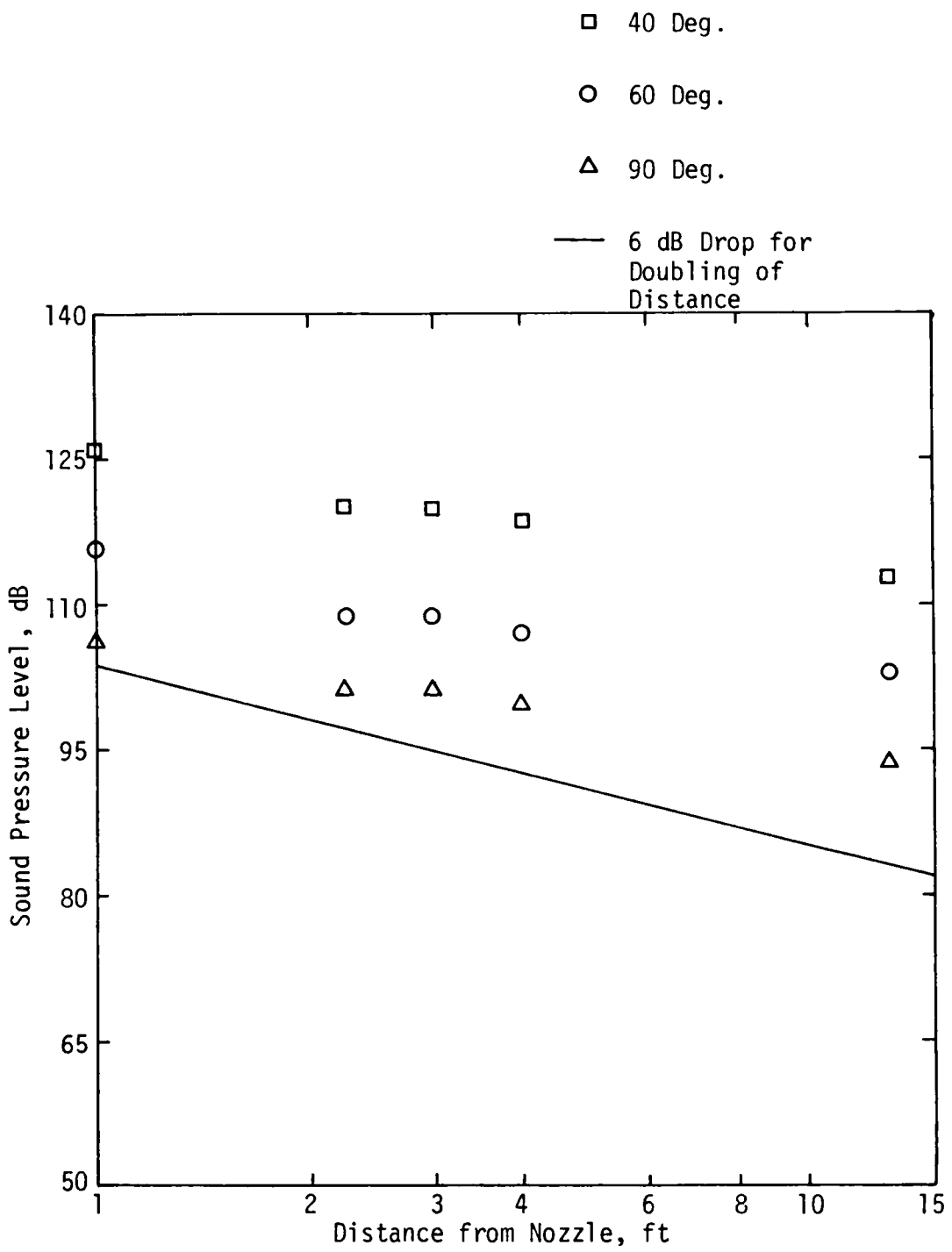

Figure 20. Radial variation of sound pressure level for Test Condition 3 at 1,000 Hz.

CHAPTER IV

CONVECTED SOURCE MODEL

4.1. Source Convection Effects

The theoretical model developed in Chapter III was under the assumption that the sound source distribution was at rest with respect to the observer. However, in an actual jet this is not the case. In fact, the elementary acoustic sources present in a jet are really fluctuating turbulent eddies which are being convected by the mean jet velocity with a characteristic velocity, the convection velocity. This motion of the source tends to beam the sound field forward and produce a directionality that is not associated with the sources themselves. In order to develop a more satisfactory model for the source distribution, it is necessary to consider the effects of convection of the sources on the sound radiation. The aerodynamic noise theory as developed by Lighthill [11] and Ffowcs Williams [12] is explained in the following sections of this chapter.

4.2. General Aerodynamic Noise Theory

The theory [11] begins from the fundamental equations of motion, expressed in terms of the mass density, ρ, and the momentum density, ρv_i, where v_i stands for the velocity vector (v_1, v_2, v_3). The equations are

$$\frac{\partial \rho}{\partial t} + \sum_{i=1}^{3} \frac{\partial(\rho v_i)}{\partial x_i} = 0 \ , \tag{4.1}$$

$$\frac{\partial(\rho v_i)}{\partial t} + \sum_{j=1}^{3} \frac{\partial(\rho v_i v_j + p_{ij})}{\partial x_j} = 0 \ . \tag{4.2}$$

These equations relate to the rate of change of mass or momentum in an elemental volume to the total mass transport or momentum transport out of the volume. The term $\rho v_i v_j$ represents direct convection of the momentum component, ρv_i, by the velocity component, v_j. The term p_{ij} represents the stress between adjacent elements of the fluid which also transfers momentum. The term p_{ij} consists of a pure pressure term, $p\delta_{ij}$ ($\delta_{ij} = 1$ for $i = j$ and $\delta i_{ij} = 0$ for $i \neq j$) and a viscous term, and is given by

$$p_{ij} = p\delta_{ij} - \mu \left(\frac{\partial v_i}{\partial x_j} + \frac{\partial v_j}{\partial x_i} - \frac{2}{3} \delta i_j \frac{\partial v_k}{\partial x_k} \right) \ .$$

However, the viscous terms in the stress tensor can be assumed to be very small and hence, neglected. Further, if it is assumed that the particle velocities, v_i are small, so that all squares of velocities can be neglected, the term $\rho v_i v_j$ can be dropped in Eq. (4.2). A third assumption used in classical acoustics is that small fluctuations in pressure and density are related to one another through the ambient speed of sound, a_o, and is given by $\partial p/\partial x_i = a_o^2 \, \partial \rho/\partial x_i$. With these assumptions, Eq. (4.2) takes the form,

$$\frac{\partial(\rho v_i)}{\partial t} + a_o^2 \frac{\partial \rho}{\partial x_i} = 0 \ . \tag{4.3}$$

Differentiating Eq. (4.1) with respect to t, and Eq. (4.3) with respect to x_i and eliminating (ρv_i) term by subtraction, gives

$$\frac{\partial^2 \rho}{\partial t^2} - a_o^2 \frac{\partial^2 \rho}{\partial x_i^2} = 0 \ . \tag{4.4}$$

However, without making any approximation, one can divide the momentum transport into two parts: firstly, the "acoustic" approximation of $a_o^2 \rho\delta_{ij}$, and secondly, the remainder, which may be written as,

$$T_{ij} = \rho v_i v_j + p_{ij} - a_o^2 \rho\delta_{ij} \ . \tag{4.5}$$

Hence, Eq. (4.2) can now be written as,

$$\frac{\partial}{\partial t}(\rho v_i) + a_o^2 \frac{\partial \rho}{\partial x_i} = - \sum_{j=1}^{3} \frac{\partial T_{ij}}{\partial x_j} \ . \tag{4.6}$$

Equations (4.6) and (4.1) state that the density fluctuations produced by a turbulent jet in the atmosphere outside of it is equivalent to the density fluctuations produced in a classical stationary acoustic medium by a system of externally applied stresses, T_{ij}. This equivalent applied stress system has the advantage that the refraction or scattering of the sound by the flow, as well as its generation, are automatically taken into account and need not be calculated separately.

By eliminating the momentum density from Eqs. (4.1) and (4.6), one can obtain,

$$\frac{\partial^2 \rho}{\partial t^2} - \sum_{i=1}^{3} a_o^2 \frac{\partial^2 \rho}{\partial x_i^2} = \sum_{i=1}^{3} \sum_{j=1}^{3} \frac{\partial^2 T_{ij}}{\partial x_i \partial x_j} . \tag{4.7}$$

Because the sound source term on the right-hand side is a summation of second derivatives of T_{ij}, the atmospheric sound field can be regarded as that due to a continuous distribution of acoustic quadrupoles, of strength T_{ij} per unit volume.

The solution of Eq. (4.7) is of the form,

$$a_o^2 (\rho - \rho_o) = \sum_{i=1}^{3} \sum_{j=1}^{3} \frac{\partial^2}{\partial x_i \partial x_j} \int_V \frac{[T_{ij}]}{4\pi R} d\tau , \tag{4.8}$$

where, V is the region of turbulent flow, R, the distance from a point in V to the point (x_1, x_2, x_3) where $a_o^2(\rho - \rho_o)$ is evaluated. The term T_{ij} is enclosed in square brackets to indicate that it should be evaluated at the retarded time, $(t - R/a_o)$, so that a wave traveling with a speed of a_o from the quadrupole reaches the observer at the current time, t.

In the far field, the terms from differentiation of 1/R with respect to x_i or x_j are not present since they fall of at least like $1/R^2$. The rate of change of retarded time, $(t - R/a_o)$, with respect to x_i gives,

$$\frac{\partial}{\partial x_i} (t - R/a_o) = \frac{-x_i}{a_o R} .$$

Using this in Eq. (4.8) leads to,

$$p - p_o = \sum_{i=1}^{3} \sum_{j=1}^{3} \frac{x_i x_j}{4\pi a_o^2 R^3} \int_V [\ddot{T}_{ij}] d\tau \qquad (4.9)$$

in the radiation field. The second time derivative, $[\ddot{T}_{ij}]$, in Eq. (4.9) results from the variability of the retarded time. In order to evaluate the total contribution from the whole jet, the statistical randomness of turbulent flow should be taken into account. It is well known that measurements made at nearby points in a turbulent flow are well correlated and the correlation drops off as the distance between the points is increased. This leads to a division of the total turbulent flow region into smaller regions, such that the quadrupole strengths are well correlated inside each of the smaller regions and are uncorrelated from one region to the next. The extent, ℓ, of each region being roughly the size of a typical energy-bearing eddy, the output from a single region of volume, say, V_e, then becomes,

$$p - p_o = \sum_{i=1}^{3} \sum_{j=1}^{3} \frac{x_i x_j}{4\pi a_o^2 R^3} [\ddot{T}_{ij}] \; . \qquad (4.10)$$

In general, the amplitudes of well-correlated sources combine linearly and for uncorrelated sources, the energy intensities combine linearly. To obtain the intensity of the radiation field, the uncorrelated outputs of each region, $\overline{(p - p_o)^2}/\rho_o a_o$, obtained from Eq. (4.10) should be added.

As a function of R, the intensity of acoustic energy from a single turbulent eddy varies as $V_e^2 \overline{\ddot{T}^2}/\rho_o a_o^5 R^2$. Here, $\overline{\ddot{T}^2}$ is a mean square fluctuation in $\ddot{T}_{ij}$. The term $\overline{\ddot{T}^2}$ can be written as $\omega^4 \overline{T^2}$, where ω is a characteristic radian frequency of fluctuation, and $\overline{T^2}$ is a characteristic mean square value of the quadrupole strength, T_{ij}. Hence, the acoustic power output per unit volume of turbulence is proportional to

$$V_e \omega^4 \overline{T^2}/\rho_o a_o^5 \ . \tag{4.11}$$

An essential assumption in this estimation is that the effect of the retarded time can be neglected within an eddy of size ℓ. This in turn requires that $\omega\ell/a_o$ be small for fluctuations at radian frequency of ω. Hence, the eddy size, ℓ, has to be small compared with the wavelength of sound it generates. This assumption is valid for low Mach numbers. However, as will be described later, ω should be observed in a moving frame of reference. The value of ω in a moving frame of reference will be smaller than that observed in a fixed frame of reference. This factor increases the range of Mach number to almost unity, for which the assumption, $\omega\ell/a_o$, is small compared to the wavelength of generated sound.

The generation of sound by turbulence discussed above will be now applied to the mechanism of sound generation in a turbulent jet.

For subsonic jets at high Reynolds numbers, the shear layer or mixing region between the jet and the atmosphere becomes fully turbulent within half a nozzle diameter of the orifice. The uniform

growth of the fully turbulent region ceases soon after x = 4D, where it reaches the axis.

In the mixing region, the fluctuations of terms, such as $\rho v_i v_j$ in the quadrupole strength, are proportional to $\rho_m U^2$, where ρ_m is the density of the fluid in the mixing region. This term changes very little with x in the mixing region and hence, can be assumed to be independent of x. The typical radian frequency, ω, falls away as U/x, while the typical eddy volume, V_e, grows as x^3. Hence, from Eq. (4.11) the acoustic power output per unit volume of a low-speed jet should vary as $\rho_m^2 U^8 / \rho_o a_o^5 x$ in the mixing region. Now, the volume per unit length increases with x; therefore, the sound emitted per unit length of jet should remain constant in this region and hence, the total up to x = 4D becomes proportional to,

$$\frac{\rho_m^2 \, U^8 \, D^2}{\rho_o \, a_o^5} \, . \tag{4.12}$$

Beyond x = 4D, the generation of sound per unit length falls off as the fluctuations in T_{ij} are reduced. Beyond x = 8D, where velocity decay is proportional to 1/x, the sound generation per unit length should fall off as $1/x^6 \ell$ by the same analysis as above. Here, ℓ is the correlation radius. The qualitative variation in acoustic power output for a free turbulent stationary jet at ambient temperature is shown in Fig. 21.

Strictly speaking, the turbulent eddies should be viewed as moving quadrupoles. Hence, they should be observed in a coordinate system that is moving at the same velocity. In such a coordinate

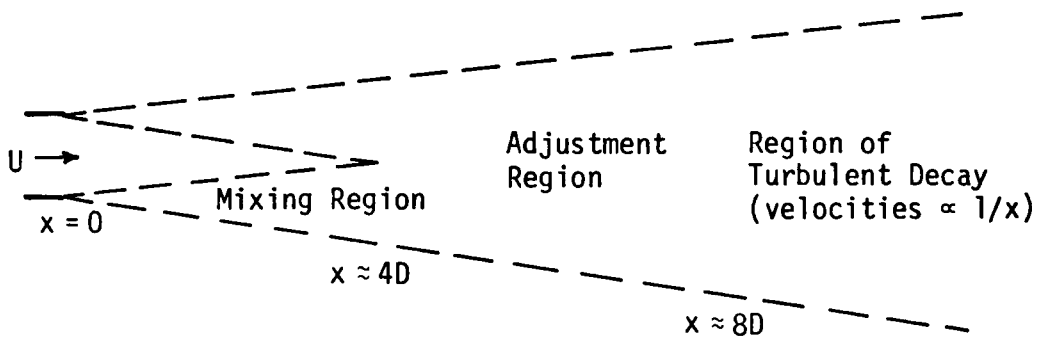

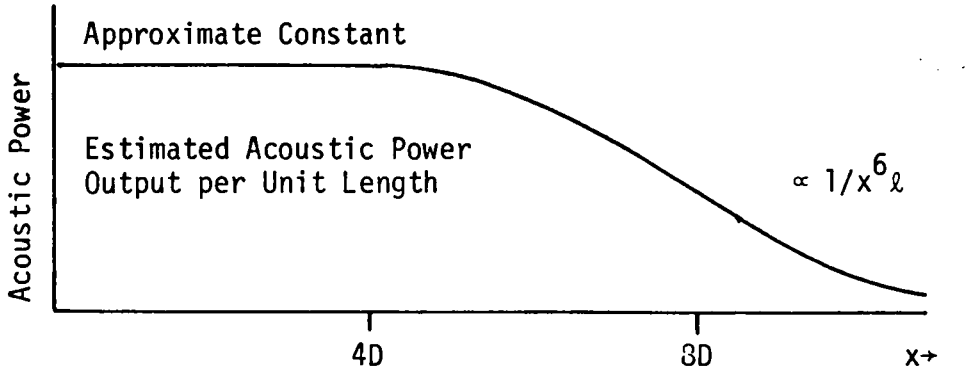

Figure 21. Stationary cold jet: measurements at Mach number 0.3 and Reynolds number 6×10^5 [11, 13].

system, the frequency of fluctuation, ω, will be smaller than that perceived in a stationary coordinate system as the variations with respect to time alone are observed in the moving coordinate system. A moving volume, V_e, with a quadrupole strength per unit volume of T_{ij} has a sound radiation field given by,

$$p - p_o = \sum_{i=1}^{3} \sum_{j=1}^{3} \frac{x_i \, x_j \, V_e[\ddot{T}_{ij}]}{4\pi \, a_o^2 \, R^3 (1-M_c \cos\phi)^3} , \qquad (4.13)$$

where, M_c is the convection Mach number and is given by the convection velocity divided by the acoustic speed in the atmosphere. The term ϕ is the angle between direction of emission and jet direction. When the the effect of convection is taken into consideration, the emission from a volume is increased compared to an unconvected quadrupole of the same strength. This is because of the increase in total emitting volume by a factor of $1/(1 - M_c \cos\phi)$ (see Fig. 22).

The mechanism of sound generation in a quadrupole is by the incomplete cancellation of the radiation from the positive and negative sources due to the time difference. The effect of convection of the quadrupoles is an augmentation of this time difference from t for an unconvected case to $t/(1 - M_c \cos\phi)$ for the convected case. Thus, two additional factors of $1/(1 - M_c \cos\phi)$ is introduced, as there are two pairs of positive and negative sources in a quadrupole.

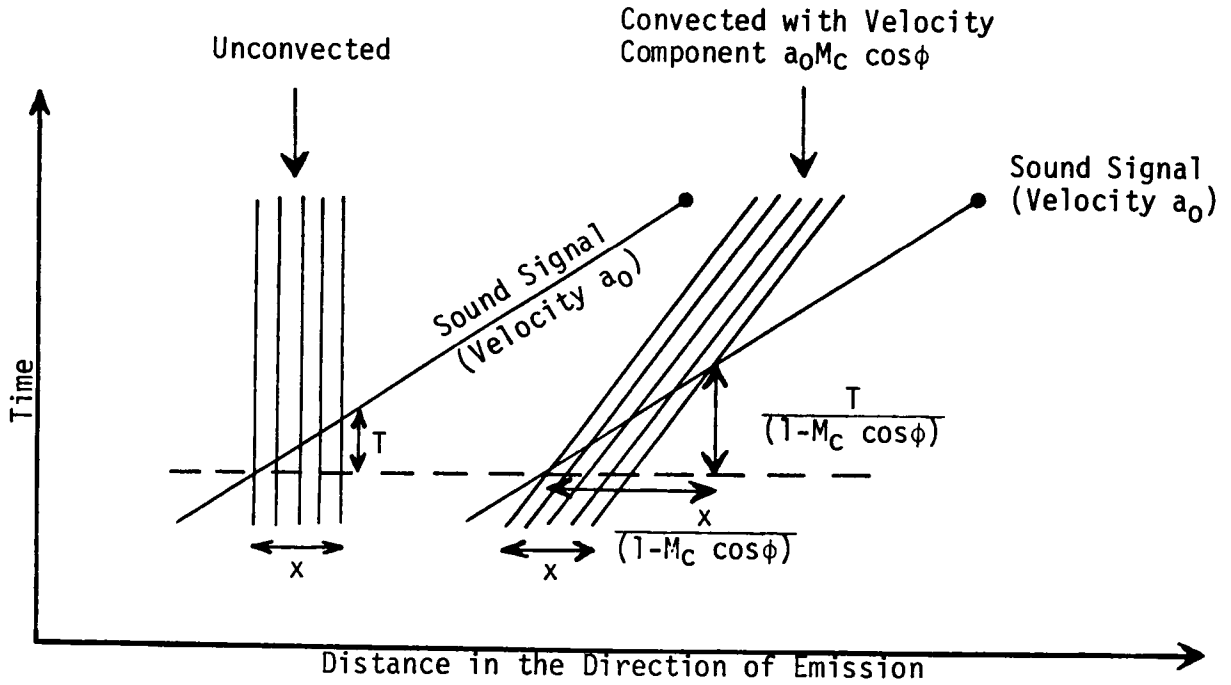

Figure 22. Increase of emitting volume and emission time differences because of convection, by the factor, $1/(1 - M_c \cos\phi)$ [11].

When the above-mentioned factors are incorporated in Eq. (4.13), the directionality factor becomes $(1 - M_c \cos\phi)^{-6}$. From Fig. 22, however, one finds that the moving eddies of extent x should be multiplied by $(1 - M_c \cos\phi)$ to obtain that number whose radiation arrives simultaneously. This, then, modifies the directionality factor to $(1 - M_c \cos\phi)^{-5}$. Hence, Eq. (4.13) takes the form,

$$\overline{(p-p_o)^2}/\rho_o a_o = \frac{V_e}{\rho_o a_o} \overline{\left(\sum_{i=1}^{3} \sum_{j=1}^{3} \frac{x_i x_j [T_{ij}]}{4\pi a_o^2 R^3} \right)^2} (1 - M_c \cos\phi)^{-5} . \quad (4.14)$$

In Eq. (4.12) it was shown that acoustic power output from the mixing region is proportional to $\rho_m^2 U^8 D^2/\rho_o a_o^5$. Using this in Eq. (4.14), an expression is obtained for the total acoustic power output from the jet up to x = 4D as,

$$\frac{\overline{(p-p_o)^2}}{\rho_o a_o} \propto \frac{\rho_m^2 U^8 D^2}{\rho_o a_o^5} \cdot \frac{1}{(1 - M_c \cos\phi)^5} . \quad (4.15)$$

This expression for power, W, can be obtained by integrating the acoustic intensity, I, over a sphere of radius R; that is,

$$W = \int I d\Omega ,$$

where, Ω is the solid angle. Hence, for a sphere, of radius R, one obtains,

$$W = 4\pi R^2 I$$

or

$$I \propto W/R^2 \ .$$

Hence, the expression for acoustic intensity as a function of R and ϕ becomes,

$$I(R,\phi) \propto \frac{\rho_m^2 \, U^8 \, D^2}{\rho_o \, a_o^5 \, R^2} \cdot \frac{1}{(1 - M_c \cos\phi)^5} \ . \qquad (4.16)$$

The preferred orientation of the quadrupoles introduces a directional effect on the sound radiation and it is assumed to be a function of ϕ. Introducing this into Eq. (4.16), the expression for acoustic intensity in the far field becomes [4, 12],

$$I(R,\phi) \propto \frac{\rho_m^2 \, U^8 \, D^2}{\rho_o \, a_o^5 \, R^2} \cdot \frac{f(\phi)}{(1 - M_c \cos\phi)^5} \ . \qquad (4.17)$$

4.3. Convection Effects on Source Model

The multipole expansion technique, described in Chapter III, used to obtain the multipole moments using the least-squares fit, tended to include the source convection effects and inherent directionality of the quadrupoles due to their preferred orientation as one parameter. This forced the least-squares fit to give more weightage to the higher order terms, which, in turn, resulted in much higher predictions for sound pressure levels in the near field (see Fig. 16, page 48). In order to improve the predicted results, the multipole moments must be forced to reflect only the source

directionality function, $f(\phi)$, for which the convection effects should be first removed from the measured far field sound pressure level data.

To carry out this procedure, the measured far field intensities were divided by the convection factor, $(1 - M_c \cos\phi)^{-5}$, prior to the determination of the multipole moments. This removes the effect of source motion from the far field sound, so that the multipole expansion includes only the inherent directionality of the source region. This, in turn, reduces the weight of the higher order terms in the expansion with their strong near field components. The computed sound field from the source distribution is then multiplied by $(1 - M_c \cos\phi)^{-5}$ to obtain the predicted sound field. However, the unknown in the convection factor, M_c, should be determined before this procedure can be carried out. A method for computing the ratio of convection velocity, V_c, to the jet velocity, U, was developed. This is explained below. The directionality effect due to convection is a maximum along $\phi = 0$, the jet axis, and a minimum at $\phi = \pi/2$. From Eq. (4.17),

$$I(R,\pi/2) \propto \frac{\rho_m^2 U^8 D^2}{\rho_o a_o^5 R^2} \cdot f(\pi/2) , \qquad (4.18)$$

$$I(R,0) \propto \frac{\rho_m^2 U^8 D^2}{\rho_o a_o^5 R^2} \frac{f(0)}{(1 - M_c \cos 0)^5} . \qquad (4.19)$$

If one assumes that the directionality function, $f(\phi)$, has weak dependence on the ϕ value for all angles of ϕ, then,

$f(\pi/2) \approx f(0)$. Dividing Eq. (4.18) by Eq. (4.19) and noting that $\cos 0 = 1$,

$$\frac{I(R,\pi/2)}{I(R,0)} = (1 - M_c)^5 \quad . \tag{4.20}$$

The acoustic intensity, I, is proportional to the mean square of the acoustic pressure. Hence,

$$\frac{\overline{p^2}(R,\pi/2)}{\overline{p^2}(R,0)} = (1 - M_c)^5 \quad . \tag{4.21}$$

Dividing the numerator and denominator on the left-hand side by the square of an acoustic reference pressure and taking the logarithm to the base 10 on both sides and multiplying by 10 throughout, Eq. (4.21) becomes,

$$10 \log \frac{\overline{p^2}(R,\pi/2)}{p_{ref}^2} - 10 \log \frac{\overline{p^2}(R,0)}{p_{ref}^2} = 50 \log(1 - M_c) \quad . \tag{4.22}$$

But sound pressure level, SPL = $10 \log \overline{p^2}/p_{ref}^2$, dB, and

$$M_c = \frac{V_c}{a_o}$$

$$= \frac{U}{a_o} \cdot \frac{V_c}{U}$$

$$= M \cdot R_c \quad ,$$

where,

$$R_c = \frac{V_c}{U} \quad .$$

Using this,

$$SPL(R,\pi/2) - SPL(R,0) = 50 \log (1 - M \cdot R_c) , \qquad (4.23)$$

from which,

$$R_c = \frac{1}{M} \left\{ 1 - 10^{\frac{[\,SPL(R,\,/2) - SPL(R,0)\,]}{50}} \right\} . \qquad (4.24)$$

The ratio of R_c was calculated for each frequency of the test condition given in Table 1, page 13, and for sound pressure levels obtained for microphone radial location of 13 feet. The sound pressure level at $\phi = 0$ appearing in the equations derived above was actually obtained by taking the average value of the sound pressure levels for ϕ = 20, 25, 30, and 35 degrees. This was done because the sound pressure level for $\phi = 0$ cannot be measured, as the microphone being directly along the jet axis would measure the pressure fluctuations of the flow rather than the acoustic pressure. The value of R_c obtained is quite reasonable and shows the expected trend that as the frequency under consideration was increased, so did the value of R_c. The reason for this may be explained as follows; the higher frequency sound sources are located further upstream compared to the lower frequency sources. The moving quadrupoles closer to the nozzle exit have a larger ratio of convection velocity to the jet exit velocity and this ratio decreases as the quadrupoles move downstream.

Figures 23 through 26 show some comparison of far field sound directivity patterns with results of the multipole expansion after the convection effects have been removed. In general, a better fit to the data was obtained with the removal of convection effects.

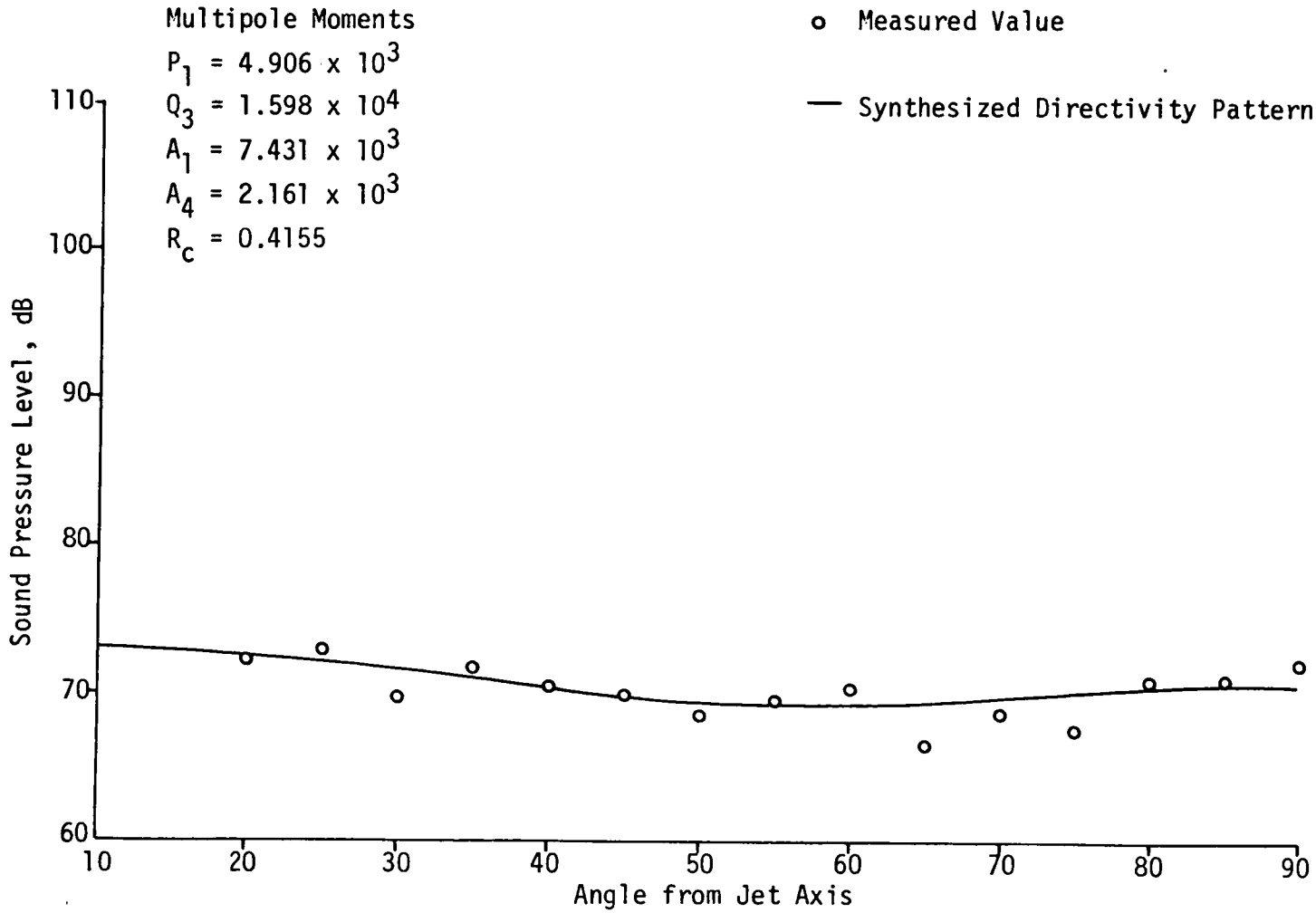

Figure 23. Comparison of measured far field sound directivity after removal of convection effects with least-squares fit for Test Condition 3 at 100 Hz.

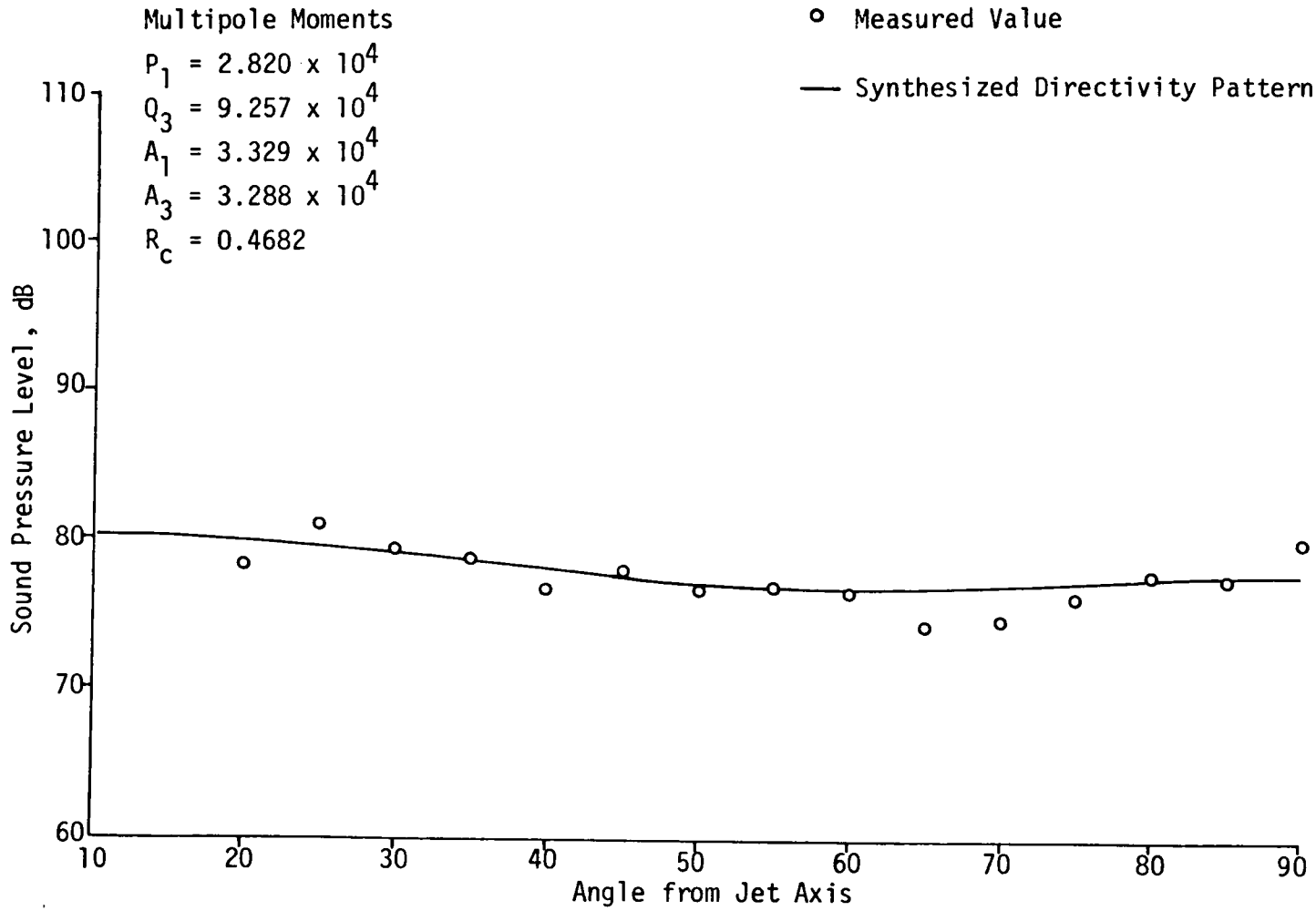

Figure 24. Comparison of measured far field sound directivity after removal of convection effects with least-squares fit for Test Condition 3 at 200 Hz.

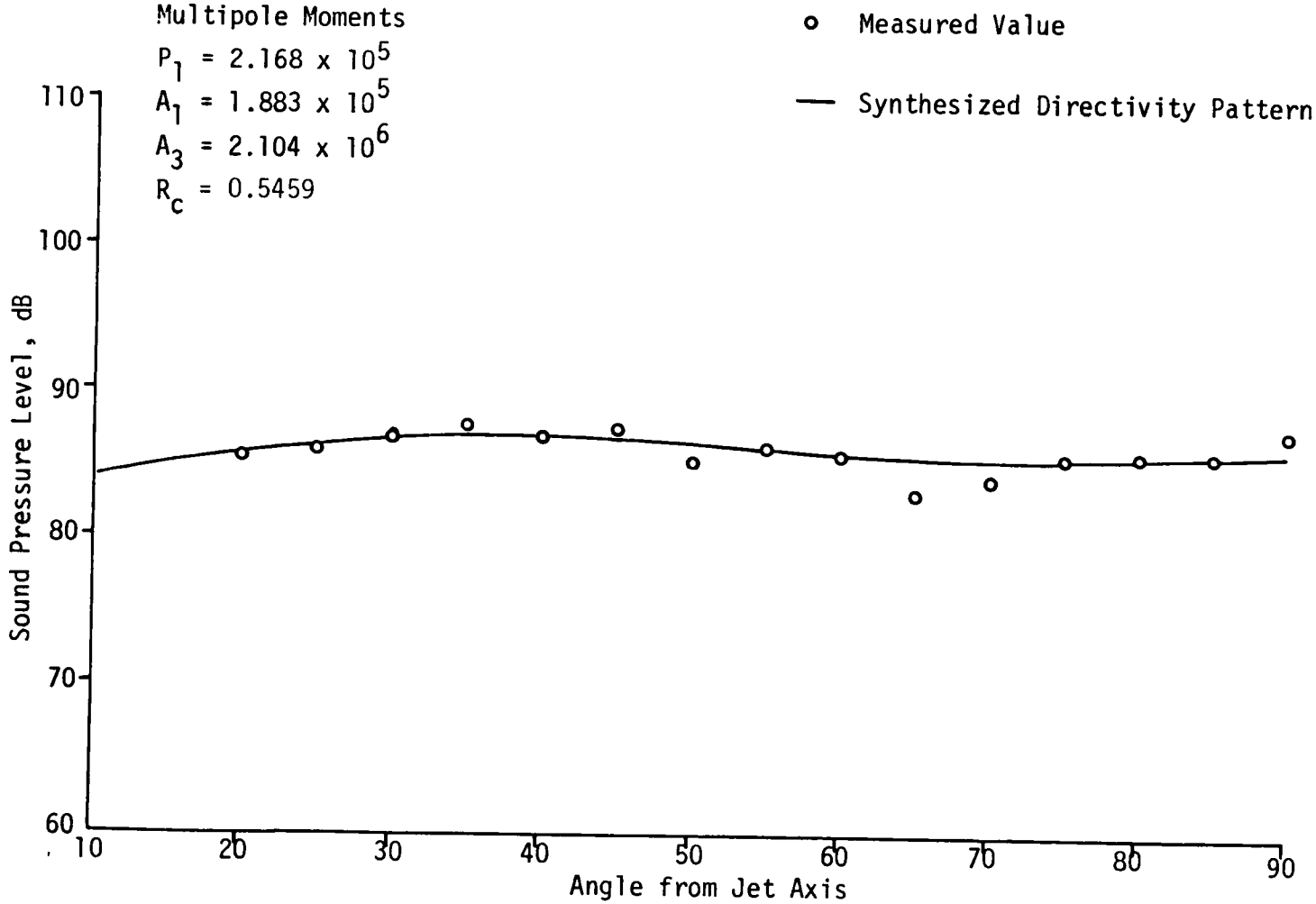

Figure 25. Comparison of measured far field sound directivity after removal of convection effects with least-squares fit for Test Condition 3 at 500 Hz.

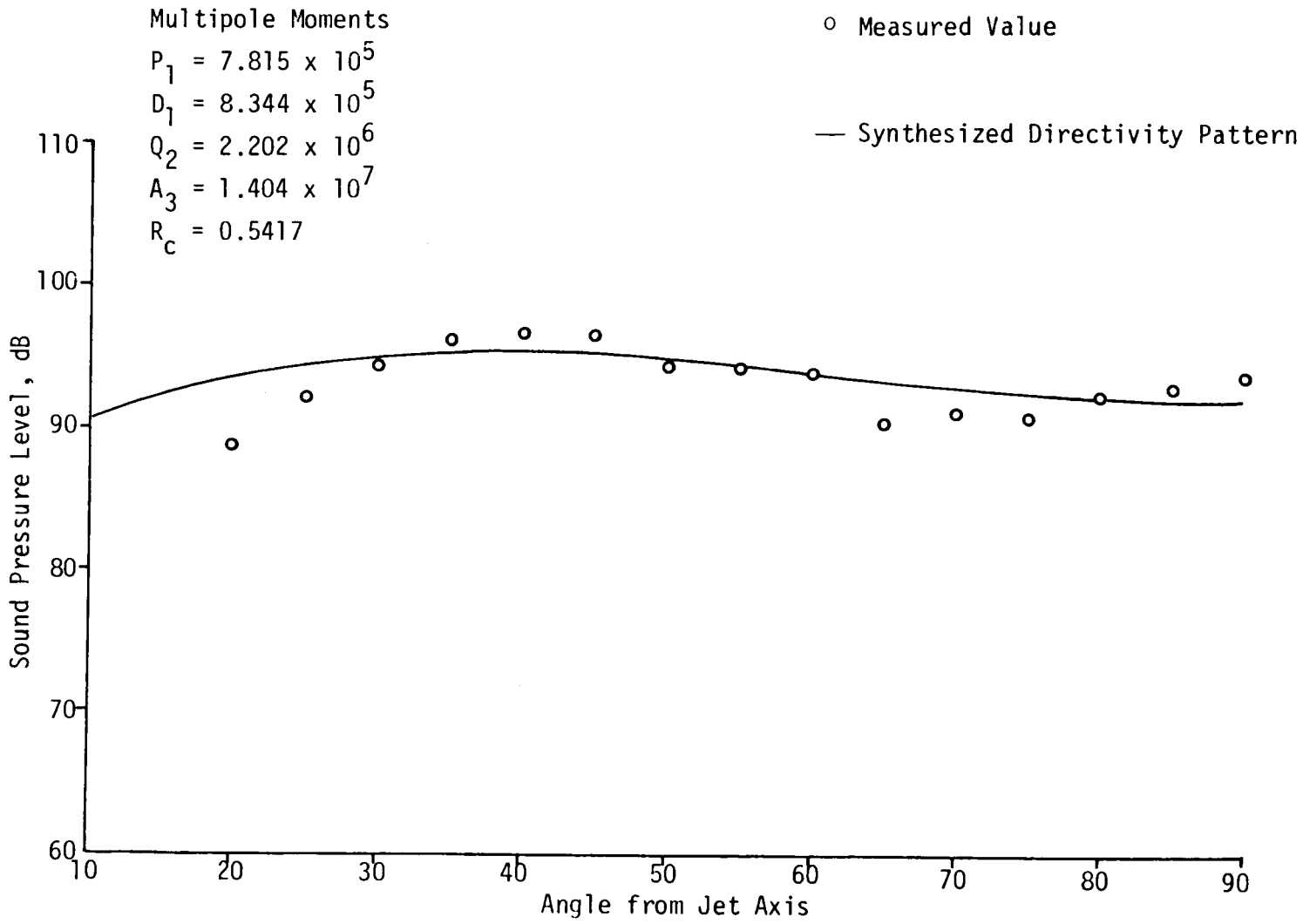

Figure 26. Comparison of measured far field sound directivity after removal of convection effects with least-squares fit for Test Condition 3 at 1,000 Hz.

4.4. Extended Source Effects

In the stationary source model described in Chapter III, for each frequency the distributed noise source of the turbulent jet was replaced by an assemblage of uncorrelated elementary sources located at the center of the nozzle exit plane. However, it is well known from jet noise theory [5] that the location of sound sources is frequency dependent. The low-frequency sound is generated by large-scale turbulent eddies, which are located further downstream than the small-scale sources of high-frequency sound. In order to account for this effect, the effective source for each one-third octave frequency band is considered to be located at a single point on the jet axis. Further, it is assumed that the location of the source is primarily a function of the Strouhal number, St = fD/U.

The near field sound pressure level at each frequency is predicted using the multipole expansion technique for various values of source location. For each source location, the RMS error between the predicted sound pressure level and the corresponding measured values are evaluated. A plot of the RMS error as a function of source location in terms of nozzle diameters is shown in Fig. 27. The approximate source location should be at the point where the RMS error is the least. This procedure is repeated for different frequencies and test conditions. A plot of the source location corresponding to the least RMS error was plotted as a function of the Strouhal number for that frequency on a log-log scale. This plot is shown in Fig. 28. In order to obtain the functional relation between

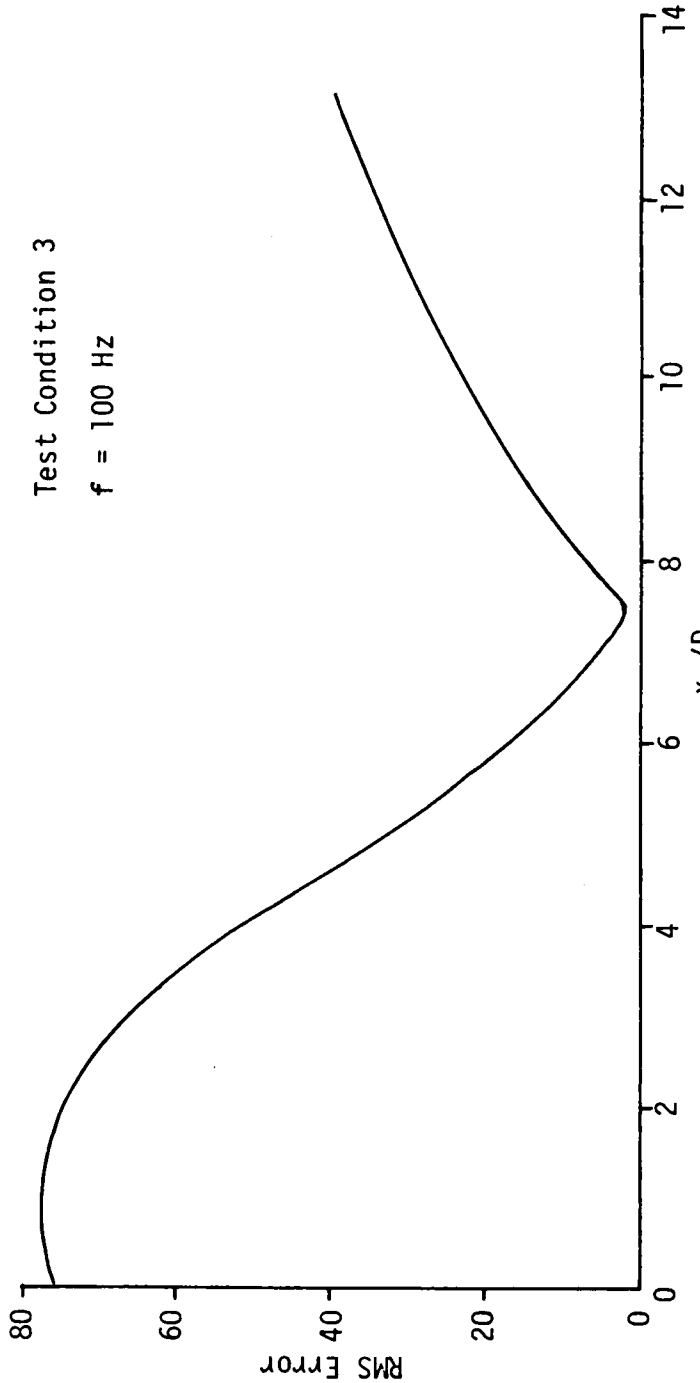

Figure 27. RMS error between microphone data at 1 ft and predicted sound level as a function of assumed source location for 100 Hz.

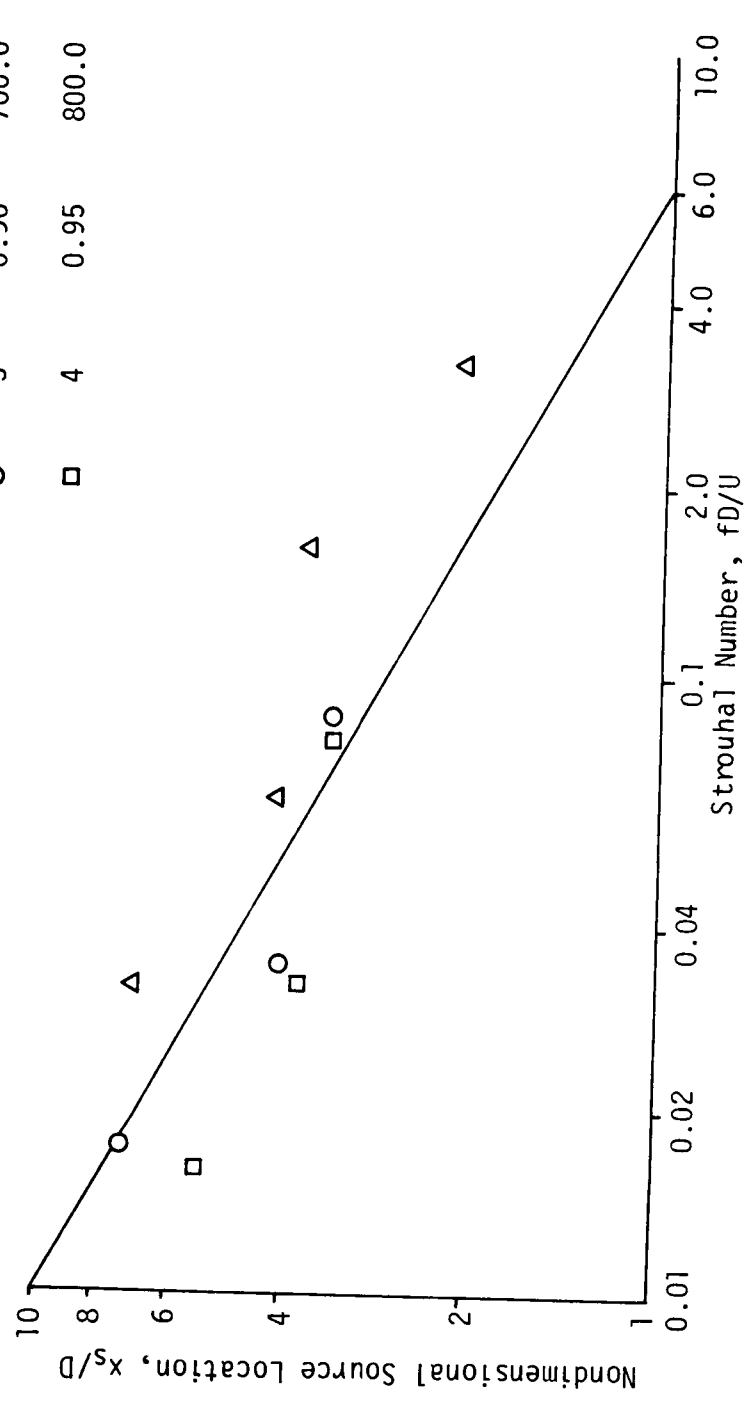

Figure 28. Optimum source location as a function of Strouhal number.

Strouhal number and the source location, the solid line in Fig. 28 is drawn as a "best fit" to the data points and specifies the relation,

$$\frac{x_s}{D} = 0.7503(St)^{-0.5624} \quad . \tag{4.25}$$

McGregor and Simcox [14] have determined peak power source location data for flow from a circular nozzle by a wall isolation technique. Their results show the same general trend as that of Fig. 28, but locate the source somewhat farther downstream for a given Strouhal number.

4.5. Results of Modified Source Modeling Procedure

The computer code for predicting the near field sound pressures based on the model developed in Chapter III was now modified to include the effect of the factors described in the last three sections. This revised model was then used to predict the near field sound pressure levels for the test conditions given in Table 1, page 13. The results of these calculations and a comparison with measured data are presented in Figs. 29 through 48. In performing these calculations, the coefficients in the multipole expansion were obtained from far field data at R = 13 feet, assuming a source location of $x_s = 0$. In all cases the multipole expansion is carried out through the octupole level and convection effects are removed before evaluation of multipole moments. In Figs. 29 through 48, all angles and distances are referred to a coordinate system fixed in the nozzle exit plane, as shown in Fig. 3, page 14, although the

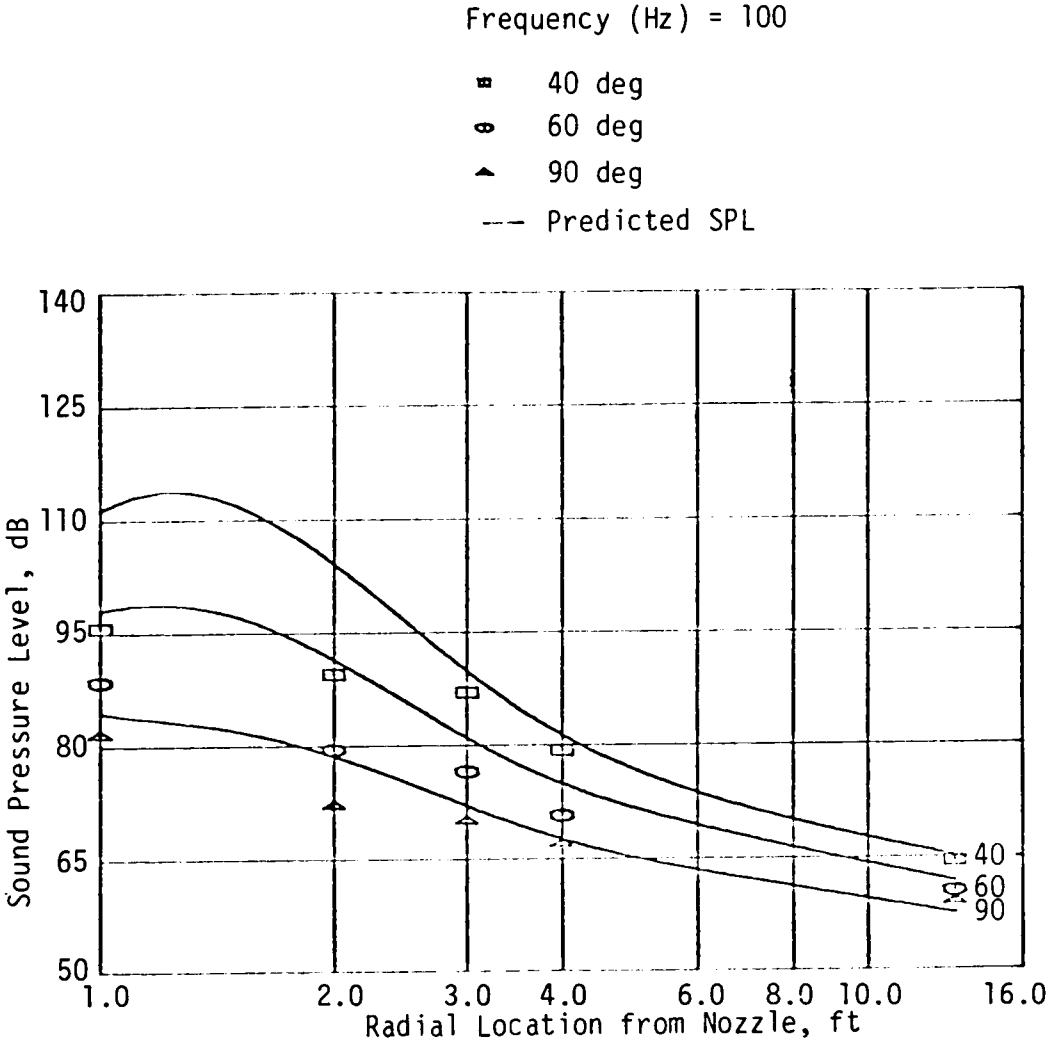

Figure 29. Comparison of measured and predicted sound pressure levels using modified source modeling technique for Test Condition 1 at 100 Hz.

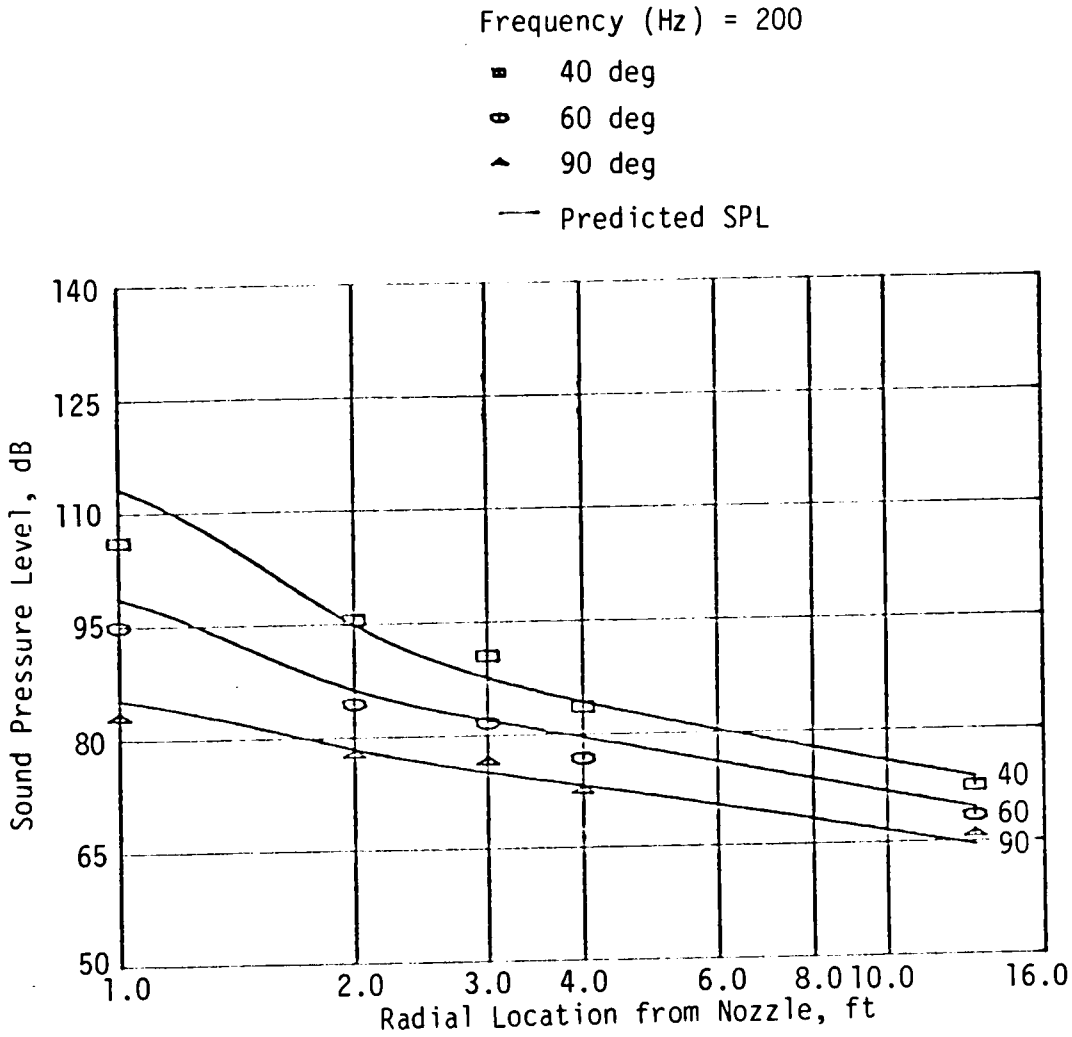

Figure 30. Comparison of measured and predicted sound pressure levels using modified source modeling technique for Test Condition 1 at 200 Hz.

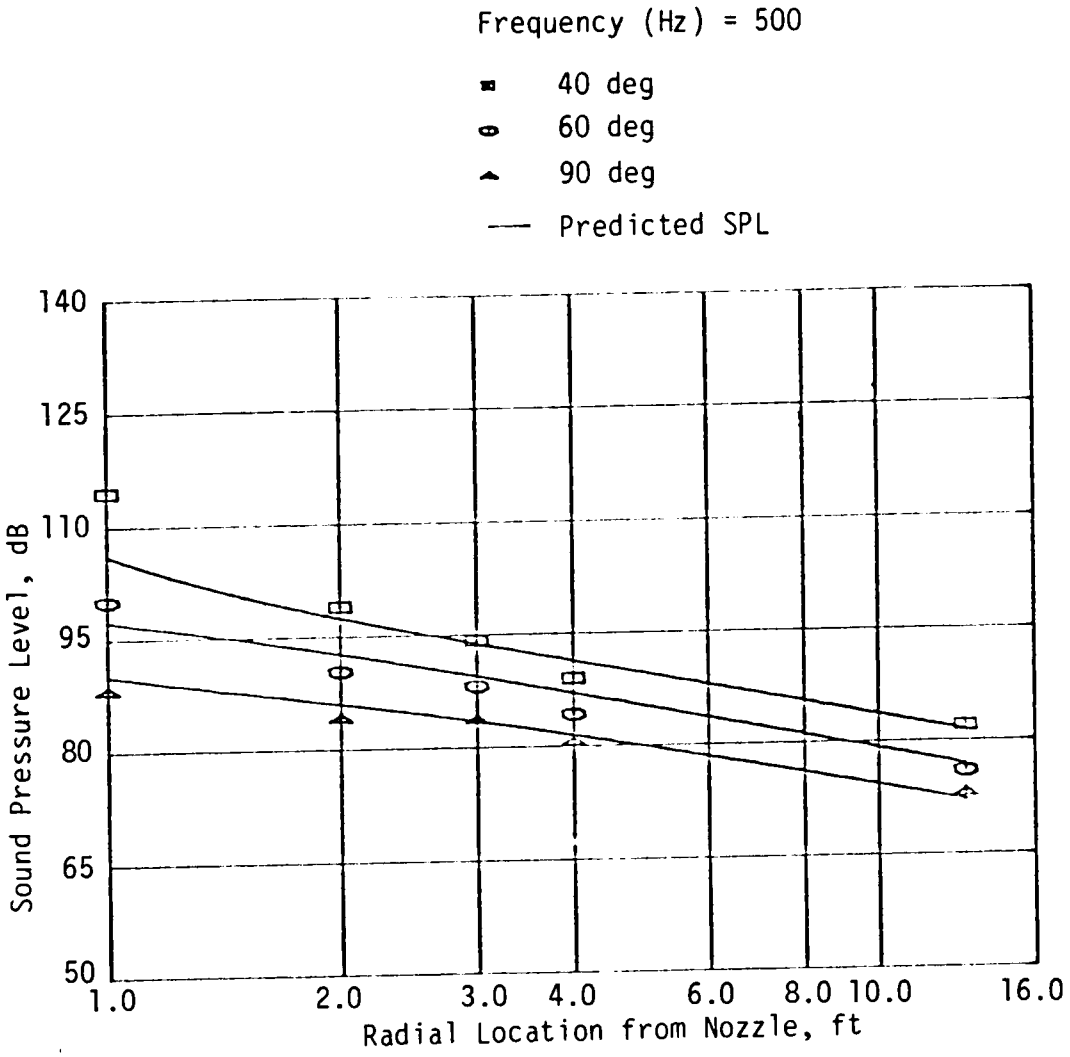

Figure 31. Comparison of measured and predicted sound pressure levels using modified source modeling technique for Test Condition 1 at 500 Hz.

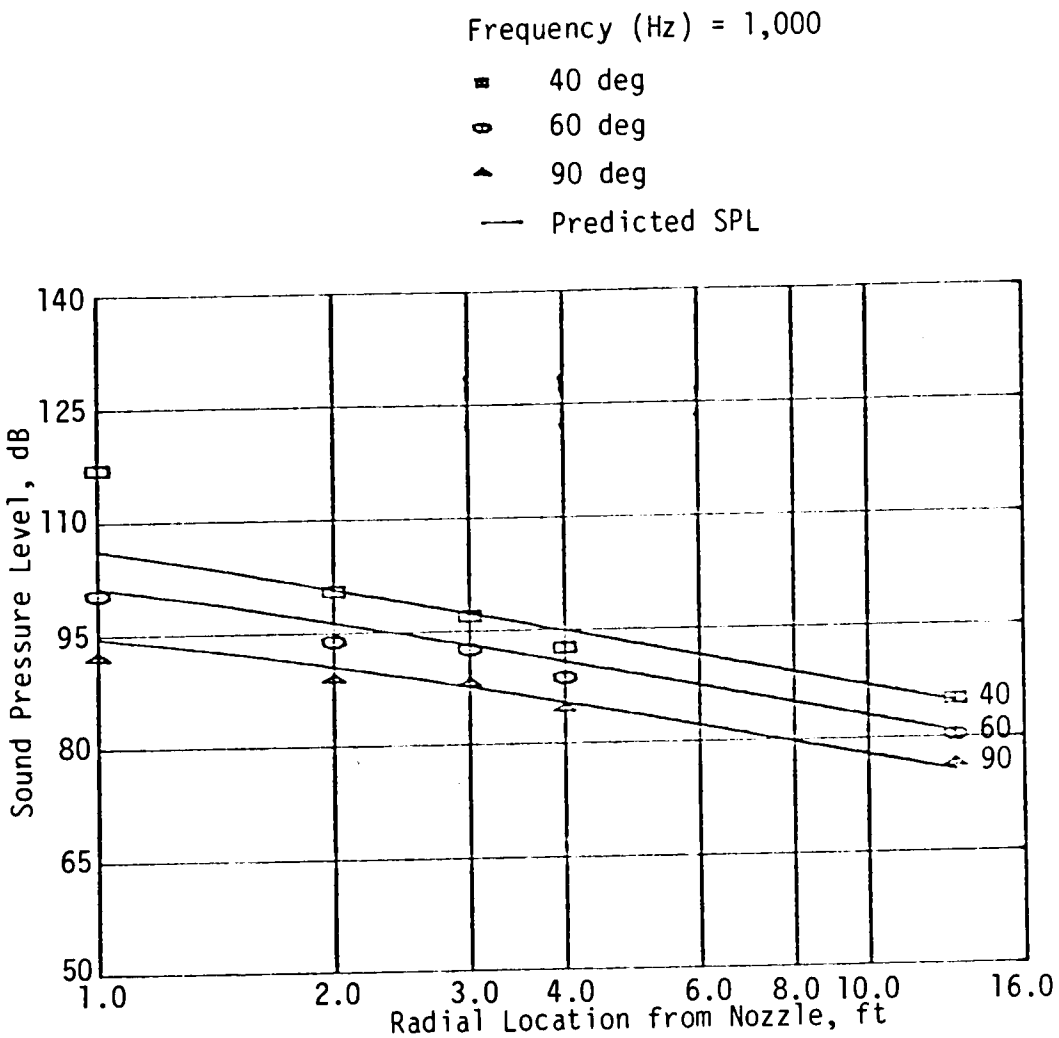

Figure 32. Comparison of measured and predicted sound pressure levels using modified source modeling technique for Test Condition 1 at 1,000 Hz.

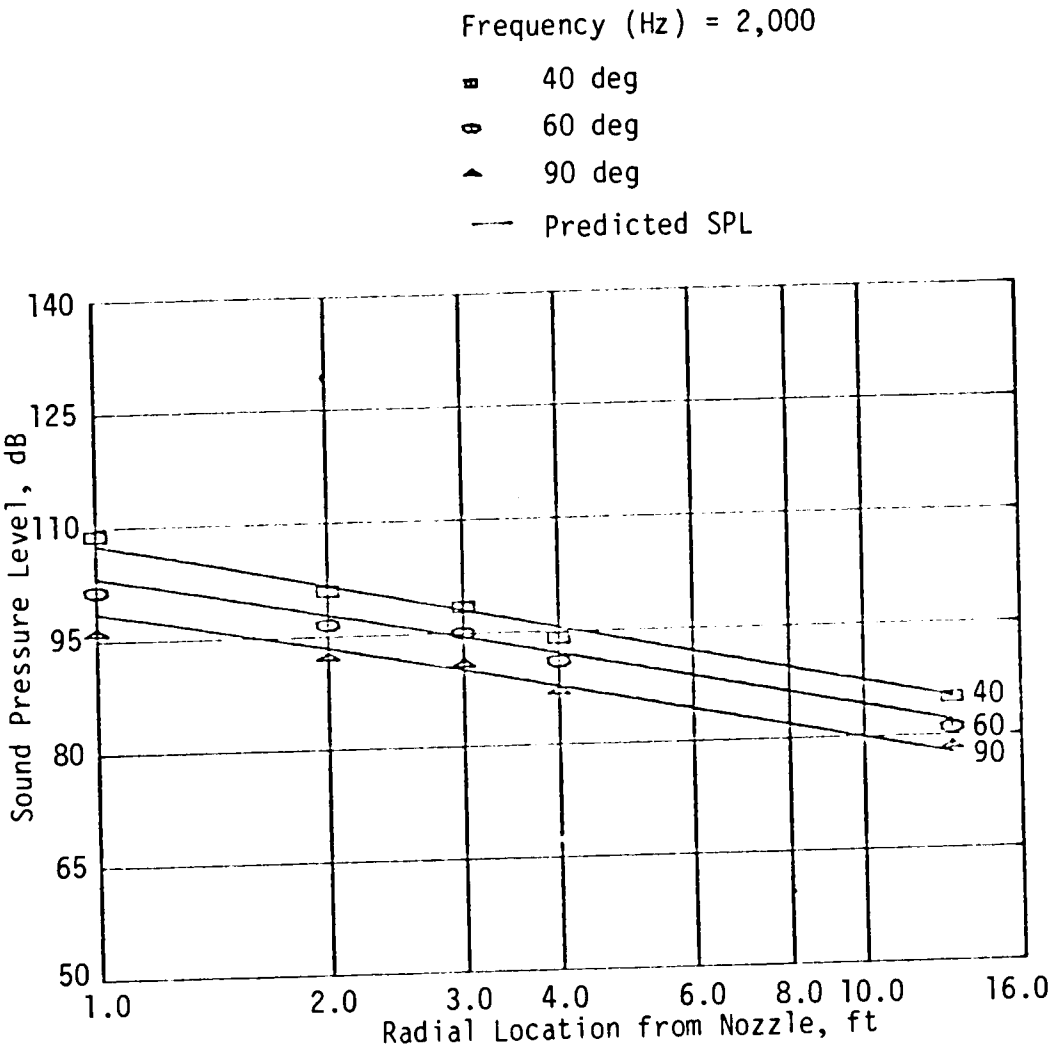

Figure 33. Comparison of measured and predicted sound pressure levels using modified source modeling technique for Test Condition 1 at 2,000 Hz.

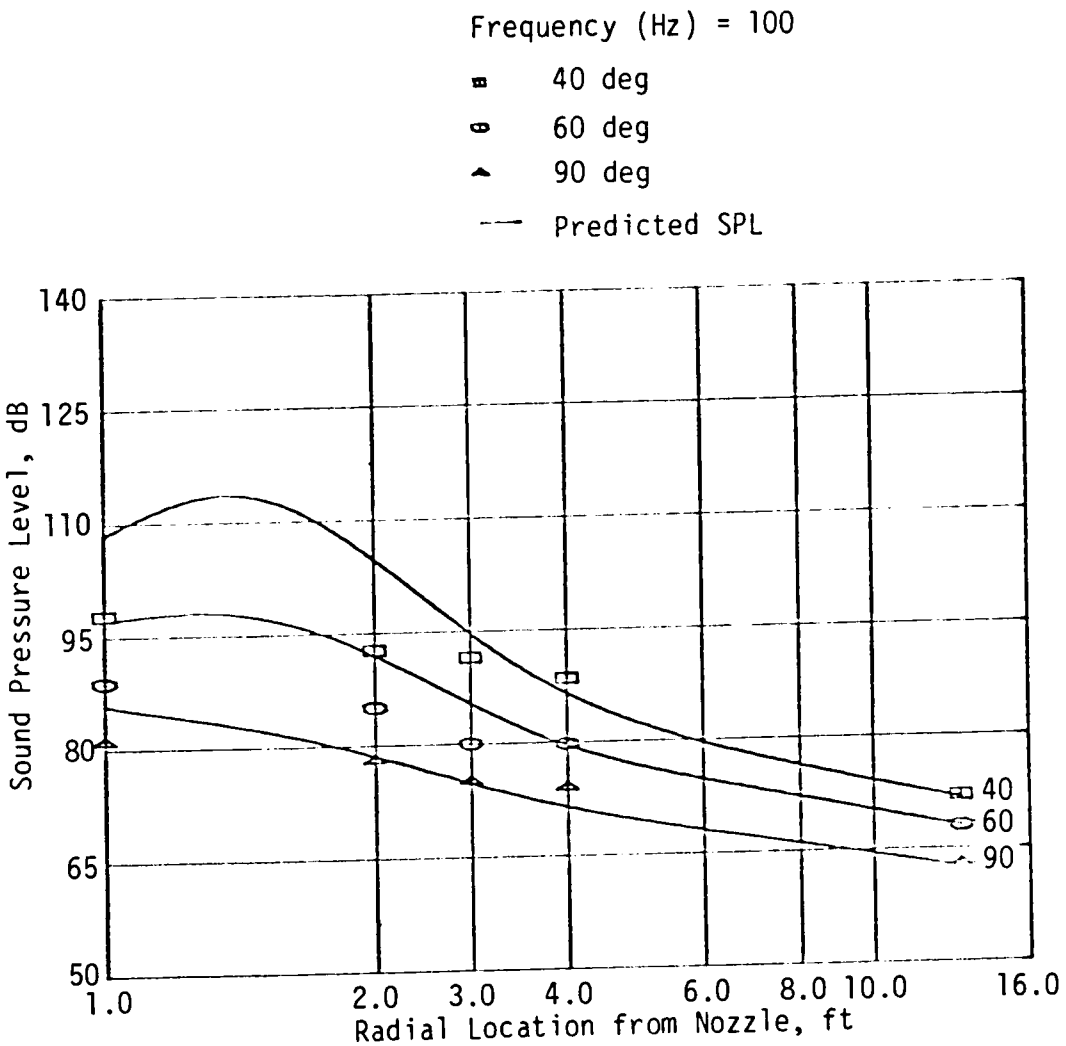

Figure 34. Comparison of measured and predicted sound pressure levels using modified source modeling technique for Test Condition 2 at 100 Hz.

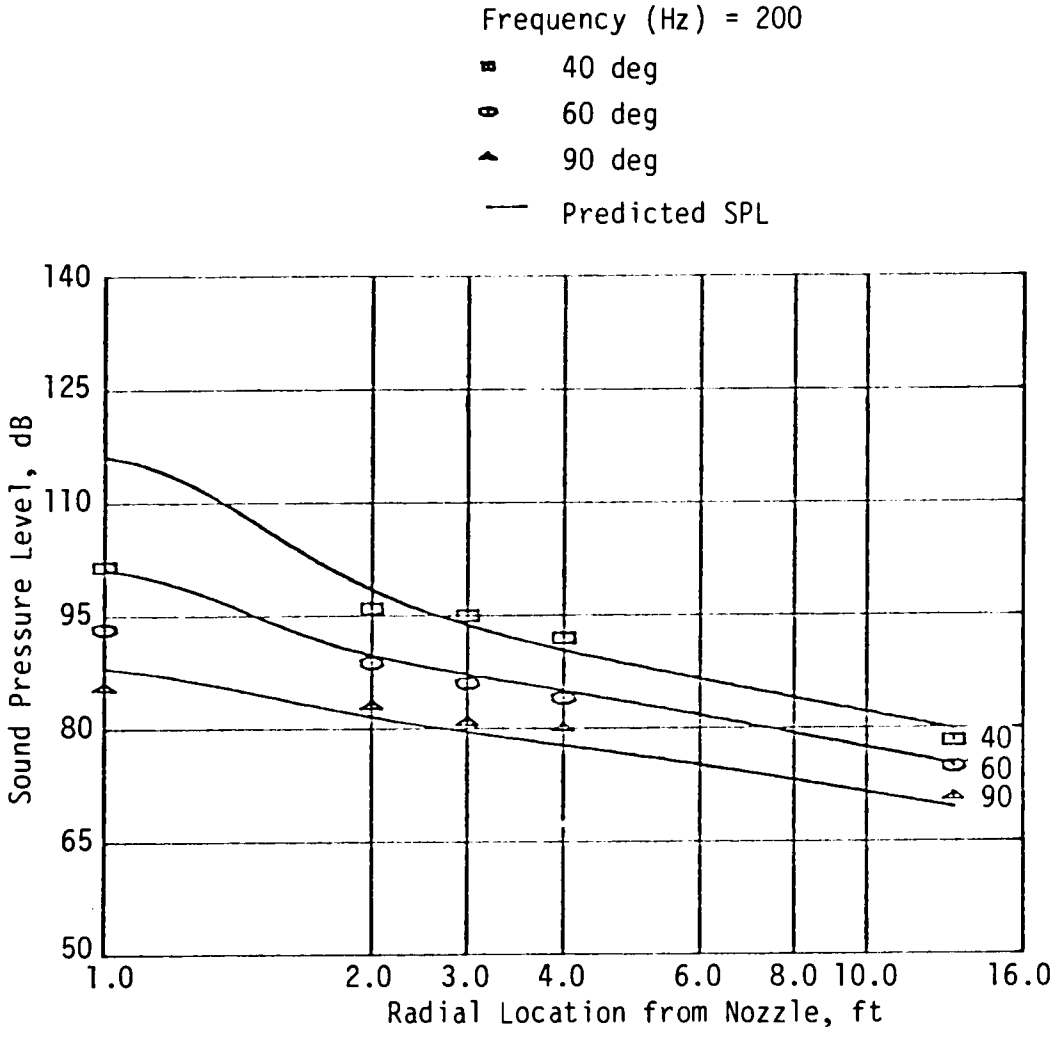

Figure 35. Comparison of measured and predicted sound pressure levels using modified source modeling technique for Test Condition 2 at 200 Hz.

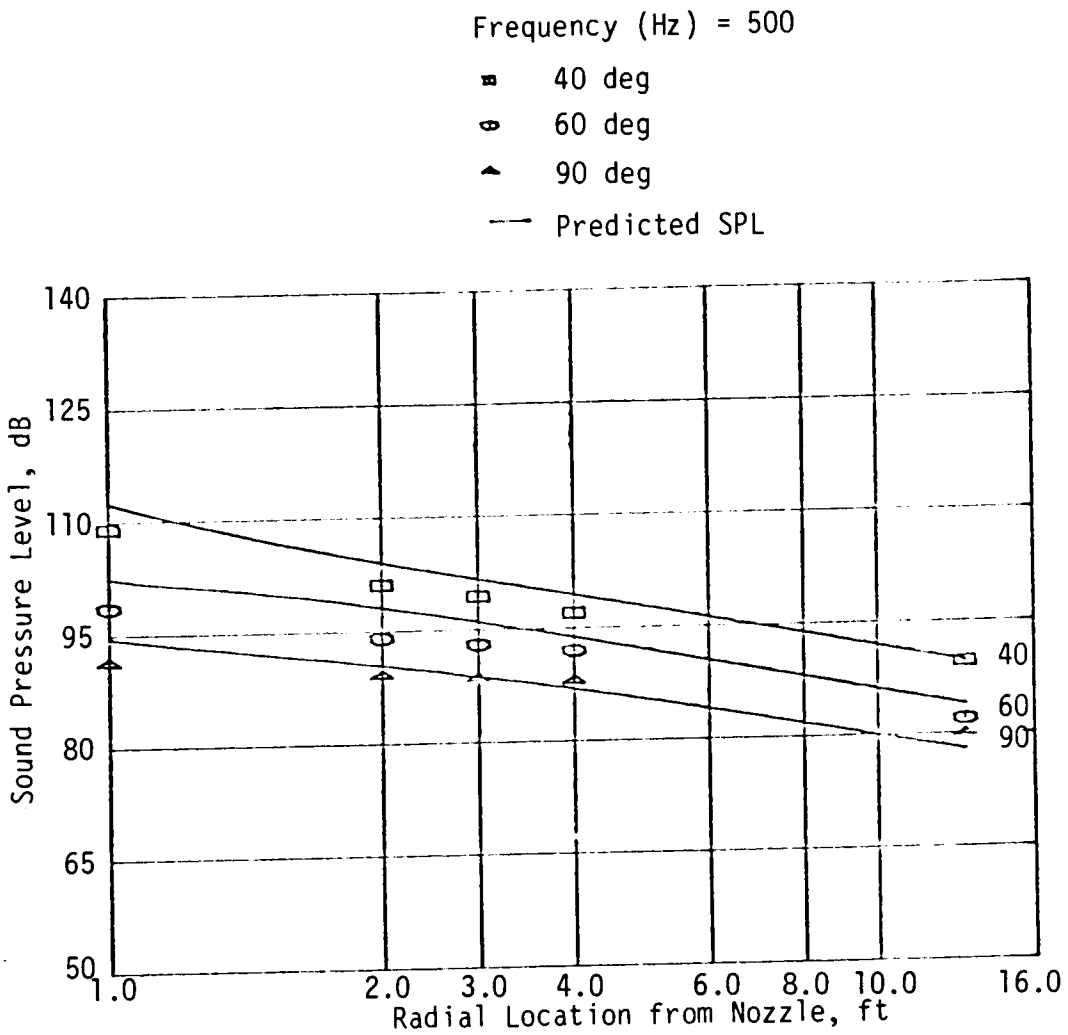

Figure 36. Comparison of measured and predicted sound pressure levels using modified source modeling technique for Test Condition 2 at 500 Hz.

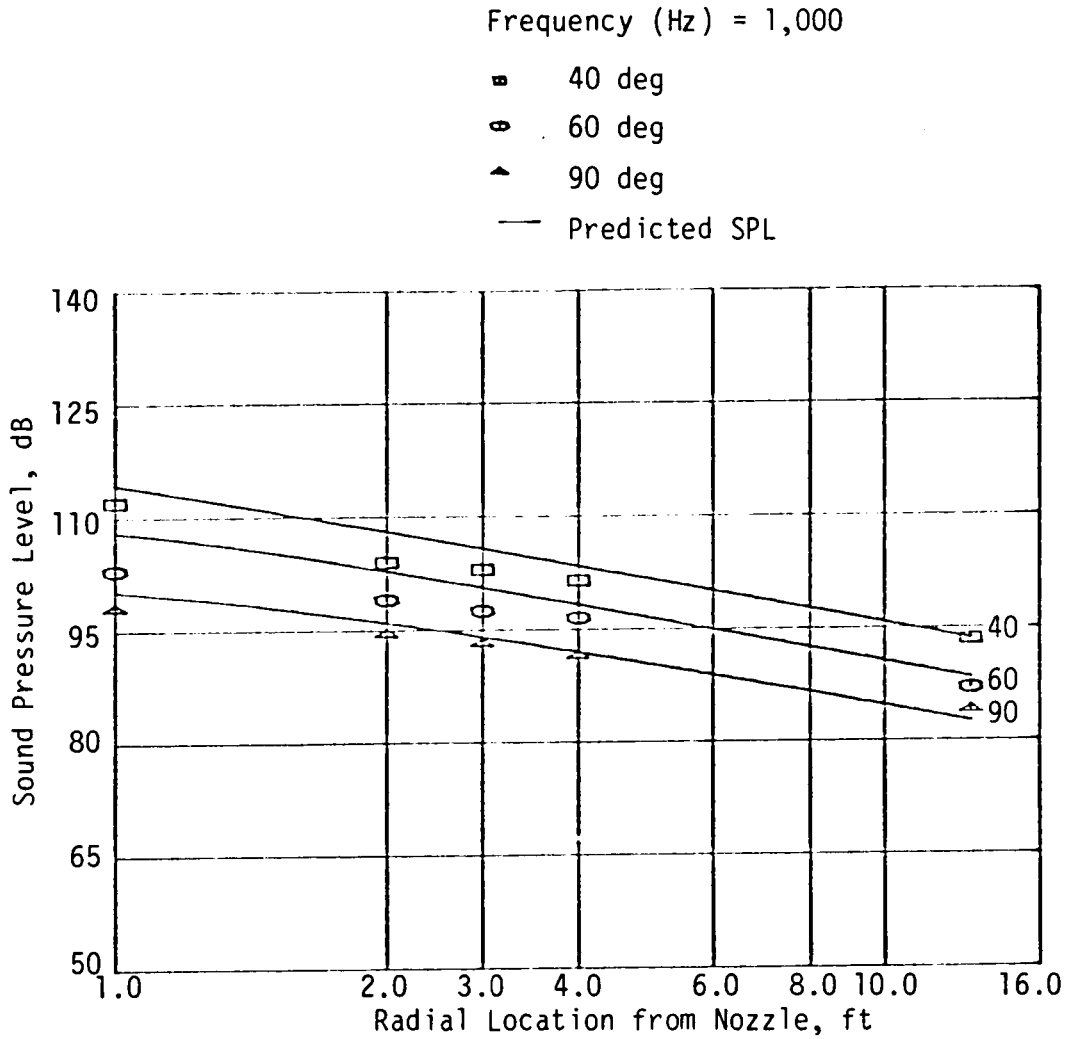

Figure 37. Comparison of measured and predicted sound pressure levels using modified source modeling technique for Test Condition 2 at 1,000 Hz.

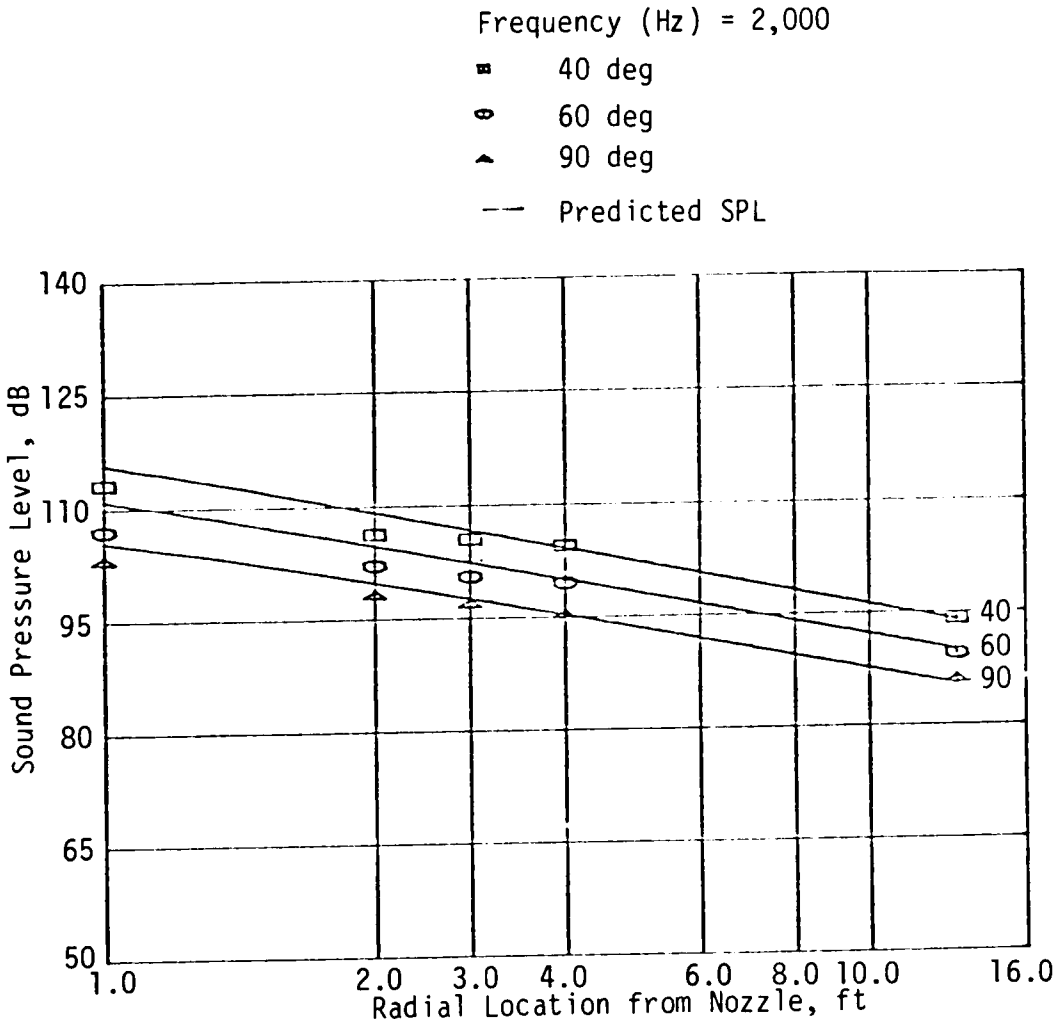

Figure 38. Comparison of measured and predicted sound pressure levels using modified source modeling technique for Test Condition 2 at 2,000 Hz.

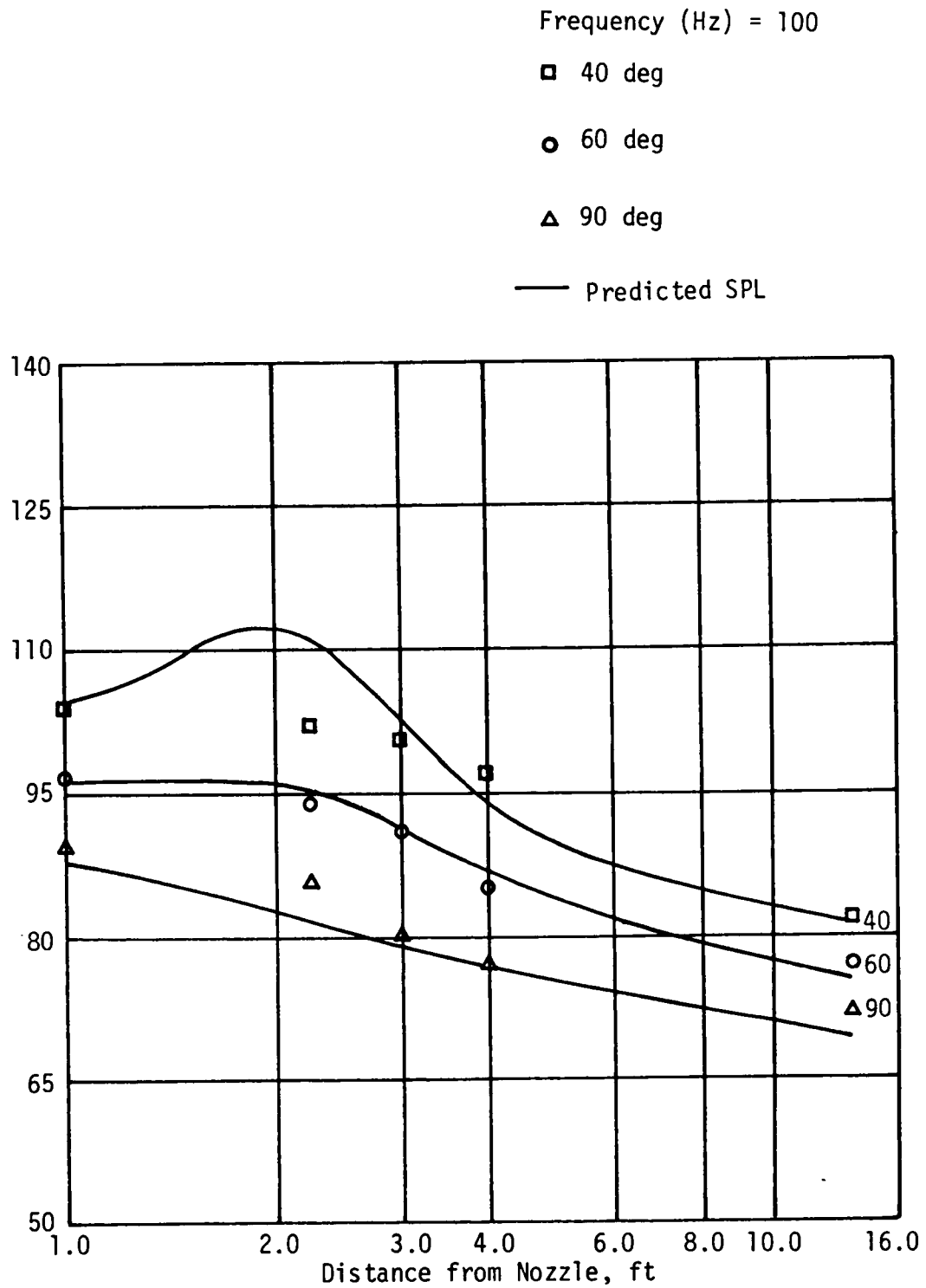

Figure 39. Comparison of measured and predicted sound pressure levels using modified source modeling technique for Test Condition 3 at 100 Hz.

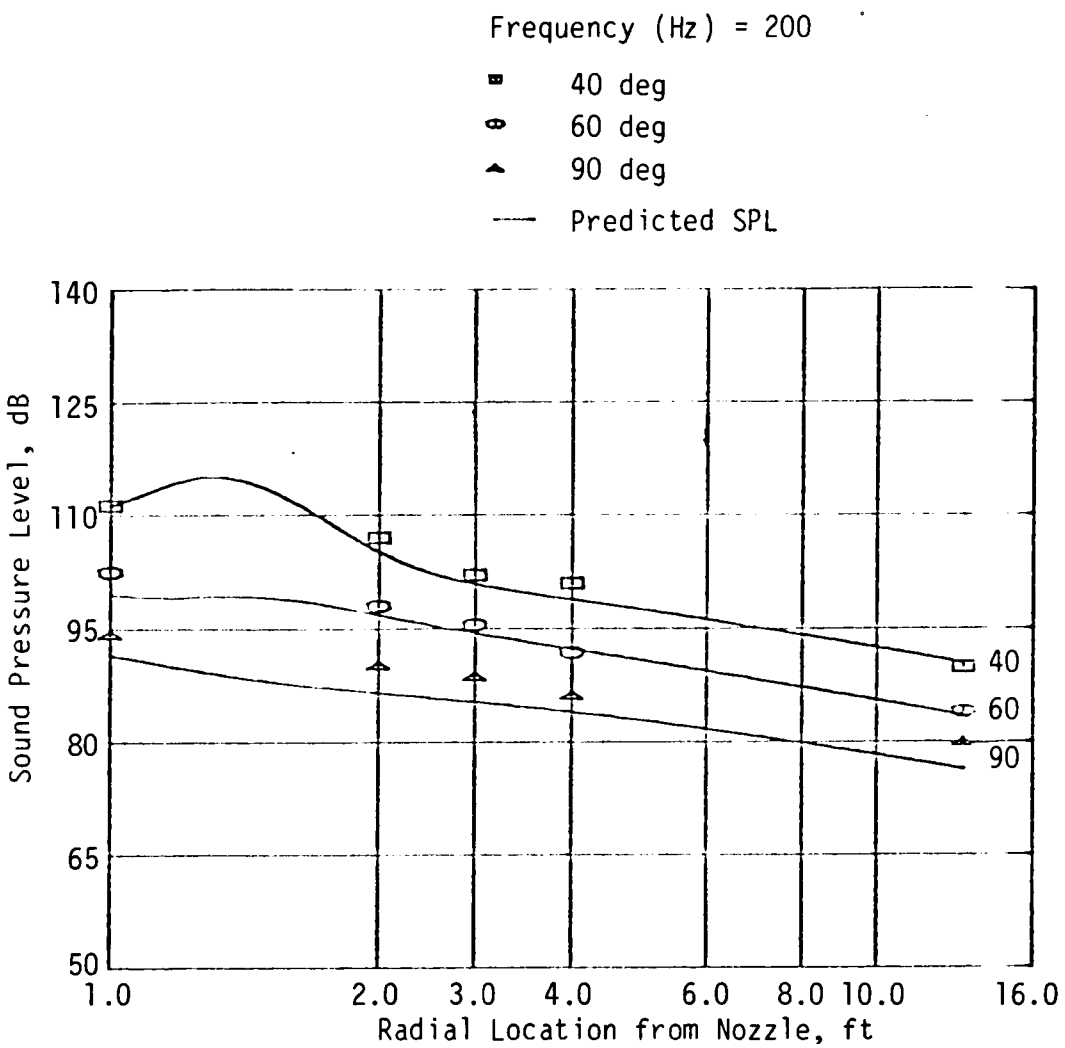

Figure 40. Comparison of measured and predicted sound pressure levels using modified source modeling technique for Test Condition 3 at 200 Hz.

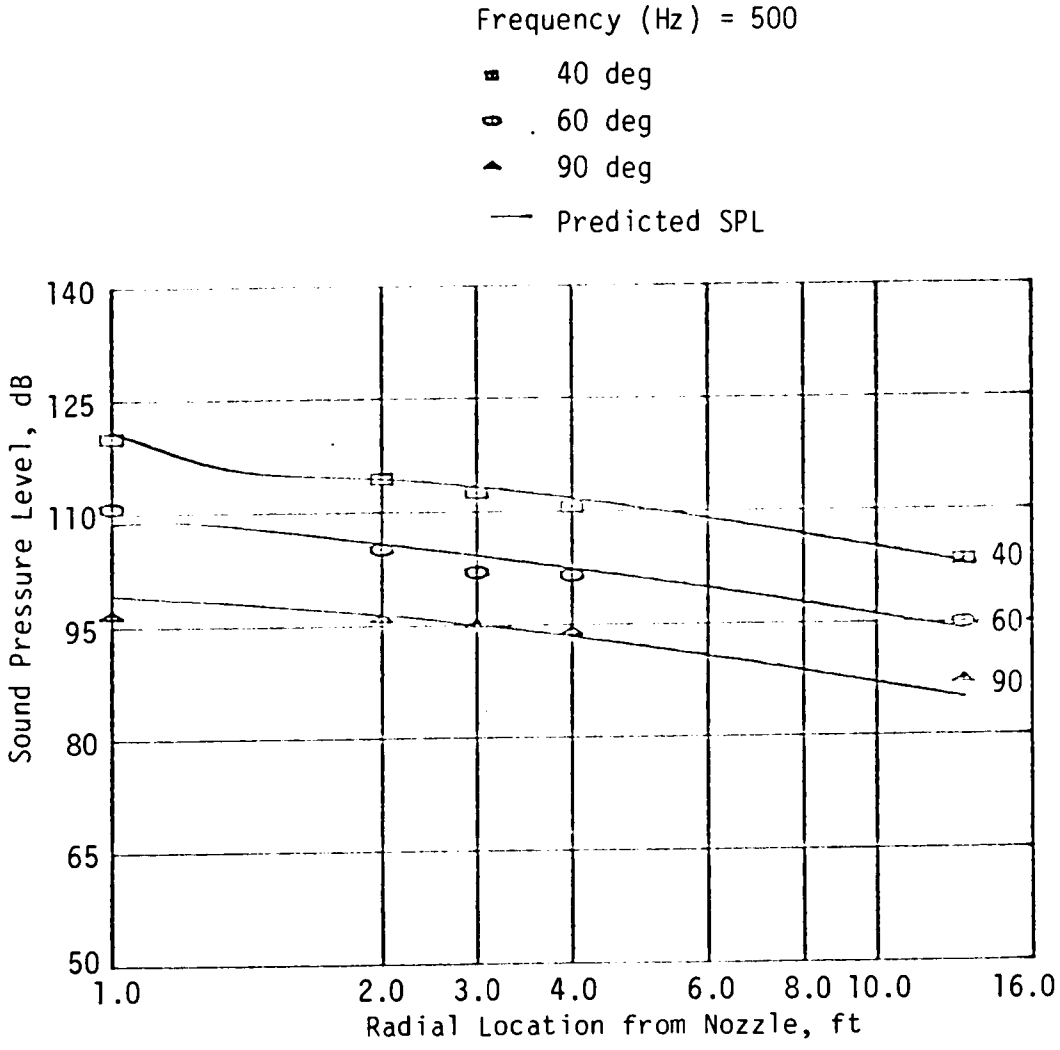

Figure 41. Comparison of measured and predicted sound pressure levels using modified source modeling technique for Test Condition 3 at 500 Hz.

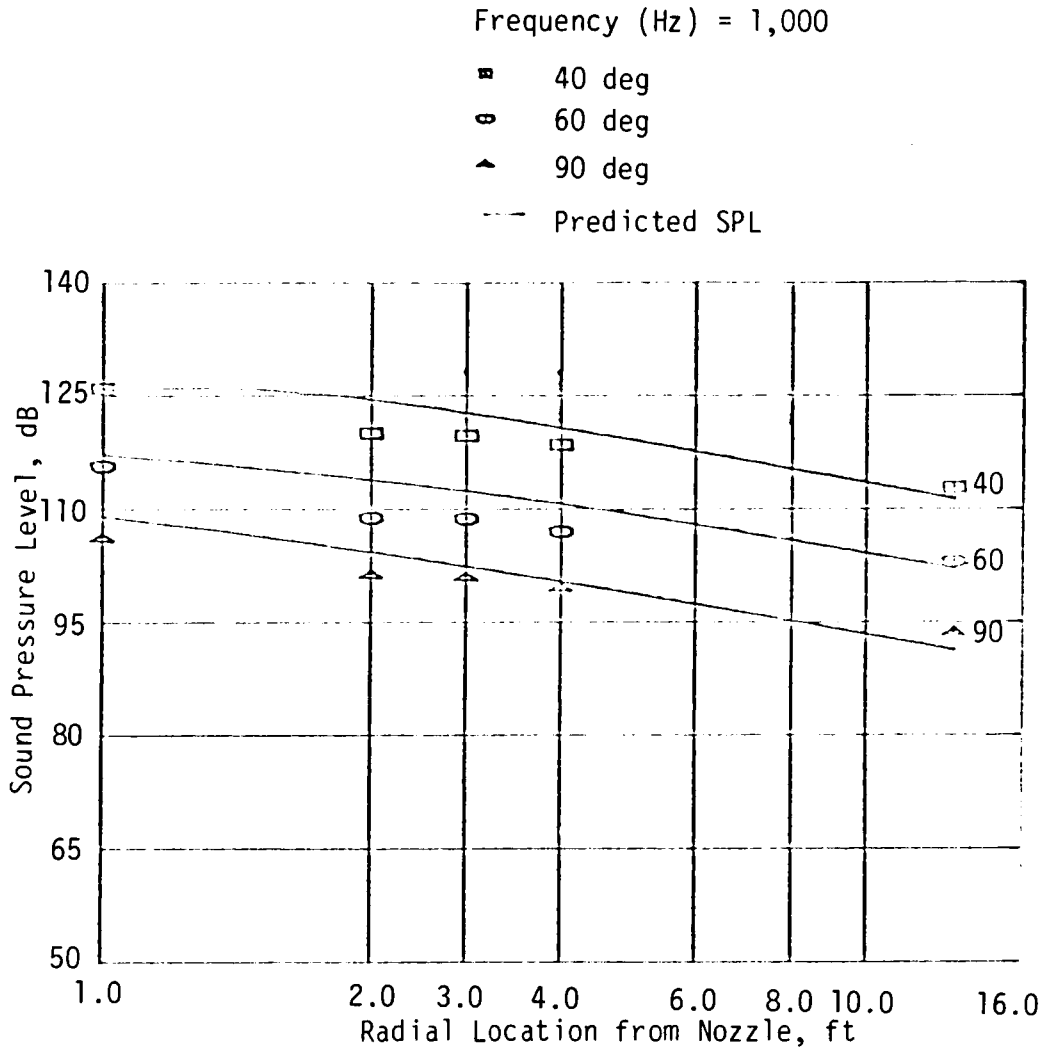

Figure 42. Comparison of measured and predicted sound pressure levels using modified source modeling technique for Test Condition 3 at 1,000 Hz.

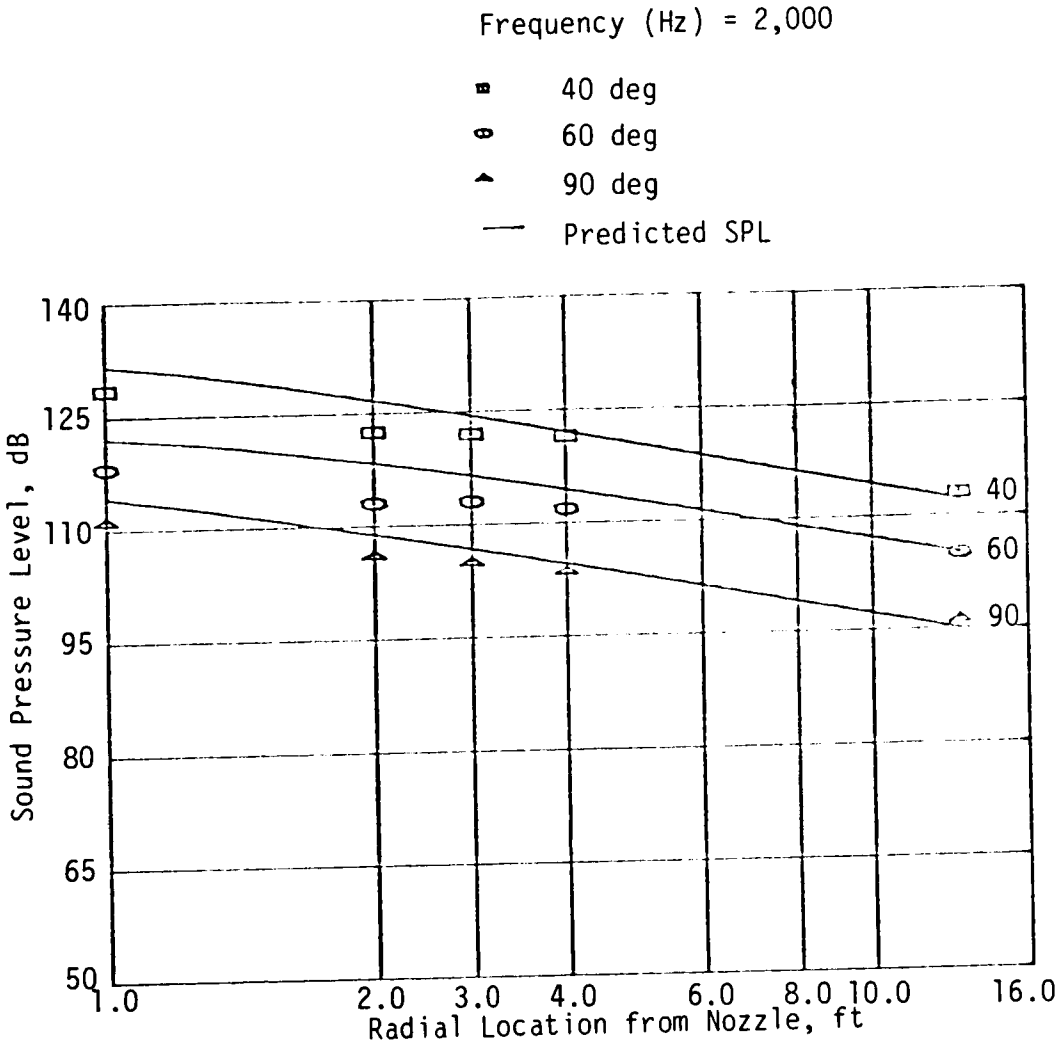

Figure 43. Comparison of measured and predicted sound pressure levels using modified source modeling technique for Test Condition 3 at 2,000 Hz.

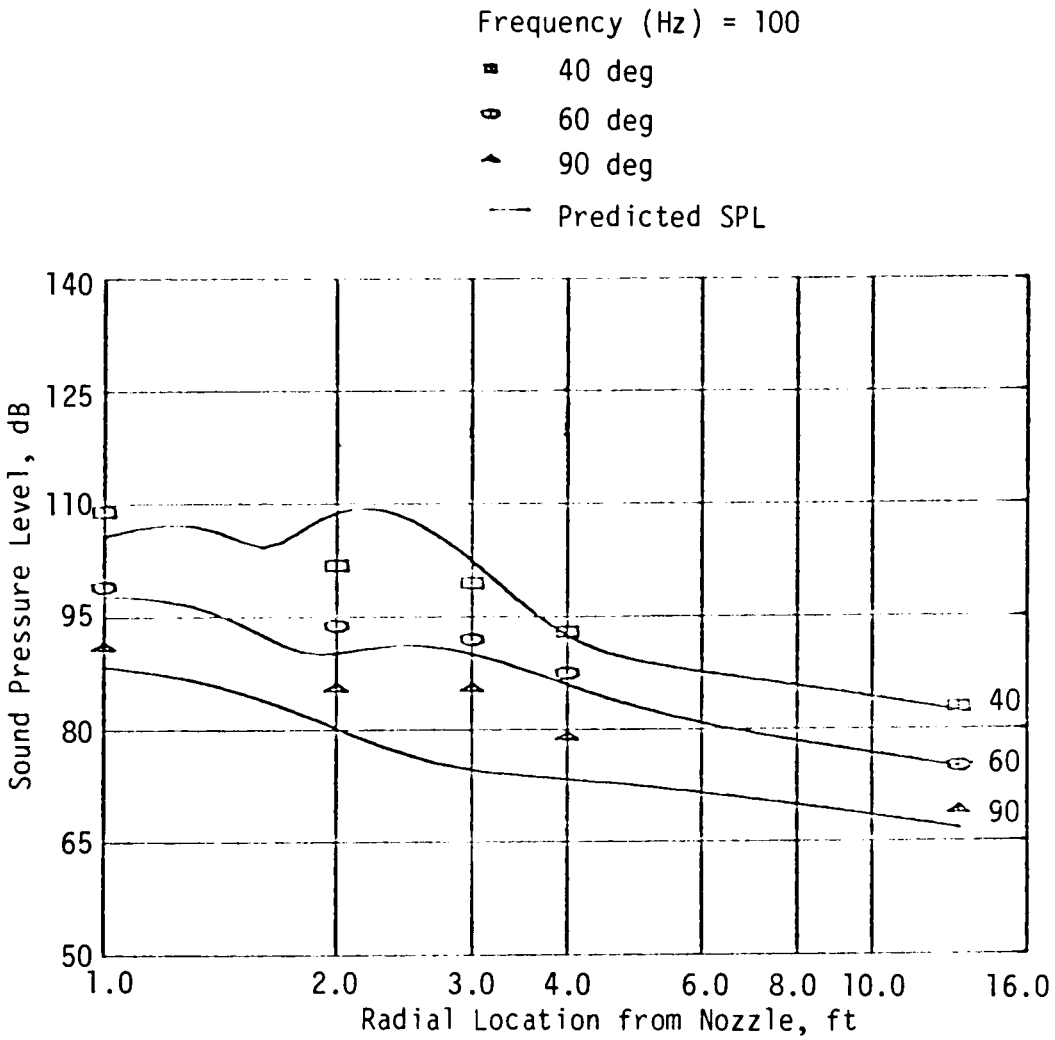

Figure 44. Comparison of measured and predicted sound pressure levels using modified source modeling technique for Test Condition 4 at 100 Hz.

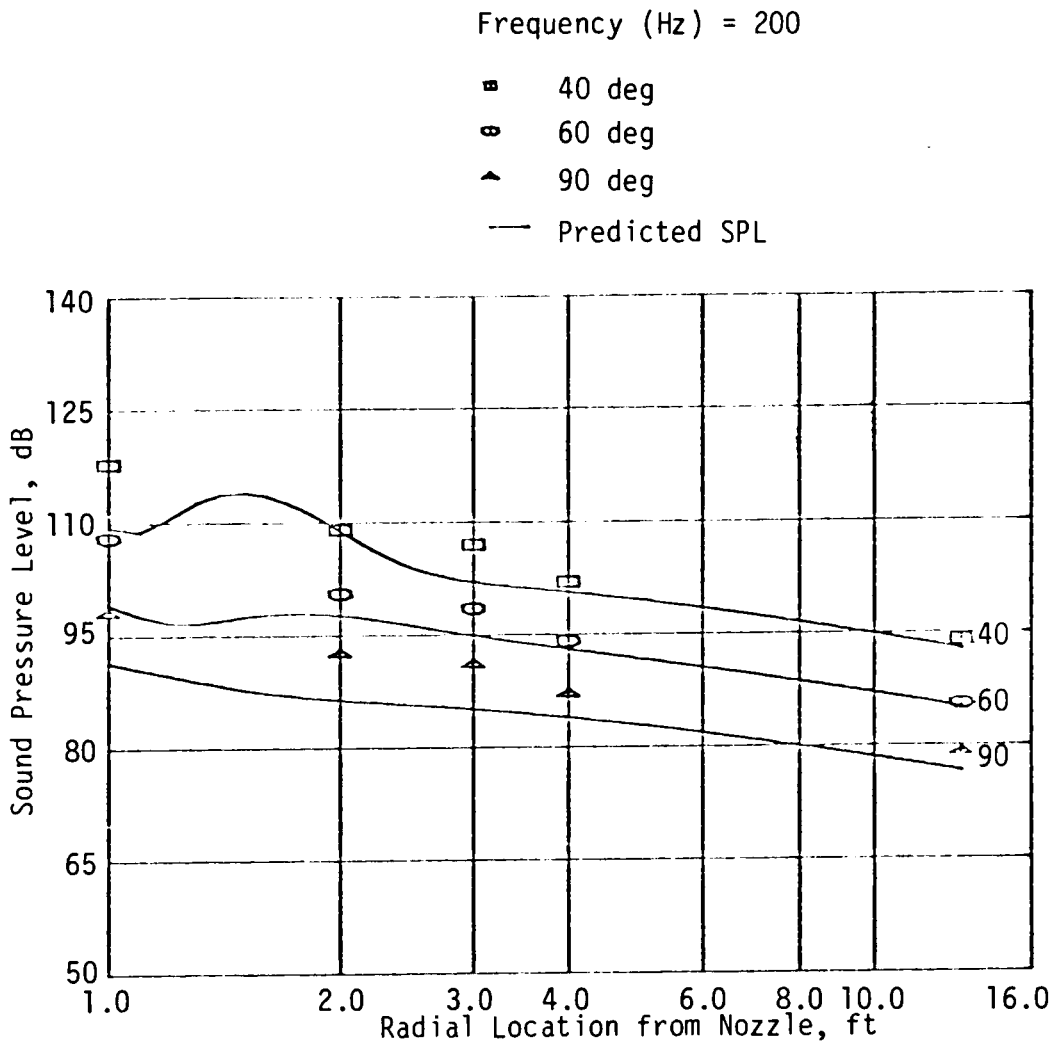

Figure 45. Comparison of measured and predicted sound pressure levels using modified source modeling technique for Test Condition 4 at 200 Hz.

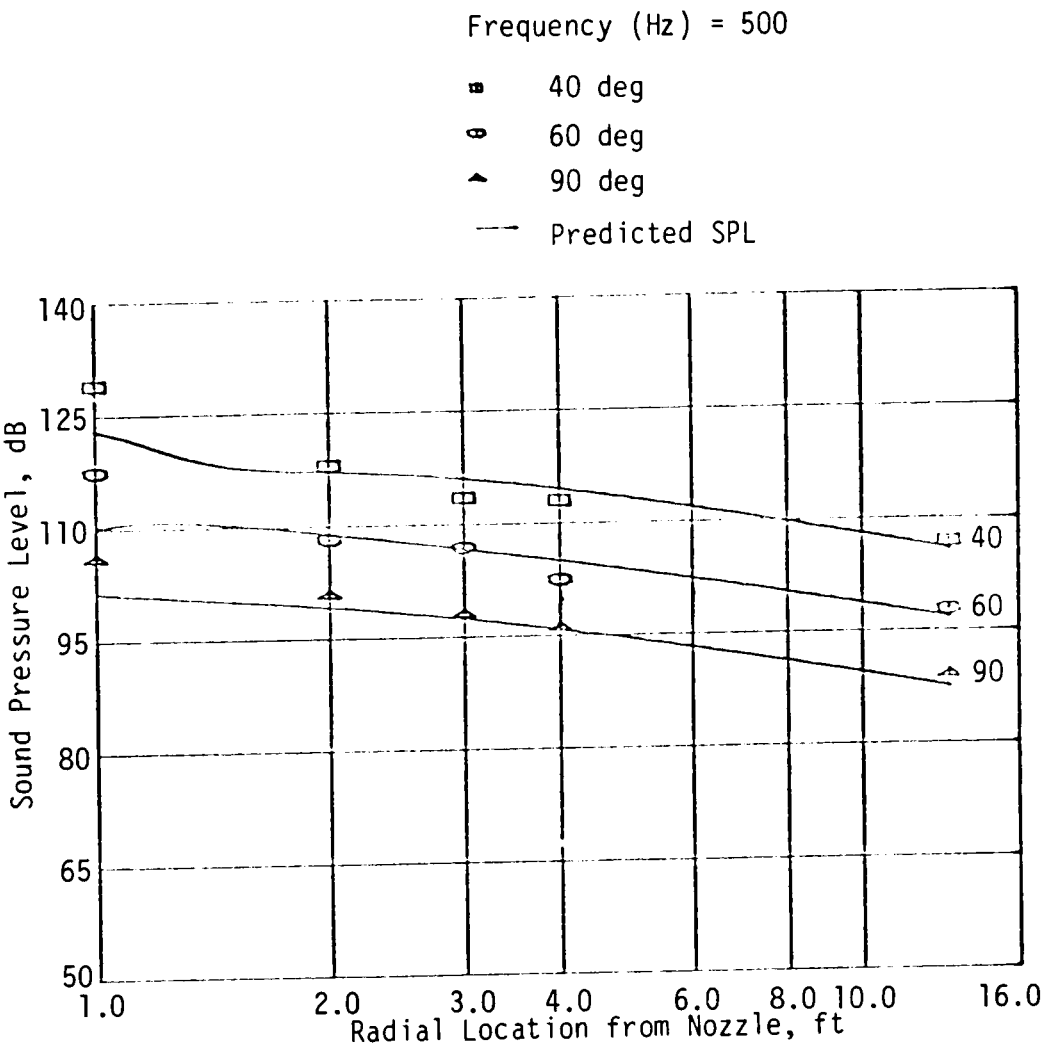

Figure 46. Comparison of measured and predicted sound pressure levels using modified source modeling technique for Test Condition 4 at 500 Hz.

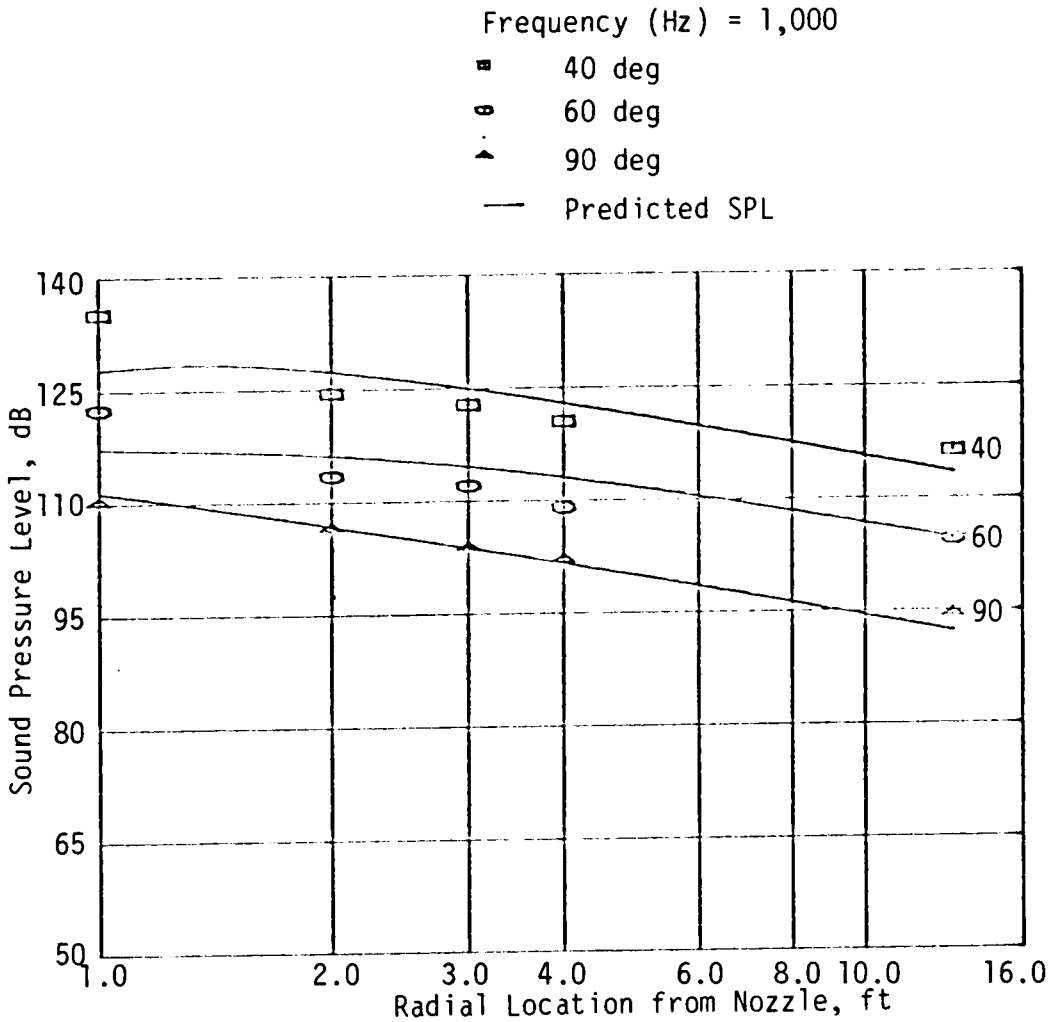

Figure 47. Comparison of measured and predicted sound pressure levels using modified source modeling technique for Test Condition 4 at 1,000 Hz.

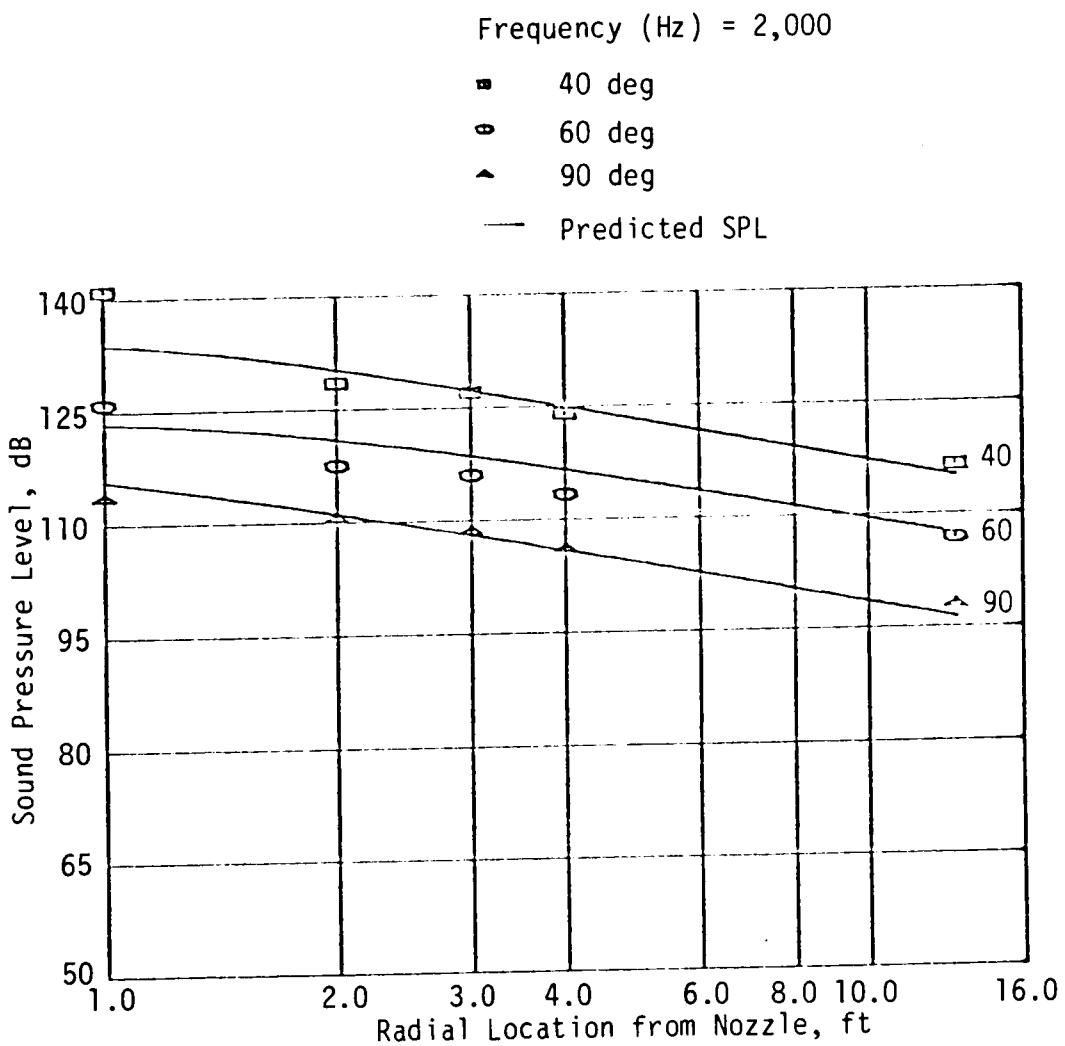

Figure 48. Comparison of measured and predicted sound pressure levels using modified source modeling technique for Test Condition 4 at 2,000 Hz.

calculations using the equations of Chapter III were made with angles and distances based on the source location for each frequency.

In general, the predicted values agree reasonably well with the microphone data. However, fairly large discrepancies still occur for measurements very close to the nozzle and for small angles to the jet axis. The microphone measurements at 90 degrees are those which are best described by the prediction scheme. This is to be expected, since in this direction the radiated sound is least affected by source convection or flow interaction effects.

As a final phase of this investigation, an attempt was made to include the Doppler effects also in the theoretical analysis. The analytical development described so far required some modifications in order to accommodate the Doppler effects. Rather than include this study as the next section of this chapter, it has been described more fully in the Appendix.

CHAPTER V

SUMMARY, CONCLUSIONS, AND RECOMMENDATIONS

5.1. Summary

The object of this study was to develop a scheme that would predict theoretically the near field noise characteristics of a subsonic axisymmetric free turbulent jet, given the sound pressures in the far field.

The main thrust during the initial stages of the investigation was to assume a stationary distributed source, which was approximated by a multipole expansion technique centered at the origin of the coordinate system. Another assumption made was that the acoustic source region and the sound field produced by it would be axisymmetric with respect to amplitude and phase on an instantaneous basis. This scheme predicted much higher values for near field sound pressures than were observed during experiments. The source region was then modeled using uncorrelated elementary sources, such as monopole, dipole, quadrupole, and so forth. The assumption of sources being stationary also had to be discarded. The source convection Mach number was calculated to evaluate the directionality effects due to convection. The inherent directionality of the sound field due to preferred orientation of the sources was also taken into account. Further, from the established theory of aerodynamic noise that sources are distributed axially as a function of their frequency (in place of the assumption that they are all located at the center of the nozzle

exit plane) was also given consideration. A functional relation between Strouhal number and source location was arrived at. With these modifications in the scheme, near field sound pressures were again predicted and compared against experimental data. Studies on the effect of Doppler shift of observed frequency were carried out.

5.2. Conclusions

A direct comparison of the predicted and measured sound pressure levels was presented in Chapter IV. The following conclusions can be made from those results.

1. The near and far acoustic fields produced by a circular jet can be reasonably well calculated using a model source region approximated by uncorrelated elementary sources.
2. The effect of source motion and the axial distribution of the sources as a function of frequency should be taken into account.
3. From this study it may be concluded that there seems to be no very strong direct near field contribution that is simply related to the far acoustic field.
4. The low-frequency sound (100 and 200 Hz) field proved to be relatively the most difficult to predict using this scheme.
5. The near sound field was theoretically predicted using only the monopole source term ($j = k = \ell = 0$). Large

deviations from the experimental results were observed. It may be concluded that the inclusion of higher order terms (up to octupole level in this study) is essential to obtain good predictions.

6. The dependence on the higher order terms mentioned in Item 5 above decreases as the frequency under consideration increases.
7. This scheme does not seem to indicate an improvement in the prediction of the near sound field by inclusion of the effect of Doppler shift of frequencies.

5.3. Recommendations

All of the tests in this study were carried out in the free field facility, where the effects of reflection from the ground and other structures were negligible. It is recommended that if the far field data were to be obtained in an enclosed space of even larger magnitude, the reflection characteristics of the enclosure should be incorporated in the prediction scheme. This is because of the conclusion that there exists no very strong direct near field contribution to the far field sound characteristics.

It is further recommended that additional study on the functional relation between Strouhal number and source frequency should be conducted. This is because the source location distance is an important factor in the prediction of the near sound field.

Further studies on estimating the ratio of convection velocity to jet exit velocity should be undertaken. It was mentioned

earlier that the sound sources are considered to be distributed along the jet axis; the lower the frequency of the source, the farther it is from the nozzle exit plane. Hence, the ratio of convection velocity to jet exit velocity should reflect the effect of this source location distance due to the velocity decay in the jet. A better method of predicting this ratio should also take into account the contribution of source location distance.

It is believed that the incorporation of a better estimate of the above-mentioned parameters in the present theoretical analysis should result in improved predictions for the near noise field.

BIBLIOGRAPHY

BIBLIOGRAPHY

1. Rayleigh, Lord. The Theory of Sound. Second edition. London: The Macmillan Company, 1896.

2. Morse, P. M. Vibration and Sound. New York: McGraw-Hill Book Company, 1948.

3. Lighthill, M. J. "On Sound Generated Aerodynamically, I, General Theory," Proceedings of the Royal Society, A211:564-587, 1952.

4. Lighthill, M. J. "On Sound Generated Aerodynamically, II, Turbulence as a Source of Sound," Proceedings of the Royal Society, A222:1-32, 1954.

5. Ribner, H. S. "The Generation of Sound by Turbulent Jets," Advances in Applied Mechanics. Vol. 8. New York: Academic Press, 1964. Pp. 104-182.

6. Lighthill, M. J. "Sound Generated Aerodynamically," Proceedings of the Royal Society, A267:147-182, 1962.

7. Ahuja, K. K., B. J. Tester, and H. K. Tanna. "Calculation of Far Field Jet Noise Spectra from Near Field Measurements Using True Source Location." American Institute of Aeronautics and Astronautics Paper No. 78-1153, presented at the Eleventh AIAA Fluid and Plasma Dynamics Conference, Seattle, Washington, July 10-12, 1978.

8. Goldstein, M. E. Aeroacoustics. New York: McGraw-Hill Book Company, 1976.

9. Mani, R., et al. "Development Technique for Inflight Jet Noise Simulation--Part II." American Institute of Aeronautics and Astronautics Paper No. 76-532, presented at the Third AIAA Aeroacoustics Conference, Palo Alto, California, July 20-23, 1976.

10. Lawson, C. L., and R. J. Hanson. Solving Least Squares Problems. New York: Prentice-Hall, 1974.

11. Lighthill, M. J. "Jet Noise." Advisory Group for Aeronautical Research and Development Paper No. AGARD-448, presented at the AGARD Specialists Meeting, "The Mechanism of Noise Generation in Turbulent Flow," Rhode-Saint-Genese, Belgium, April 1963.

12. Ffowcs Williams, J. E. "The Noise from Turbulence Convected at High Speed," Philosophical Transactions of the Royal Society, A225:469-503, 1963.

13. Laurence, J. C. "Intensity Scale and Spectra of Turbulence in Mixing Region of Free Subsonic Jet," National Advisory Committee for Aeronautics Report 1292, Washington, D. C., April 1956.

14. MacGregor, G. R., and C. D. Simcox. "Location of Acoustic Sources in Jet Flow by Means of Wall Isolation Technique." American Institute of Aeronautics and Astronautics Paper No. 73-1041, presented at the AIAA Aeroacoustics Conference, Seattle, Washington, October 15-17, 1973.

15. Lush, P. A. "Measurements of Subsonic Jet Noise and Comparison with Theory," Journal of Fluid Mechanics, 46(Part 3):477-500, April 1971.

APPENDIX

APPENDIX

DOPPLER SHIFT OF OBSERVED FREQUENCIES FOR CONVECTED ACOUSTIC SOURCES IN A TURBULENT JET

For an acoustic source of a given source frequency, f_s, being convected with a Mach number of M_c in a turbulent jet, the frequency as perceived by the microphone (the observed frequency) is a function of the convective Mach number and polar angle, ϕ, of the observation point. The relation between the observed frequency, f, and the source frequency is given by,

$$f_s = f(1 - M_c \cos\phi) \ . \qquad (A.1)$$

In other words, f_s is a frequency observed in a frame of reference convected at a Mach number, M_c. This frequency is related to f, observed in a stationary frame of reference, through the Doppler factor as given in Eq. (A.1). In a strict sense, it is more relevant to estimate the near sound field characteristics from the far field data for a given source frequency than for a given observed frequency. The procedure adopted for this modification and the results of the same are described below.

The first step in this direction is selecting a source frequency and calculating the observed frequencies for different values of polar angle, ϕ, and convection Mach number, M_c. However, in the present analysis, M_c is an unknown at this stage, as this value was obtained from Eqs. (4.18) through (4.24), explained in Chapter IV.

The estimation of convection velocity, V_c, requires as input the far field sound pressure levels for ϕ = 20, 25, 30, 35, and 90 degrees. The sound pressure levels used so far have been for selected observed frequencies. For a selected source frequency, the sound pressure level can be obtained only by knowing the value of M_c, as the frequency spectrum is based on observed frequencies. This necessitated that the ratio of convection to the jet exit Mach number be fixed a priori. A value of 0.6 was chosen for this ratio. Knowing the jet exit Mach number from the flow conditions, the value of the convection Mach number can now be determined by using Eq. (A.1). The observed frequencies can now be obtained for a given source frequency and various values of ϕ. It should be borne in mind that at present there is not enough conclusive theory in aerodynamic noise literature that prescribes an exact value for this ratio. Lush [15], for example, assumed a value of 0.65 for this ratio in his study on jet noise. Further, the ratio of M_c/M strictly will not be a constant and would depend on the acoustic source frequency, as the source location is different for each frequency. This somewhat oversimplified assumption of a constant value for this ratio was used in the present study due to, mainly, two reasons: (1) to get an idea as to how easily the present analysis is amenable to the incorporation of Doppler shift effects, and (2) as mentioned earlier, the lack of any information on the functional relation existing between the ratio, M_c/M, and frequency in aeroacoustics literature.

For each of the source frequencies of 100, 200, 500, 1,000, 2,000, 5,000, and 10,000 Hz, the corresponding observed frequencies

were calculated using Eq. (A.1) for each test condition given in Table 1, page 13. The sound pressure levels for each observed frequency were read off from the recorded spectra. The value of ϕ again ranged from ϕ = 20 degrees to ϕ = 90 degrees, with an increment of 5 degrees. These values of far field sound pressure levels were used to evaluate the strengths of the uncorrelated elementary sources. The near field sound pressure levels were again predicted, as described in Chapter IV.

A comparison of the measured sound pressure levels and the corresponding predicted values for some of the source frequencies are shown in Figs. 49 through 51. Equation (4.25) was used to predict the source locations from the Strouhal number.

As evident from these figures, the inclusion of Doppler shift did not produce the expected improvement in the prediction of sound pressure levels. However, this study proved helpful in a better understanding of the following about the theoretical model that was developed:

1. The non-negative least-squares fit computer program which predicted the multipole moment strengths was sensitive to the input values of the far field sound pressure levels. These values in this case depended upon a proper choice of the ratio of M_c/M. The misgivings about assuming a constant value for this ratio have already been discussed.
2. The expression for source location requires further refinement. A series of predictions of sound pressure levels was made by varying arbitrarily the constant and

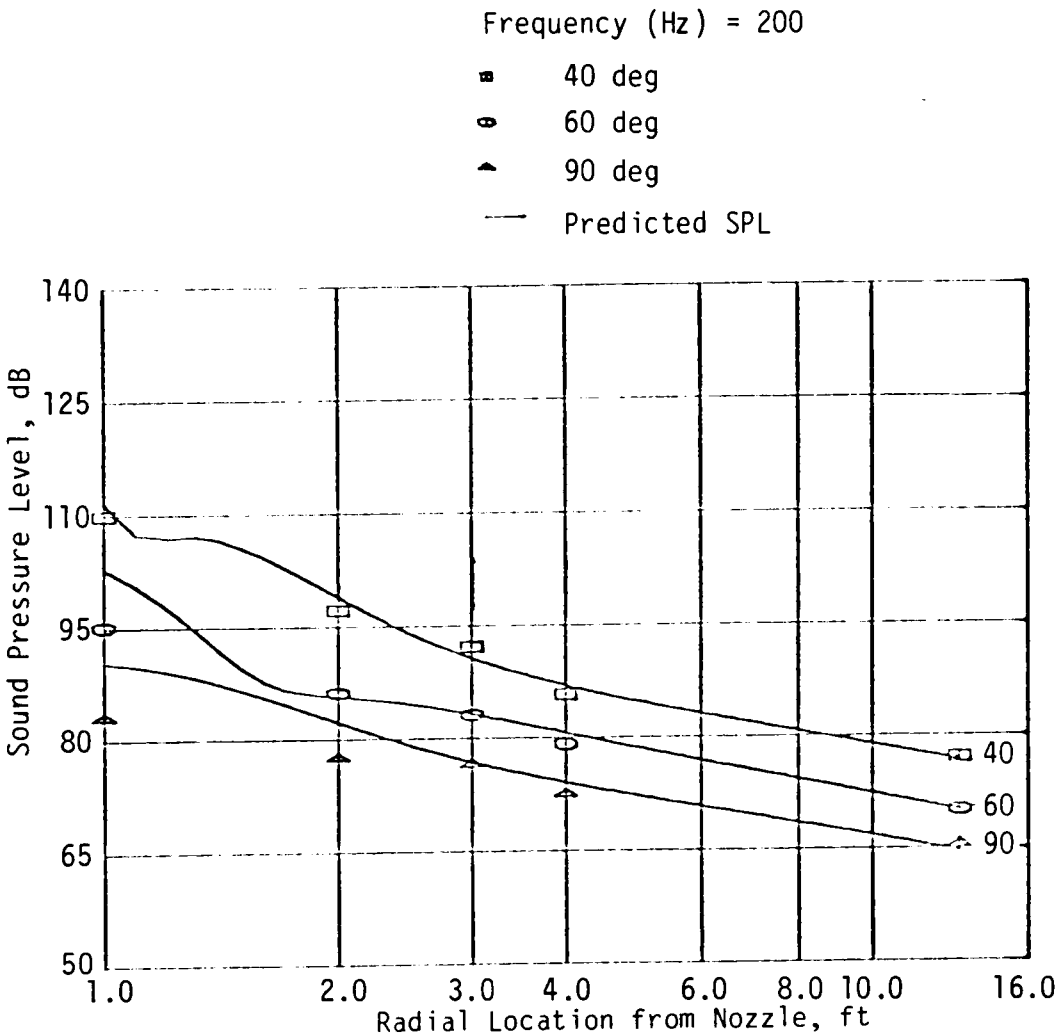

Figure 49. Comparison of measured and predicted sound pressure levels after Doppler shift correction for Test Condition 1.

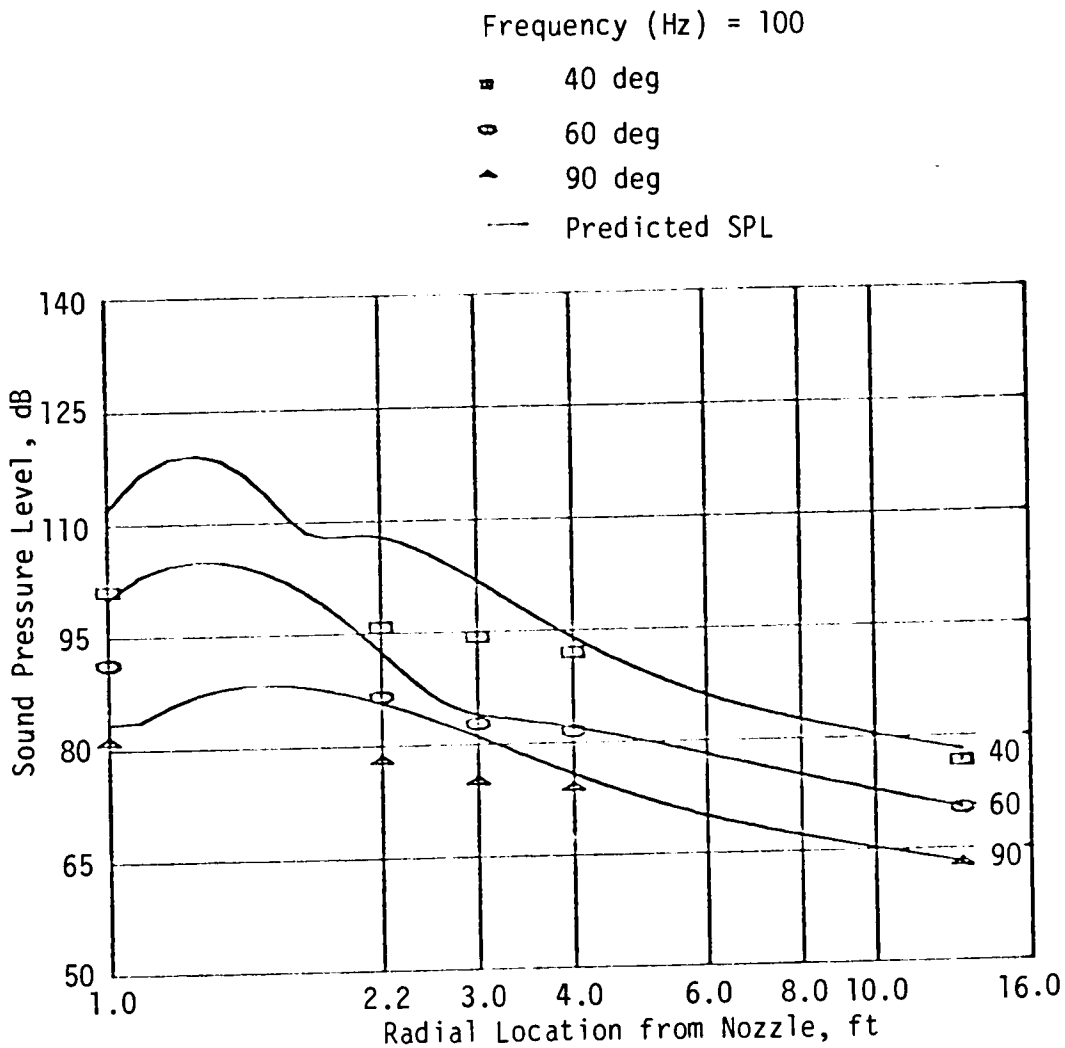

Figure 50. Comparison of measured and predicted sound pressure levels after Doppler shift correction for Test Condition 2.

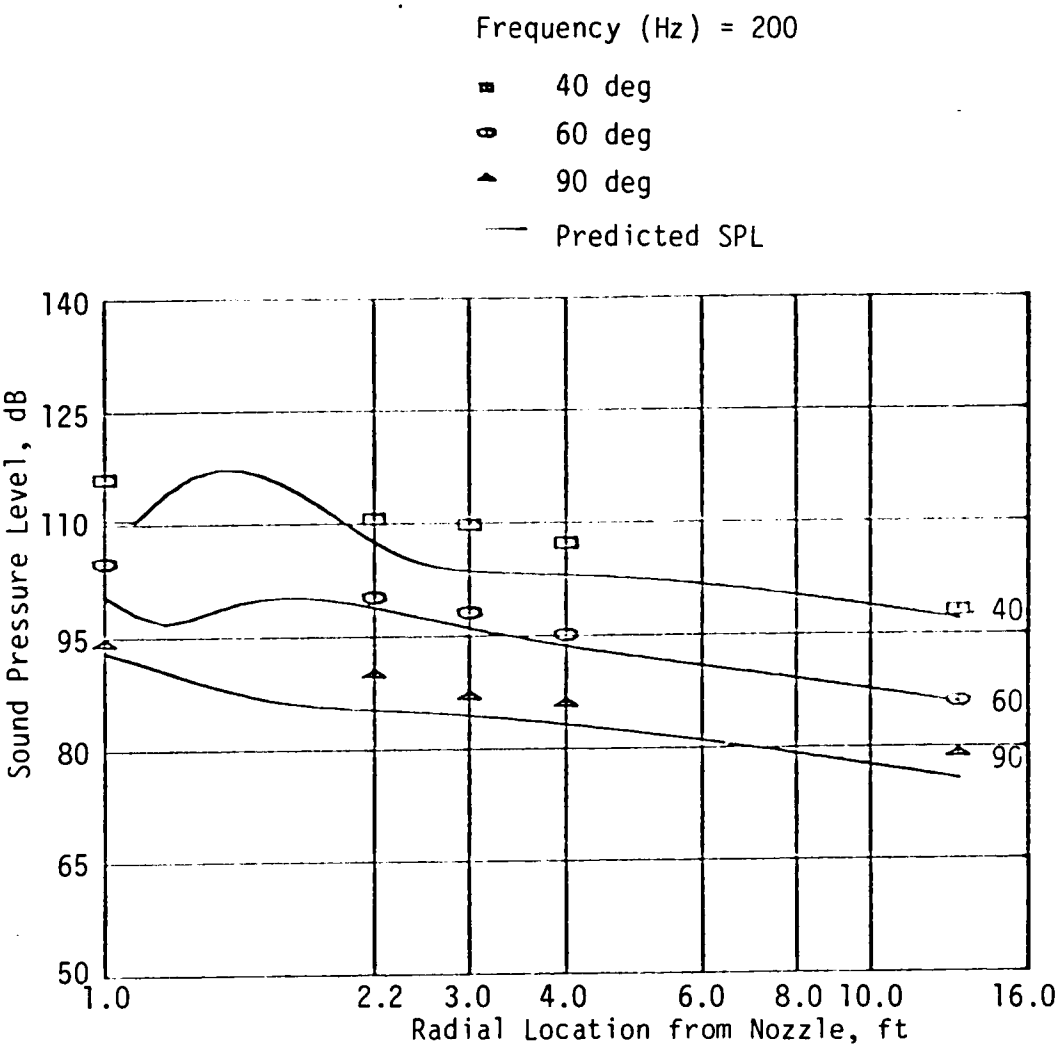

Figure 51. Comparison of measured and predicted sound pressure levels after Doppler shift correction for Test Condition 3.

exponent appearing in Eq. (4.25). The improvements in the results observed were not uniform over the complete range of frequencies and test conditions. These results are not presented here due to their voluminous nature.

It is strongly felt that the source modeling technique described here can be adapted to reflect the effects of Doppler shift if more light can be thrown upon the above-mentioned points through further research in the field of aerodynamic noise.

VITA

Sundaram C. Venkitarama was born in the city of Palghat in the State of Kerala in India on March 30, 1951. After graduating with a Bachelor of Science (Engineering) degree in Mechanical Engineering from N. S. S. Engineering College, Palghat, in 1972, he joined the Indian Institute of Technology in Madras, India, in 1973. He graduated with a Master of Technology (M. Tech) in Mechanical Engineering in 1975. He worked as an Engineering Trainee and later as an Engineer at Instrumentation, Ltd., in India until February 1977. He joined The University of Tennessee Space Institute in March 1977 and graduated with a Ph.D. degree in Mechanical Engineering in December 1981. Presently, he is employed as a Senior Engineer in the Research Division of Wyle Laboratories in Huntsville, Alabama.